

HEAT TRANSFER ENHANCEMENT WITH NANOFUIDS

A THESIS SUBMITTED TO  
THE GRADUATE SCHOOL OF NATURAL AND APPLIED SCIENCES  
OF  
MIDDLE EAST TECHNICAL UNIVERSITY

BY

SEZER ÖZERİNÇ

IN PARTIAL FULFILLMENT OF THE REQUIREMENTS  
FOR  
THE DEGREE OF MASTER OF SCIENCE  
IN  
MECHANICAL ENGINEERING

MAY 2010

Approval of the thesis:

**HEAT TRANSFER ENHANCEMENT WITH NANOFUIDS**

submitted by **SEZER ÖZERİNÇ** in partial fulfillment of the requirements for the degree of **Master of Science in Mechanical Engineering Department, Middle East Technical University** by,

Prof. Dr. Canan Özgen  
Dean, Graduate School of **Natural and Applied Sciences**

\_\_\_\_\_

Prof. Dr. Suha Oral  
Head of Department, **Mechanical Engineering**

\_\_\_\_\_

Asst. Prof. Dr. Almıla Güvenç Yazıcıoğlu  
Supervisor, **Mechanical Engineering Dept., METU**

\_\_\_\_\_

Prof. Dr. Sadık Kakaç  
Co-Supervisor, **Mechanical Engineering Dept., TOBB ETÜ**

\_\_\_\_\_

**Examining Committee Members:**

Assoc. Prof. Dr. Derek K. Baker  
Mechanical Engineering Dept., METU

\_\_\_\_\_

Asst. Prof. Dr. Almıla Güvenç Yazıcıoğlu  
Mechanical Engineering Dept., METU

\_\_\_\_\_

Prof. Dr. Sadık Kakaç  
Mechanical Engineering Dept., TOBB ETÜ

\_\_\_\_\_

Prof. Dr. Tülay Özbelge  
Chemical Engineering Dept., METU

\_\_\_\_\_

Asst. Prof. Dr. Tuba Okutucu Özyurt  
Mechanical Engineering Dept., METU

\_\_\_\_\_

**Date:**

**May 10, 2010**

**I hereby declare that all information in this document has been obtained and presented in accordance with academic rules and ethical conduct. I also declare that, as required by these rules and conduct, I have fully cited and referenced all material and results that are not original to this work.**

Name, Last name : Sezer Özerinç

Signature :

## **ABSTRACT**

### **HEAT TRANSFER ENHANCEMENT WITH NANOFLUIDS**

Özerinç, Sezer

M.S., Mechanical Engineering Department

Supervisor : Asst. Prof. Dr. Almila Güvenç Yazıcıoğlu

Co-Supervisor : Prof. Dr. Sadık Kakaç

May 2010, 147 pages

A nanofluid is the suspension of nanoparticles in a base fluid. Nanofluids are promising fluids for heat transfer enhancement due to their anomalously high thermal conductivity. At present, there is significant discrepancy in nanofluid thermal conductivity data in the literature. On the other hand, thermal conductivity enhancement mechanisms of nanofluids have not been fully understood yet. In the first part of this study, a detailed literature review about the thermal conductivity of nanofluids is performed. Experimental studies are discussed in terms of the effects of some parameters such as particle volume fraction, particle size, and temperature on the thermal conductivity of nanofluids. Enhancement mechanisms proposed to explain nanofluid thermal conductivity are also summarized and associated thermal conductivity models are explained. Predictions of some thermal conductivity models are compared with the experimental data and discrepancies are indicated.

Research about the forced convection of nanofluids is important for the practical application of nanofluids in heat transfer devices. Recent experiments showed that heat transfer enhancement of nanofluids exceeds the thermal conductivity enhancement of nanofluids. This extra enhancement might be

explained by thermal dispersion, which occurs due to the random motion of nanoparticles in the flow. In the second part of the present study, in order to examine the validity of a thermal dispersion model available in the literature, hydrodynamically fully developed, thermally developing laminar flow of  $\text{Al}_2\text{O}_3/\text{water}$  nanofluid inside a straight circular tube under constant wall temperature and constant wall heat flux boundary conditions is numerically analyzed. Finite difference method with Alternating Direction Implicit Scheme is utilized in the analysis. Numerical results are compared with experimental and numerical data in the literature and good agreement is observed especially with experimental data. The agreement can be considered as an indication of the validity of the thermal dispersion model for explaining nanofluid heat transfer. In addition to the numerical study, a theoretical analysis is also performed, which shows that the usage of classical heat transfer correlations for heat transfer analysis of nanofluids is not valid.

**Keywords:** Nanofluids, Thermal Conductivity, Heat Transfer Enhancement, Forced Convection, Numerical Analysis

## ÖZ

### NANOAKIŞKANLAR KULLANARAK TAŞINIMLA ISI TRANSFERİNİN ARTIRILMASI

Özerinç, Sezer

Yüksek Lisans, Makina Mühendisliği Bölümü

Tez Yöneticisi : Yrd. Doç. Dr. Almıla Güvenç Yazıcıoğlu

Ortak Tez Yöneticisi : Prof Dr. Sadık Kakaç

Mayıs 2010, 147 sayfa

Nanoparçacıkların bir sıvı içerisindeki süspansiyonları nanoakışkan olarak adlandırılır. Nanoakışkanlar yüksek ısı iletim katsayıları sebebiyle ısı transferi artırımı için gelecek vaat etmektedirler. An itibariyle, literatürde nanoakışkanların ısı iletim katsayıları ile ilgili çelişkili sonuçlar mevcuttur. Öte yandan söz konusu ısı iletim katsayısı artışına sebep olan mekanizmalar henüz tam olarak anlaşılamamıştır. Bu çalışmanın ilk bölümünde, nanoakışkanların ısı iletim katsayıları ile ilgili detaylı bir literatür taraması yapılmıştır. Deneysel çalışmalar, hacimsel parçacık oranı, parçacık boyutu ve sıcaklık gibi parametrelerin ısı iletim katsayısına etkisinin incelenmesi suretiyle özetlenmiştir. Ayrıca, nanoakışkan ısı iletim katsayısı artışlarını açıklamak için önerilen mekanizmalar ve ilgili ısı iletim katsayısı modelleri açıklanmıştır. Bu modellerin öngörülerini deneysel sonuçlarla karşılaştırılmış, gözlemlenen çelişkiler vurgulanmıştır.

Zorlanmış taşınım ile nanoakışkan ısı transferi konusundaki araştırmalar, nanoakışkanların ısı transferi ekipmanlarında kullanılabilmesi açısından önem arz etmektedir. Son dönemde yapılan deneysel çalışmalar, nanoakışkanlarla elde edilen ısı transferi artırımının, ilgili ısı iletim katsayısı artırımından yüksek

olduğunu göstermiştir. Bu ilave artışın, nanoparçacıkların akış içerisindeki rastlantısal hareketleri sonucu oluşan ısı dağılım olayı ile açıklanabileceği düşünülmektedir. Bu çalışmanın ikinci bölümünde, literatürde mevcut olan bir ısı dağılım modelinin geçerliliğini incelemek amacıyla,  $Al_2O_3$ /su nanoakışkanının dairesel kesitli düz bir kanal içerisindeki hidrodinamik olarak tam gelişmiş, termal olarak gelişmekte olan laminer akışı, sabit duvar sıcaklığı ve sabit duvar ısı akısı sınır şartları altında sayısal olarak incelenmiştir. Analizde, Değişken Yönlü Kapalı Metot aracılığı ile sonlu farklar analizi uygulanmıştır. Sayısal sonuçlar literatürdeki deneysel ve sayısal sonuçlarla karşılaştırılmış ve özellikle deneysel sonuçlar ile uyumluluk gözlenmiştir. Söz konusu uyumluluk, ısı dağılım modelinin nanoakışkan ısı transferini açıklamak için uygun bir model olduğu yönünde değerlendirilebilir. Sayısal çalışmaya ek olarak yapılan teorik çalışmada, klasik ısı transferi eşilişkilerinin nanoakışkan ısı transferi analizi için kullanılmasının uygun olmadığı gösterilmiştir.

**Anahtar Kelimeler:** Nanoakışkan, Isıl İletim Katsayısı, Isı Transferi Artırımı, Zorlanmış Taşınım, Sayısal Analiz

*To My Parents*



## ACKNOWLEDGMENTS

Firstly, I would like to express my sincere gratitude to my supervisor Asst. Prof. Dr. Almıla Güvenç Yazıcıođlu and my co-supervisor Prof. Dr. Sadık Kakaç for their guidance and encouragement throughout my study. I have experienced an excellent academic study under their supervision and their invaluable recommendations and support helped me to plan my further academic studies in the best way.

I would like to give my special thanks to Asst. Prof. Dr. Cüneyt Sert and Dr. Barbaros Çetin for their helpful comments regarding the numerical aspects of my study.

I would like to thank to my colleagues Altuđ Özçelikkale, Fahri Erinç Hızır and Cem Gözükara for the useful discussions we experienced in all steps of my study.

This thesis would not have been possible without the support of my family. I am grateful to them for their never-ending love, patience and encouragement.

Lastly, I would like to thank to TÜBİTAK for its financial support during my academic study.

## TABLE OF CONTENTS

ABSTRACT.....	iv
ÖZ.....	vi
ACKNOWLEDGMENTS.....	ix
TABLE OF CONTENTS.....	x
LIST OF TABLES.....	xvi
LIST OF FIGURES.....	xvii
NOMENCLATURE.....	xx
CHAPTERS	
1. INTRODUCTION.....	1
1.1 Improving Heat Transfer Efficiency.....	1
1.2 Nanofluids.....	2
1.2.1 Introduction.....	2
1.2.2 Particle Material and Base Fluid.....	2
1.2.3 Particle Size.....	3
1.2.4 Particle Shape.....	3
1.2.5 Production Methods.....	3
1.2.5.1 Production of Nanoparticles.....	3
1.2.5.2 Production of Nanofluids.....	3
1.3 Thermal Conductivity of Nanofluids.....	4
1.4 Heat Transfer Enhancement with Nanofluids.....	5
2. THERMAL CONDUCTIVITY OF NANOFUIDS.....	6

2.1	Introduction.....	6
2.2	Literature Survey.....	7
2.2.1	Experimental Studies.....	7
2.2.1.1	Thermal Conductivity Measurement Methods.....	7
2.2.1.2	Effects of Some Parameters on Thermal Conductivity of Nanofluids.....	7
2.2.1.2.1	Particle Volume Fraction.....	8
2.2.1.2.2	Particle Material.....	9
2.2.1.2.3	Base Fluid.....	11
2.2.1.2.4	Particle Size.....	13
2.2.1.2.5	Particle Shape.....	15
2.2.1.2.6	Temperature.....	16
2.2.1.2.7	Clustering.....	19
2.2.1.2.8	pH Value.....	19
2.2.1.3	Possible Reasons of Discrepancy in Experimental Data.....	20
2.2.2	Theoretical Studies.....	24
2.2.2.1	Classical Models.....	24
2.2.2.2	Enhancement Mechanisms.....	25
2.2.2.2.1	Brownian Motion of Nanoparticles.....	25
2.2.2.2.2	Clustering of Nanoparticles.....	27
2.2.2.2.3	Liquid Layering around Nanoparticles.....	29
2.2.2.2.4	Ballistic Phonon Transport in Nanoparticles.....	31

2.2.2.2.5	Near Field Radiation.....	32
2.2.2.3	Models of Nanofluid Thermal Conductivity.....	32
2.2.2.3.1	Models Based on Brownian Motion.....	32
2.2.2.3.2	Models Based on Clustering.....	38
2.2.2.3.3	Models Based on Liquid Layering.....	40
2.3	Comparison of Thermal Conductivity with Experimental Data.....	47
2.3.1	Particle Volume Fraction.....	47
2.3.2	Particle Size.....	49
2.3.3	Temperature.....	55
2.4	Concluding Remarks.....	59
3.	CONVECTIVE HEAT TRANSFER WITH NANOFLUIDS –	
	LITERATURE SURVEY AND THEORETICAL ANALYSIS .....	61
3.1	Introduction.....	61
3.2	Literature Survey.....	61
3.2.1	Experimental Studies.....	62
3.2.2	Theoretical Studies.....	64
3.2.3	Numerical Studies.....	67
3.3	Thermophysical Properties of Nanofluids.....	69
3.3.1	Density.....	69
3.3.2	Specific Heat.....	69
3.3.3	Viscosity.....	69
3.3.3.1	Experimental Studies.....	70
3.3.3.2	Theoretical Models.....	71

3.3.4	Thermal Conductivity.....	73
3.4	Theoretical Analysis.....	74
3.4.1	Introduction.....	74
3.4.2	Heat Transfer Coefficient Enhancement.....	75
3.4.2.1	Constant Wall Heat Flux Boundary Condition.....	75
3.4.2.2	Constant Wall Temperature Boundary Condition....	79
3.4.3	Effect of Thermal Conductivity on Fully Developed Heat Transfer.....	82
3.4.4	Concluding Remarks.....	85
4.	CONVECTIVE HEAT TRANSFER WITH NANOFUIDS – EXPLANATION AND VERIFICATION OF NUMERICAL ANALYSIS.....	86
4.1	Introduction.....	86
4.2	Geometry in Consideration.....	86
4.2.1	Constant Wall Temperature Boundary Condition.....	87
4.2.2	Constant Wall Heat Flux Boundary Condition.....	87
4.3	Modeling of Nanofluid Flow.....	88
4.3.1	Single Phase Approach.....	88
4.3.2	Thermal Dispersion Model.....	89
4.3.3	Thermophysical Properties.....	89
4.3.4	Variation of Thermal Conductivity with Temperature.....	90
4.4	Governing Equations.....	90
4.4.1	Constant Wall Temperature Boundary Condition.....	93

4.4.2	Constant Wall Heat Flux Boundary Condition.....	94
4.5	Numerical Method.....	95
4.5.1	Finite Difference Method.....	95
4.5.2	Discretization of the Boundary Nodes.....	96
4.5.3	Alternating Direction Implicit Scheme.....	97
4.6	Code Verification.....	99
4.6.1	Determination of Optimum Solution Parameters.....	99
4.6.2	Comparison of the Results with Graetz Solution.....	102
4.6.2.1	Constant Wall Temperature Boundary Condition...	102
4.6.2.2	Constant Wall Heat Flux Boundary Condition.....	103
4.7	Concluding Remarks.....	104
5.	CONVECTIVE HEAT TRANSFER WITH NANOFUIDS –	
	RESULTS OF NUMERICAL ANALYSIS.....	105
5.1	Introduction.....	105
5.2	Constant Wall Temperature Boundary Condition.....	105
5.2.1	Heat Transfer Coefficient Enhancement.....	106
5.2.1.1	Comparison of Results with Experimental Data....	106
5.2.1.2	Comparison of Results with Numerical Data.....	107
5.2.2	Further Analysis.....	109
5.2.2.1	Local Nusselt Number.....	109
5.2.2.2	Effect of Particle Size.....	110
5.2.2.3	Effects of Heating and Cooling.....	112
5.3	Constant Wall Heat Flux Boundary Condition.....	113

5.3.1	Local Heat Transfer Coefficient.....	114
5.3.1.1	Comparison of Results with Experimental Data....	114
5.3.1.2	Comparison of Results with Numerical Data.....	115
5.3.2	Further Analysis.....	117
5.3.2.1	Local Nusselt Number.....	117
5.3.2.2	Effect of Particle Size.....	119
5.3.2.3	Effects of Heating and Cooling.....	120
5.4	Concluding Remarks.....	122
6.	CONCLUSION.....	124
6.1	Summary.....	124
6.2	Conclusion.....	125
6.3	Suggestions for Future Work.....	127
	REFERENCES.....	129
APPENDICES		
A.	SAMPLE CALCULATIONS.....	141
A.1.	Average Heat Transfer Coefficient Enhancement Ratio.....	141
A.2.	Fully Developed Heat Transfer Coefficient.....	143
B.	FLOWCHART OF THE NUMERICAL SOLUTION.....	146

## LIST OF TABLES

### TABLES

Table 1	Summary of Experimental Studies of Thermal Conductivity Enhancement.....	21
Table 2	$\beta$ Values for Different Nanoparticles to be Used in Eq. (13).....	35
Table 3	Viscosity Models for Nanofluids.....	73
Table 4	Thermal Conductivity and Heat Transfer Coefficient Values for Pure Water and $\text{Al}_2\text{O}_3$ /Water Nanofluid, Room Temperature.....	84
Table 5	Thermal Conductivity and Heat Transfer Coefficient Values for Pure Water and $\text{Al}_2\text{O}_3$ /Water Nanofluid, $T = 50^\circ\text{C}$ .....	84
Table 6	Fully Developed Nusselt Number and Heat Transfer Coefficient Values Obtained from the Numerical Solution for Pure Water and $\text{Al}_2\text{O}_3$ /Water Nanofluid with Different Particle Volume Fractions.....	110
Table 7	Average Heat Transfer Coefficient of $\text{Al}_2\text{O}_3$ /Water Nanofluid according to the Present Numerical Study and the Numerical Study of Bianco et al. ....	117
Table 8	Fully Developed Nusselt Number and Heat Transfer Coefficient Values Obtained from the Numerical Solution for Pure Water and $\text{Al}_2\text{O}_3$ /Water Nanofluid with Different Particle Volume Fractions.....	119



## LIST OF FIGURES

### FIGURES

Figure 1	Schematic Illustration Representing the Clustering Phenomenon.....	27
Figure 2	Schematic Illustration Representing the Liquid Layering Around Nanoparticles.....	29
Figure 3	Comparison of the Experimental Results of the Thermal Conductivity Ratio for Al <sub>2</sub> O <sub>3</sub> /Water Nanofluid with Theoretical Models as a Function of Particle Volume Fraction at a Particle Size around 40 nm.....	48
Figure 4	Comparison of the Experimental Results of the Thermal Conductivity Ratio for Al <sub>2</sub> O <sub>3</sub> /Water Nanofluid with Theoretical Models as a Function of Particle Volume Fraction at a Particle Size around 40 nm.....	49
Figure 5	Comparison of the Experimental Results of the Thermal Conductivity Ratio for Al <sub>2</sub> O <sub>3</sub> /Water Nanofluid with Hamilton and Crosser Model as a Function of the Particle Size at Various Values of the Particle Volume Fraction.....	51
Figure 6	Comparison of the Experimental Results of the Thermal Conductivity Ratio for Al <sub>2</sub> O <sub>3</sub> /Water Nanofluid with Xue and Xu Model as a Function of the Particle Size at Various Values of the Particle Volume Fraction.....	52
Figure 7	Comparison of the Experimental Results of the Thermal Conductivity Ratio for 1 vol.% Al <sub>2</sub> O <sub>3</sub> /Water Nanofluid with Theoretical Models as a Function of Particle Size.....	53
Figure 8	Comparison of the Experimental Results of the Thermal Conductivity Ratio for 3 vol.% Al <sub>2</sub> O <sub>3</sub> /Water Nanofluid with Theoretical Models as a Function of Particle Size.....	54

Figure 9	Comparison of the Experimental Results of the Thermal Conductivity Ratio for Al <sub>2</sub> O <sub>3</sub> /Water Nanofluid with Koo and Kleinstreuer Model as a Function of Temperature at Various Values of Particle Volume Fraction.....	56
Figure 10	Comparison of the Experimental Results of the Thermal Conductivity Ratio for Al <sub>2</sub> O <sub>3</sub> /Water Nanofluid with Jang and Choi Model as a Function of Temperature at Various Values of Particle Volume Fraction.....	57
Figure 11	Comparison of the Experimental Results of the Thermal Conductivity Ratio for Al <sub>2</sub> O <sub>3</sub> /Water Nanofluid with Sitprasert et al. Model as a Function of Temperature at Various Values of Particle Volume Fraction.....	58
Figure 12	Variation of Average Heat Transfer Coefficient Enhancement Ratio with Reynolds Number for Different Particle Volume Fractions of the Cu/Water Nanofluid.....	79
Figure 13	Variation of Average Heat Transfer Coefficient Enhancement Ratio with Peclet Number for Different Particle Volume Fractions of the Al <sub>2</sub> O <sub>3</sub> /Water Nanofluid.....	81
Figure 14	Schematic View of the Problem Considered in the Numerical Analysis.....	87
Figure 15	Schematic View of the Problem Considered in the Numerical Analysis.....	88
Figure 16	Variation of Local Nusselt Number in Axial Direction for the Solutions with Different Number of Nodes.....	100
Figure 17	Variation of Local Nusselt Number in Axial Direction for the Solutions with Different Number of Nodes.....	101
Figure 18	Variation of Local Nusselt Number in Axial Direction According to the Numerical Results and Graetz Solution.....	103
Figure 19	Variation of Local Nusselt Number in Axial Direction According to the Numerical Results and Graetz Solution.....	104

Figure 20	Variation of Average Heat Transfer Coefficient Enhancement Ratio with Peclet Number for Different Particle Volume Fractions of the Al <sub>2</sub> O <sub>3</sub> /Water Nanofluid.....	107
Figure 21	Variation of Average Heat Transfer Coefficient Enhancement Ratio with Peclet Number for Different Particle Volume Fractions of the Al <sub>2</sub> O <sub>3</sub> /Water Nanofluid.....	108
Figure 22	Variation of Local Nusselt Number with Dimensionless Axial Position for Pure Water and Al <sub>2</sub> O <sub>3</sub> /Water Nanofluid.....	110
Figure 23	Variation of Average Heat Transfer Coefficient Enhancement Ratio with Peclet Number for Different Particle Sizes of the 1 vol.% Al <sub>2</sub> O <sub>3</sub> /Water Nanofluid.....	112
Figure 24	Variation of Average Heat Transfer Coefficient Enhancement Ratio with Peclet Number for Heating and Cooling of the 2 vol.% Al <sub>2</sub> O <sub>3</sub> /Water Nanofluid.....	113
Figure 25	Variation of Local Heat Transfer Coefficient with Dimensionless Axial Position for Pure Water and 3 vol.% Al <sub>2</sub> O <sub>3</sub> /Water Nanofluid.....	115
Figure 26	Variation of Local Heat Transfer Coefficient with Reynolds Number for Pure Water and 3 vol.% Al <sub>2</sub> O <sub>3</sub> /Water Nanofluid.....	116
Figure 27	Variation of Local Nusselt Number with Dimensionless Axial Position for Pure Water and Al <sub>2</sub> O <sub>3</sub> /Water Nanofluid.....	118
Figure 28	Variation of Local Heat Transfer Coefficient with Dimensionless Axial Position for Different Particle Sizes of 4 vol.% Al <sub>2</sub> O <sub>3</sub> /Water Nanofluid.....	120
Figure 29	Variation of Local Heat Transfer Coefficient with Dimensionless Axial Position for Heating and Cooling of the 4 vol.% Al <sub>2</sub> O <sub>3</sub> /Water Nanofluid and Pure Water.....	121
Figure 30	Flowchart of the Numerical Solution Discussed in Chapters 4 and 5.....	147

## NOMENCLATURE

$Br$	Brinkman number
$c_p$	specific heat capacity, J/kgK
$d$	tube diameter, m
$d_p$	nanoparticle diameter, m
$Gz$	Graetz number, $ud^2 / \alpha L$
$h$	average heat transfer coefficient, W/m <sup>2</sup> K
$h_{fd}$	fully developed heat transfer coefficient, W/m <sup>2</sup> K
$h_x$	local heat transfer coefficient, W/m <sup>2</sup> K
$k$	thermal conductivity, W/mK
$L$	tube length, m
$n$	empirical shape factor
$Nu$	average Nusselt number, $hd / k$
$Nu_{fd}$	fully developed Nusselt number, $h_{fd}d / k$
$Nu_x$	local Nusselt number, $h_x d / k$
$p$	pressure, Pa
$Pe$	Peclet number, $ud / \alpha$
$Pr$	Prandtl number, $\nu / \alpha$
$q''$	heat flux, W/m <sup>2</sup>
$r$	radius, m
$r_0$	tube radius, m
$Re$	Reynolds number, $ud / \nu$
$t$	nanolayer thickness, m
$T$	temperature, K
$u_m$	mean flow velocity, m/s
$u_r$	radial flow velocity, m/s
$u_x$	axial flow velocity, m/s
$u_\theta$	tangential flow velocity, m/s

## Greek letters

$\alpha$	thermal diffusivity, m <sup>2</sup> /s
$\theta$	dimensionless temperature
$\kappa_B$	Boltzmann constant, $1.3807 \times 10^{-23}$ J/K
$\mu$	dynamic viscosity, Pa·s
$\nu$	kinematic viscosity, m <sup>2</sup> /s
$\rho$	density, kg/m <sup>3</sup>
$\phi$	particle volume fraction
$\psi$	sphericity

## Subscripts

$b$	bulk mean
$cl$	cluster
$d$	dispersed
$eff$	effective
$f$	base fluid
$fd$	fully developed
$i$	inlet
$l$	liquid nanolayer
$nf$	nanofluid
$o$	outlet
$p$	nanoparticle
$w$	wall
$x$	local

## **CHAPTER 1**

### **INTRODUCTION**

#### **1.1. Improving Heat Transfer Efficiency**

Heat transfer plays an important role in numerous applications. For example, in vehicles, heat generated by the prime mover needs to be removed for proper operation. Similarly, electronic equipments dissipate heat, which requires a cooling system. Heating, ventilating, and air conditioning systems also include various heat transfer processes. Heat transfer is the key process in thermal power stations. In addition to these, many production processes include heat transfer in various forms; it might be the cooling of a machine tool, pasteurization of food, or the temperature adjustment for triggering a chemical process. In most of these applications, heat transfer is realized through some heat transfer devices; such as, heat exchangers, evaporators, condensers, and heat sinks. Increasing the heat transfer efficiency of these devices is desirable, because by increasing efficiency, the space occupied by the device can be minimized, which is important for applications with compactness requirements. Furthermore, in most of the heat transfer systems, the working fluid is circulated by a pump, and improvements in heat transfer efficiency can minimize the associated power consumption.

There are several methods to improve the heat transfer efficiency. Some methods are utilization of extended surfaces, application of vibration to the heat transfer surfaces, and usage of microchannels. Heat transfer efficiency can also be improved by increasing the thermal conductivity of the working fluid. Commonly used heat transfer fluids such as water, ethylene glycol, and engine oil have relatively low thermal conductivities, when compared to the thermal conductivity of solids. High thermal conductivity of solids can be used to increase the thermal conductivity of a fluid by adding small solid particles to that fluid. The feasibility of the usage of such suspensions of solid particles with sizes on the order of

millimeters or micrometers was previously investigated by several researchers and significant drawbacks were observed. These drawbacks are sedimentation of particles, clogging of channels and erosion in channel walls, which prevented the practical application of suspensions of solid particles in base fluids as advanced working fluids in heat transfer applications [1,2].

## **1.2. Nanofluids**

### **1.2.1. Introduction**

With the recent improvements in nanotechnology, the production of particles with sizes on the order of nanometers (nanoparticles) can be achieved with relative ease. As a consequence, the idea of suspending these nanoparticles in a base liquid for improving thermal conductivity has been proposed recently [3,4]. Such suspension of nanoparticles in a base fluid is called a nanofluid. Due to their small size, nanoparticles fluidize easily inside the base fluid, and as a consequence, clogging of channels and erosion in channel walls are no longer a problem. It is even possible to use nanofluids in microchannels [5,6]. When it comes to the stability of the suspension, it was shown that sedimentation of particles can be prevented by utilizing proper dispersants.

### **1.2.2. Particle Material and Base Fluid**

Many different particle materials are used for nanofluid preparation.  $\text{Al}_2\text{O}_3$ ,  $\text{CuO}$ ,  $\text{TiO}_2$ ,  $\text{SiC}$ ,  $\text{TiC}$ ,  $\text{Ag}$ ,  $\text{Au}$ ,  $\text{Cu}$ , and  $\text{Fe}$  nanoparticles are frequently used in nanofluid research. Carbon nanotubes are also utilized due to their extremely high thermal conductivity in the longitudinal (axial) direction.

Base fluids mostly used in the preparation of nanofluids are the common working fluids of heat transfer applications; such as, water, ethylene glycol and engine oil. In order to improve the stability of nanoparticles inside the base fluid, some additives are added to the mixture in small amounts.

### **1.2.3. Particle Size**

Nanoparticles used in nanofluid preparation usually have diameters below 100 nm. Particles as small as 10 nm have been used in nanofluid research [7]. When particles are not spherical but rod or tube-shaped, the diameter is still below 100 nm, but the length of the particles may be on the order of micrometers. It should also be noted that due to the clustering phenomenon, particles may form clusters with sizes on the order of micrometers.

### **1.2.4. Particle Shape**

Spherical particles are mostly used in nanofluids. However, rod-shaped, tube-shaped and disk-shaped nanoparticles are also used. On the other hand, the clusters formed by nanoparticles may have fractal-like shapes.

### **1.2.5. Production Methods**

#### **1.2.5.1. Production of Nanoparticles**

Production of nanoparticles can be divided into two main categories, namely, physical synthesis and chemical synthesis. Yu et al. [8] listed the common production techniques of nanofluids as follows.

Physical Synthesis: Mechanical grinding, inert-gas-condensation technique.

Chemical Synthesis: Chemical precipitation, chemical vapor deposition, micro-emulsions, spray pyrolysis, thermal spraying.

#### **1.2.5.2. Production of Nanofluids**

There are mainly two methods of nanofluid production, namely, two-step technique and one-step technique. In the two-step technique, the first step is the production of nanoparticles and the second step is the dispersion of the nanoparticles in a base fluid. Two-step technique is advantageous when mass



production of nanofluids is considered, because at present, nanoparticles can be produced in large quantities by utilizing the technique of inert gas condensation [9]. The main disadvantage of the two-step technique is that the nanoparticles form clusters during the preparation of the nanofluid which prevents the proper dispersion of nanoparticles inside the base fluid [8].

One-step technique combines the production of nanoparticles and dispersion of nanoparticles in the base fluid into a single step. There are some variations of this technique. In one of the common methods, named direct evaporation one-step method, the nanofluid is produced by the solidification of the nanoparticles, which are initially gas phase, inside the base fluid [7]. The dispersion characteristics of nanofluids produced with one-step techniques are better than those produced with two-step technique [8]. The main drawback of one-step techniques is that they are not proper for mass production, which limits their commercialization [8].

### **1.3. Thermal Conductivity of Nanofluids**

Studies regarding the thermal conductivity of nanofluids showed that high enhancements of thermal conductivity can be achieved by using nanofluids. It is possible to obtain thermal conductivity enhancements larger than 20% at a particle volume fraction smaller than 5% [10-12]. Such enhancement values exceed the predictions of theoretical models developed for suspensions with larger particles. This is considered as an indication of the presence of additional thermal transport enhancement mechanisms of nanofluids.

There are many experimental and theoretical studies in the literature regarding the thermal conductivity of nanofluids. In Chapter 2, a detailed review of these studies is presented and experimental data in the literature are compared with the theoretical models of nanofluid thermal conductivity.

#### **1.4. Heat Transfer Enhancement with Nanofluids**

Increase in the thermal conductivity of the working fluid improves the efficiency of the associated heat transfer process. When forced convection in tubes is considered, it is expected that heat transfer coefficient enhancement obtained by using a nanofluid is equal to the enhancement in thermal conductivity of the nanofluid, due to the definition of Nusselt number. However, research about the convective heat transfer of nanofluids indicated that the enhancement of heat transfer coefficient exceeds the thermal conductivity enhancement of nanofluids [13-16]. In order to explain this extra enhancement, several models were proposed by researchers.

Chapter 3 first provides some review of experimental, theoretical and numerical research about the convective heat transfer of nanofluids. Then, a theoretical analysis regarding the prediction of heat transfer performance of nanofluids by utilizing classical correlations of convective heat transfer is performed. In Chapter 4, a numerical approach for the analysis of convective heat transfer of nanofluids based on a thermal dispersion model proposed by Xuan and Roetzel [17] is described and the accuracy of the numerical method is verified. In Chapter 5, associated numerical results are discussed in order to gain insight into the underlying mechanisms of convective heat transfer enhancement with nanofluids. Finally, in Chapter 6, the thesis study is summarized, important conclusions are indicated, and some suggestions for future work are provided.

In Appendix A, sample calculations are provided for the determination of fully developed and average heat transfer coefficient of nanofluid flow inside straight circular tubes.

In Appendix B, a general flowchart of the numerical analysis performed for the determination of nanofluid heat transfer is provided.

## CHAPTER 2

### THERMAL CONDUCTIVITY OF NANOFLUIDS

The study presented in this chapter is previously published as a review paper in *Microfluidics and Nanofluidics* [18].

#### 2.1. Introduction

In the last decade, a significant amount of experimental and theoretical research was made to investigate the thermophysical behavior of nanofluids. In these studies, it was observed that a high thermal conductivity enhancement could be obtained with nanofluids, even in the case of very small particle volume fractions. Furthermore, most of the experimental work showed that the thermal conductivity enhancement obtained by using nanoparticle suspensions was much higher than that obtained by using conventional suspensions with particles that are millimeter- or micrometer-sized. Many researchers proposed theoretical models to explain and predict those anomalous thermal conductivity ratios, defined as thermal conductivity of the nanofluid ( $k_{nf}$ ) divided by the thermal conductivity of the base fluid ( $k_f$ ) [18].

In this chapter, experimental studies on thermal conductivity enhancement with nanofluids are reviewed. Theoretical attempts made to explain the associated thermal conductivity enhancement mechanisms are also outlined. In addition to these, theoretical models proposed for the determination of thermal conductivity of nanofluids are summarized, predictions of the models are compared with experimental findings, and significant discrepancies are indicated.

There are many reviews available in the literature about nanofluid research [8,19-23]. In all of the nanofluid thermal conductivity reviews, both theoretical models and experimental results are discussed. However, most of the time, a detailed comparison between theoretical models and experimental results is not

provided. In this chapter, a systematic comparison between recent theoretical models especially developed for nanofluids and experimental results is provided. It is thought that such an analysis provides important information about the validity of the proposed models and the associated thermal conductivity enhancement mechanisms.

## **2.2. Literature Survey**

### **2.2.1. Experimental Studies**

#### **2.2.1.1. Thermal Conductivity Measurement Methods**

In thermal conductivity measurements of nanofluids, the transient hot-wire technique is the most commonly used method [24-27]. A modified transient hot-wire method is required in the measurements, since nanofluids conduct electricity. The modification is made by insulating the wire. Some other methods such as steady-state parallel-plate technique, temperature oscillation technique, microhot strip method, and optical beam deflection technique have also been utilized by some researchers [28-31].

#### **2.2.1.2. Effects of Some Parameters on Thermal Conductivity of Nanofluids**

Experimental studies show that thermal conductivity of nanofluids depends on many factors such as particle volume fraction, particle material, particle size, particle shape, base fluid material, and temperature. Amount and types of additives and the acidity of the nanofluid were also shown to be effective in the thermal conductivity enhancement [18].

In the following sections, experimental studies about the thermal conductivity of nanofluids are summarized. In each section, a specific parameter that is effective on thermal conductivity is discussed.

### 2.2.1.2.1. Particle Volume Fraction

There are many studies in the literature about the effect of particle volume fraction, which is the volumetric concentration of the nanoparticles in the nanofluid, on the thermal conductivity of nanofluids. Masuda et al. [3] measured the thermal conductivity of nanofluids containing Al<sub>2</sub>O<sub>3</sub> (13 nm), SiO<sub>2</sub> (12 nm), and TiO<sub>2</sub> (27 nm) nanoparticles (values in parentheses indicate the average particle diameter). This is the first experimental study regarding the thermal conductivity of nanofluids. Water was used as the base fluid and a two-step method was utilized for the preparation of nanofluids. An enhancement as high as 32.4% was observed for the effective thermal conductivity of 4.3 vol.% Al<sub>2</sub>O<sub>3</sub>/water nanofluid at 31.85°C (all percentage enhancement values are indicated according to the expression  $100(k_{nf} - k_f)/k_f$  throughout the discussion). It was found that thermal conductivity enhancement increases linearly with particle volume fraction. Lee et al. [32] studied the room temperature thermal conductivity of nanofluids by dispersing Al<sub>2</sub>O<sub>3</sub> (38.5 nm) and CuO (23.6 nm) nanoparticles, which were produced by gas condensation method, in water and ethylene glycol. Similar to the study of Masuda et al. [3], a linear relationship was observed between thermal conductivity and particle volume fraction (thermal conductivity increases with particle volume fraction). Highest enhancement was 20%, which was observed for 4 vol.% CuO/ethylene glycol nanofluid. A similar study was performed by Wang et al. [28], who examined the thermal conductivity performance of nanofluids with Al<sub>2</sub>O<sub>3</sub> (28 nm) and CuO (23 nm) nanoparticles. For the case of 8 vol.% Al<sub>2</sub>O<sub>3</sub>/water nanofluid, thermal conductivity enhancement as high as 40% was achieved. For water- and ethylene glycol-based nanofluids, thermal conductivity ratio showed a linear relationship with particle volume fraction and the lines representing this relation were found to be coincident.

Particle volume fraction is a parameter that is investigated in almost all of the experimental studies and the results are usually in agreement qualitatively. Most of the researchers report increasing thermal conductivity with increasing particle volume fraction and the relation found is usually linear [18]. However,

there are also some studies which indicate nonlinear behavior. An example is the study made by Murshed et al. [33]. They measured the thermal conductivity of TiO<sub>2</sub>/deionized water nanofluid at room temperature by using transient hot-wire method. Volume fraction of nanoparticles was varied between 0.5 and 5%. A nonlinear relationship was observed between thermal conductivity ratio and particle volume fraction, especially at low volume fractions. The authors noted that the nonlinear behavior might be due to the cetyltrimethyl ammonium bromide (CTAB) surfactant, application of sonication for a long time, or hydrophobic surface forces involved. Choi et al. [34] investigated the thermal conductivity of nanofluids prepared by dispersing multiwalled carbon nanotubes (MWCNT) in oil. They also found a nonlinear relation between thermal conductivity ratio and particle volume fraction. According to the authors, such a nonlinear relation is an indication of interactions between particles. It was concluded that despite the fact that particle volume fraction is very small, nanotubes interact with each other due to the very high particle concentration ( $10^{11}$  particles/cm<sup>3</sup>).

#### **2.2.1.2.2. Particle Material**

Most of the studies show that particle material is an important parameter that affects the thermal conductivity of nanofluids. At first glance, it might be thought that the difference in the thermal conductivities of particle materials is the main reason of this effect. However, studies show that particle type may affect the thermal conductivity of nanofluids in other ways. For example, Lee et al. [32] considered the thermal conductivity of nanofluids with Al<sub>2</sub>O<sub>3</sub> and CuO nanoparticles as mentioned in the previous section and they found that nanofluids with CuO nanoparticles showed better enhancement when compared to the nanofluids prepared using Al<sub>2</sub>O<sub>3</sub> nanoparticles. It should be noted that Al<sub>2</sub>O<sub>3</sub>, as a material, has higher thermal conductivity than CuO. Therefore, thermal conductivity of particle material may not be the dominant parameter that determines the thermal conductivity of the nanofluid. According to the authors, the key factor is the fact that Al<sub>2</sub>O<sub>3</sub> nanoparticles formed relatively larger clusters

when compared to CuO nanoparticles. That might be an explanation if the main mechanism of thermal conductivity enhancement is accepted to be the Brownian motion of nanoparticles, since the effect of Brownian motion diminishes with increasing particle size. However, it should also be noted that there are some studies that consider the clustering of nanoparticles as a thermal conductivity enhancement mechanism. Another study that considers the effect of nanoparticle type was made by Chopkar et al. [35]. They dispersed  $\text{Al}_2\text{Cu}$  and  $\text{Ag}_2\text{Al}$  nanoparticles into water and ethylene glycol. 1 vol.% oleic acid was added as the surfactant. Measurements were made at room temperature. It was found that  $\text{Ag}_2\text{Al}$  nanoparticles enhanced thermal conductivity slightly more when compared to  $\text{Al}_2\text{Cu}$  nanoparticles. According to the authors, this is due to the fact that the thermal conductivity of  $\text{Ag}_2\text{Al}$  is higher when compared to  $\text{Al}_2\text{Cu}$ .

Effect of particle material is much more pronounced when carbon nanotubes are used for the preparation of nanofluids. Choi et al. [34] studied the thermal conductivity enhancement of oil based nanofluids containing MWCNT with a mean diameter of around 25 nm and length around 50  $\mu\text{m}$ . The base fluid used was synthetic poly ( $\alpha$ -olefin) oil. Measurements were conducted at room temperature. 160% enhancement (a thermal conductivity ratio of 2.6) was observed for 1 vol.% MWCNT/oil nanofluid. The authors noted that such an anomalous enhancement might be due to the liquid nanolayers forming around the nanotubes. On the other hand, the fact that heat is transported ballistically inside the nanotubes improves the conduction of heat in the tubes, but the effect of this factor is not dominant according to the authors. It should also be noted that the shape of nanotubes might also be effective in the anomalous enhancement values. The length of the nanotubes is on the order of micrometers, and this enables rapid heat conduction across relatively large distances, which is not possible for spherical nanoparticles as long as there is no clustering. Another study about nanofluids with carbon nanotubes was made by Assael et al. [36]. They compared the nanofluids containing double-walled CNT (DWCNT) and MWCNT. For DWCNT, average outer diameter was 5 nm and average inner diameter was larger than 2.5 nm. It was noted that MWCNT also exist in the samples with DWCNT.

For MWCNT, length was larger than 10  $\mu\text{m}$  and average outer diameter was 130 nm. Thickness of the walls was determined to be around 90 graphitic layers (about 30 nm) with interlayer distance around 0.34 nm. CTAB and Nanospense AQ were added to the nanofluids and ultrasonic vibration was applied in order to obtain proper dispersion. Transient hot-wire method was used in the measurements. A thermal conductivity enhancement as high as 34% was achieved for the 0.6 vol.% MWCNT/water nanofluid, whereas the 0.75 vol.% DWCNT/water nanofluid showed only 3% enhancement. The authors noted that the reason of such low enhancement was that the size of the DWCNT reached the order of micrometers due to clustering effects.

It should also be noted that the mean-free path of phonons in nanoparticles may be smaller than the size of the nanoparticles. In such a condition, heat transfer mechanism inside the particles is not diffusion but heat is transported ballistically. When this fact is considered, relating the superior enhancement characteristics of a specific nanoparticle material to its high bulk thermal conductivity is not reasonable [18].

### **2.2.1.2.3. Base Fluid**

According to the conventional thermal conductivity models such as the Maxwell model [37], as the base fluid thermal conductivity of a mixture decreases, the thermal conductivity ratio (thermal conductivity of nanofluid ( $k_{nf}$ ) divided by the thermal conductivity of base fluid ( $k_f$ )) increases. When it comes to nanofluids, the situation is more complicated due to the fact that the viscosity of the base fluid affects the Brownian motion of nanoparticles and that in turn affects the thermal conductivity of the nanofluid [38]. Moreover, Lee [39] examined the effect of electric double layer forming around nanoparticles on the thermal conductivity of nanofluids and showed that the thermal conductivity and thickness of the layer depends on the base fluid. It is difficult to determine the quantitative effects of these factors completely. Therefore, systematic experiments are required that will



show the effect of base fluid on the thermal conductivity of nanofluids. Some experimental studies made in this area are summarized below.

In the previously mentioned study of Wang et al. [28],  $\text{Al}_2\text{O}_3$  and CuO nanoparticles were used to prepare nanofluids with several base fluids; water, ethylene glycol, vacuum pump fluid, and engine oil. With  $\text{Al}_2\text{O}_3$  nanoparticles, the highest thermal conductivity ratio was observed when ethylene glycol was used as the base fluid. Engine oil showed somewhat lower thermal conductivity ratios than ethylene glycol. Water and pump fluid showed even smaller ratios, respectively. With CuO nanoparticles, only ethylene glycol- and water-based nanofluids were prepared and it is interesting to note that they showed exactly the same thermal conductivity ratios for the same particle volume fraction. The effect of the base fluid on the thermal conductivity of nanofluids was also analyzed by Xie et al. [40]. Nanofluids with  $\text{Al}_2\text{O}_3$  nanoparticles were prepared by using different base fluids; deionized water, glycerol, ethylene glycol, and pump oil. In addition, ethylene glycol-water and glycerol-water mixtures with different volume fractions were also used as base fluids and the variation of the thermal conductivity ratio with thermal conductivity of the base fluid mixture was examined. It was seen that, thermal conductivity ratio decreased with increasing thermal conductivity of the base fluid. Results were compared with a theoretical analysis made by Hasselman and Johnson [41]. Theoretical results were found to be nearly independent of the thermal conductivity of the base fluid, being contrary to the experimental data. However, it should be noted that these experimental results are in agreement with the Maxwell model [37] qualitatively. Chopkar et al. [35] also analyzed the effect of base fluid by comparing water and ethylene glycol.  $\text{Al}_2\text{Cu}$  and  $\text{Ag}_2\text{Al}$  nanoparticles were used in the study and it was found that water-based nanofluids showed a higher thermal conductivity ratio. It should be noted that more than 100% enhancement was obtained for the 2.0 vol.%  $\text{Ag}_2\text{Al}(30\text{ nm})/\text{water}$  nanofluid.

Base fluid effect was also investigated with MWCNT nanofluids. Ethylene glycol and synthetic engine oil were used as base fluids in the experiments conducted by Liu et al. [42]. Thermal conductivity of nanofluids were measured

by a transient hot-wire method. 1 vol.% MWCNT/ethylene glycol nanofluid showed 12.4% thermal conductivity enhancement, whereas for 2 vol.% MWCNT/synthetic engine oil nanofluid, enhancement was 30%. It was observed that higher enhancements were achieved with synthetic engine oil as the base fluid, in general.

#### **2.2.1.2.4. Particle Size**

Particle size is another important parameter of thermal conductivity of nanofluids. It is possible to produce nanoparticles of various sizes, generally ranging between 5 and 100 nm. Eastman et al. [43] studied Cu nanoparticles, with ethylene glycol as the base fluid. By using a one-step production method, suspensions with Cu nanoparticles smaller than 10 nm were obtained. Thioglycolic acid less than 1 vol.% was added to some of the samples for stabilizing purposes and those samples showed much better enhancement when compared to samples without thioglycolic acid. A 40% increase in thermal conductivity was observed at a particle volume fraction of 0.3% (with thioglycolic acid). To make a comparison, it should be noted that in the study of Lee et al. [32], the researchers obtained 20% enhancement with 4 vol.% CuO(23.6 nm)/ethylene glycol nanofluid. As a result of the anomalous enhancements obtained, Eastman et al. [43] concluded that the size of the nanoparticles is an important factor that affects the thermal conductivity enhancement, which is contrary to the predictions of conventional models such as Hamilton and Crosser model [44], which does not take the effect of particle size on thermal conductivity into account. Chopkar et al. [45] prepared nanofluids by dispersing  $Al_{70}Cu_{30}$  nanoparticles into ethylene glycol. Nanoparticles were obtained by mechanical alloying. By transmission electron microscopy, they illustrated the fact that there is no significant clustering in the samples. They varied the particle size between 9 and 83 nm and they showed that thermal conductivity enhancement decreases with increasing particle size. For 0.5 vol.% nanofluid, thermal conductivity enhancement decreased from 38 to 3% by increasing the particle size from 9 to 83 nm. In another study, Chopkar et al. [35]

investigated the effect of particle size on the thermal conductivity of water- and ethylene glycol-based nanofluids with  $\text{Al}_2\text{Cu}$  and  $\text{Ag}_2\text{Al}$  nanoparticles. Nanoparticles with sizes varying between 30 and 120 nm were used in the study. For all four types of nanofluids, it was observed that thermal conductivity enhancement increases with decreasing particle size.

Another systematic particle size dependence study for the thermal conductivity of nanofluids was made by Beck et al. [27] for  $\text{Al}_2\text{O}_3$ /water and  $\text{Al}_2\text{O}_3$ /ethylene glycol nanofluids. Particle size was varied between 8 and 282 nm. HCl was added to the nanofluids to adjust the pH value to 4. Conductivity measurements were carried out by a transient hot-wire method at room temperature. It was observed that for the same particle volume fraction, thermal conductivity ratio decreases with decreasing particle size. This effect is more pronounced for nanofluids with particles smaller than 50 nm. As a result of the experimental findings, it was concluded that nanoparticle thermal conductivity decrease with decreasing particle size is responsible for the observed size dependence of the thermal conductivity of nanofluids. It should be noted that these results are not in agreement with the aforementioned studies. The results also contradict with the effect of Brownian motion, since the effect of Brownian motion decreases with increasing particle size, which decreases the associated thermal conductivity enhancement.

Mintsa et al. [46] measured the thermal conductivity of  $\text{Al}_2\text{O}_3$ /water nanofluids. Two different sizes of  $\text{Al}_2\text{O}_3$  nanoparticles were used in the experiment (36 and 47 nm). Particle volume fraction was varied between 0 and 18% and temperature was varied between 20 and 50°C. It was observed that the thermal conductivity enhancements were nearly the same for the two different particle sizes of  $\text{Al}_2\text{O}_3$  nanoparticles at room temperature. However, at higher temperatures,  $\text{Al}_2\text{O}_3$ /water nanofluid with smaller particles showed higher enhancement. The experimental results were compared with theoretical models and it was concluded that the model proposed by Chon et al. [10] predicted their experimental data well. On the contrary, when the temperature dependent thermal conductivity data of  $\text{Al}_2\text{O}_3$ /water nanofluid provided by Murshed et al. [47], Das

et al. [11], and Chon and Kihm [48] is compared, it is seen that the thermal conductivity ratio is not much different from each other for significantly different particle sizes (80, 38.4, and 47 nm, respectively).

The general trend in the experimental data is that the thermal conductivity of nanofluids increases with decreasing particle size. This trend is theoretically supported by two mechanisms of thermal conductivity enhancement; Brownian motion of nanoparticles and liquid layering around nanoparticles [18]. However, there is also a significant amount of contradictory data in the literature that indicate decreasing thermal conductivity with decreasing particle size. In fact, for the case of nanofluids with  $\text{Al}_2\text{O}_3$  nanoparticles, such results are more common than the results showing increasing thermal conductivity with decreasing particle size [18]. The associated data for  $\text{Al}_2\text{O}_3$ /water nanofluids is illustrated in Section 2.3.2. It is thought that the data indicating decreasing thermal conductivity with decreasing particle size may be the result of severe clustering of nanoparticles in the associated samples. Although clustering at a certain level may improve thermal conductivity enhancement, excessive clustering creates an opposite effect due to associated sedimentation [49]. At this point, it is important to note that Feng et al. [50] showed that clustering effects are more pronounced in nanofluid samples with smaller particles. This may explain the results in which nanofluids with smaller particles show lower enhancement.

#### **2.2.1.2.5. Particle Shape**

There are mainly two particle shapes used in nanofluid research; spherical particles and cylindrical particles. Cylindrical particles usually have a large length-to-diameter ratio. The thermal conductivity of SiC/distilled water and SiC/ethylene glycol nanofluids were investigated by Xie et al. [51]. Two types of nanoparticles were used for the preparation of nanofluids; spherical particles with 26 nm average diameter and cylindrical particles with 600 nm average diameter. It was found that 4.2 vol.% water-based nanofluid with spherical particles had a thermal conductivity enhancement of 15.8%, whereas 4 vol.% nanofluid with

cylindrical particles had a thermal conductivity enhancement of 22.9%. The authors compared the results with the Hamilton and Crosser model [44]. It was noted that Hamilton and Crosser model was successful in predicting the enhancement in cylindrical particles, whereas it underestimated the values associated with nanofluids with spherical particles. Another study related to the particle shape was made by Murshed et al. [33]. They measured the thermal conductivity of TiO<sub>2</sub>/deionized water nanofluid. Two types of nanoparticles were used, spherical particles (15 nm) and rod-shaped particles (10 nm in diameter and 40 nm in length). Stability and dispersion of nanoparticles were improved by using oleic acid and CTAB surfactants. For nanofluids with spherical particles, a maximum enhancement of 29.7% was obtained at 5 vol.%. At the same volume fraction, rod-shaped nanoparticles showed an enhancement of 32.8%.

In addition to these experimental results, the fact that nanofluids with carbon nanotubes (which are cylindrical in shape) generally show greater thermal conductivity enhancement than nanofluids with spherical particles should also be considered. As a result, one can conclude that cylindrical nanoparticles provide higher thermal conductivity enhancement than spherical particles. One of the possible reasons of this is the rapid heat transport along relatively larger distances in cylindrical particles since cylindrical particles usually have lengths on the order of micrometers [18]. However, it should be noted that nanofluids with cylindrical particles usually have much larger viscosities than those with spherical nanoparticles [52]. As a result, the associated increase in pumping power is large and this reduces the feasibility of usage of nanofluids with cylindrical particles.

#### **2.2.1.2.6. Temperature**

In conventional suspensions of solid particles (with sizes on the order of millimeters or micrometers) in liquids, thermal conductivity of the mixture depends on temperature only due to the dependence of thermal conductivity of base liquid and solid particles on temperature [18]. However, in case of nanofluids, change of temperature affects the Brownian motion of nanoparticles

and clustering of nanoparticles [53], which results in dramatic changes of thermal conductivity of nanofluids with temperature. Masuda et al. [3] measured the thermal conductivity of water-based nanofluids containing  $\text{Al}_2\text{O}_3$ ,  $\text{SiO}_2$ , and  $\text{TiO}_2$  nanoparticles at different temperatures. Thermal conductivity ratio decreased with increasing temperature, which is contradictory to many findings in the literature. The temperature dependence of the thermal conductivity of  $\text{Al}_2\text{O}_3$ (38.4 nm)/water and  $\text{CuO}$ (28.6 nm)/water nanofluids was studied by Das et al. [11]. Thermal diffusivity was measured by using a temperature oscillation technique and then thermal conductivity was calculated. Several measurements were made at different temperatures varying between 21 and 51°C. It was seen that for 1 vol.%  $\text{Al}_2\text{O}_3$ /water nanofluid, thermal conductivity enhancement increased from 2% at 21°C to 10.8% at 51°C. Temperature dependence of 4 vol.%  $\text{Al}_2\text{O}_3$  nanofluid was much more significant. From 21 to 51°C, enhancement increased from 9.4 to 24.3%. A linear relationship between thermal conductivity ratio and temperature was observed at both 1 and 4 vol.% cases.

Li and Peterson [12] also investigated the effect of temperature on thermal conductivity of  $\text{CuO}$ (29 nm)/water and  $\text{Al}_2\text{O}_3$ (36 nm)/water nanofluids. For both nanofluid types, it was observed that at a constant particle volume fraction thermal conductivity ratio increased with temperature. In addition, it was noted that for  $\text{Al}_2\text{O}_3$ /water nanofluid, the dependence of thermal conductivity ratio on particle volume fraction became more pronounced with increasing temperature. A regression analysis based on the experimental data showed that particle volume fraction dependence of thermal conductivity is much higher than the temperature dependence. For the  $\text{Al}_2\text{O}_3$ /water nanofluid and  $\text{CuO}$ /water nanofluid, two correlations were proposed for the determination of the thermal conductivity. Another study regarding the temperature dependence of thermal conductivity was made by Turgut et al. [54]. They measured the thermal conductivity of  $\text{TiO}_2$ (21 nm)/deionized water nanofluid. Nanofluids used in the experiment were prepared by a two-step method and ultrasonic vibration was applied to the samples. 3 $\omega$  method was used in the measurements. Measurements were made at different temperatures; 13, 23, 40, and 55°C. Particle volume fraction of the sample

nanofluids were varied between 0.2 and 3 vol.%. It was noted that the results of the analysis can be well predicted by conventional theoretical models such as Hamilton and Crosser model [44]. It was also observed that thermal conductivity ratio does not vary with temperature significantly. This observation is contradictory with the aforementioned studies. The results can be considered as an indication of the importance of the usage of surfactants in nanofluids, because no surfactant was used in this study.

Temperature dependence of thermal conductivity of nanofluids was also investigated for the case of nanofluids with carbon nanotubes. Ding et al. [24] measured the thermal conductivity of MWCNT/water nanofluid. Ultrasonic vibration was applied to samples. First Gum Arabic was added to the samples in order to obtain better dispersion and to adjust the pH value, then the nanofluid was homogenized with a high shear homogenizer. Transient hot-wire method was applied for thermal conductivity measurements. No information was given about the size of MWCNT but from the provided scanning electron microscopy images, a very rough estimation of nanotube diameter could be made as 40 nm. Measurements were made at three different temperatures; 20, 25, and 30°C. Particle weight fraction was varied between 0.1 and 1%. It was found that thermal conductivity ratio increases with both particle volume fraction and temperature. However, at 20 and 25°C, increase of thermal conductivity ratio with particle volume fraction stopped after 0.5 wt%. On the other hand, at 30°C, thermal conductivity ratio continued to increase after 0.5 wt%. A maximum enhancement of 80% was achieved at 30°C for 1 wt% of MWCNT/water nanofluid. At 20°C, the associated enhancement decreased to 10%.

Thermal conductivity research of nanofluids in terms of temperature dependence is not limited to the aforementioned studies. Other research efforts about the dependence of thermal conductivity on temperature for various nanofluids exist [47,55-57].

#### **2.2.1.2.7. Clustering**

Clustering is the formation of larger particles through aggregation of nanoparticles. Clustering effect is always present in nanofluids and it is an effective parameter in thermal conductivity. Hong et al. [58] investigated this effect for Fe(10 nm)/ethylene glycol nanofluids. The thermal conductivity of nanofluids were determined as a function of the duration of the application of the ultrasonic vibration, which was varied between 0 min, that is, no vibration applied, and 70 min. It was seen that thermal conductivity ratio increased with increasing vibration time and the rate of this increase became smaller for longer vibration time. Furthermore, the variation of thermal conductivity of nanofluid with time after the application of vibration was investigated and it was found that thermal conductivity decreased as time progressed. Variation of average size of clusters was also determined as a function of time after the application of vibration and it was noted that cluster size increases with time. As a result of these observations, it was concluded that the size of the clusters formed by the nanoparticles had a major influence on the thermal conductivity. In addition, the variation of thermal conductivity ratio of the Fe/ethylene glycol nanofluid with particle volume fraction was found to be nonlinear. It was stated that this behavior is due to the fact that nanoparticles in the nanofluids with high volume fractions formed clusters at a higher rate. It should be noted that Zhu et al. [59] also examined the effect of nanoparticle clustering, on the thermal conductivity of Fe<sub>3</sub>O<sub>4</sub>/water nanofluid and noted that clustering and nanoparticle alignment were mainly responsible for the anomalous thermal conductivity enhancement. Theoretical aspects of clustering of nanoparticles are discussed in Section 2.2.2.2.2.

#### **2.2.1.2.8. pH Value**

The number of studies regarding the pH value of nanofluids is limited when compared to the studies regarding the other parameters. Xie et al. [60] measured the thermal conductivity of nanofluids, which are prepared by dispersing Al<sub>2</sub>O<sub>3</sub>



nanoparticles into water, ethylene glycol, and pump oil. They reported significant decrease in thermal conductivity ratio with increasing pH values. It was also observed that the rate of change of thermal conductivity with particle volume fraction was dependent on pH value. Thermal conductivity enhancement of 5 vol.%  $\text{Al}_2\text{O}_3$ /water nanofluid was 23% when pH is equal to 2.0 and it became 19% when pH is equal to 11.5. The authors related the dependence of thermal conductivity on pH to the fact that as the difference between the isoelectric point of  $\text{Al}_2\text{O}_3$  nanoparticles and pH value of the solution increases, mobility of nanoparticles increases, which improve the micro-convection effect. Wang et al. [61] also investigated the effect of pH on the thermal conductivity of nanofluids. They considered Cu/water and  $\text{Al}_2\text{O}_3$ /water nanofluids, as the dispersant, sodium dodecylbenzene sulfonate, was added to the samples. They obtained optimum values of pH (approximately 8.0 for  $\text{Al}_2\text{O}_3$ /water and 9.5 for Cu/water nanofluids) for maximum thermal conductivity enhancement. It should also be noted that the thermal conductivity of base fluid does not change significantly with pH. The authors related the observed phenomenon to the fact that at the optimum value of pH, surface charge of nanoparticles increases, which creates repulsive forces between nanoparticles. As a result of this effect, severe clustering of nanoparticles is prevented (excessive clustering may result in sedimentation, which decreases thermal conductivity enhancement). Another study regarding the pH of nanofluids was presented by Murshed et al. [62]. They investigated the thermal conductivity of  $\text{TiO}_2$ /water nanofluid and observed a decrease in the thermal conductivity with increasing pH value. However, this decrease is not significant, only 2% change was observed when pH value was increased from 3.4 to 9.

### **2.2.1.3. Possible Reasons of Discrepancy in Experimental Data**

Yu et al. [8] systematically analyze the effects of most of the parameters discussed in the previous sections by comparing various experimental data and tabulating the significant results. Partially based on the tables provided by Yu et al. [8], aforementioned experimental studies on thermal conductivity of nanofluids are

summarized in Table 1. When Table 1 is observed, it is seen that there exists significant discrepancies in experimental data.

**Table 1.** Summary of experimental studies of thermal conductivity enhancement

	Particle Type	Base Fluid <sup>a</sup>	Particle Volume Fraction (%)	Particle Size (nm)	Maximum Enhancement (%) <sup>b</sup>	Notes
<b>Masuda et al. [3]</b>	Al <sub>2</sub> O <sub>3</sub>	water	1.30–4.30	13	32.4	31.85°C – 86.85°C
	SiO <sub>2</sub>	water	1.10–2.40	12	1.1	
	TiO <sub>2</sub>	water	3.10–4.30	27	10.8	
<b>Lee et al. [32]</b>	Al <sub>2</sub> O <sub>3</sub>	water / EG	1.00–4.30 / 1.00–5.00	38.4	10 / 18	Room temperature
	CuO	water / EG	1.00–3.41 / 1.00–4.00	23.6	12 / 23	
<b>Wang et al. [28]</b>	Al <sub>2</sub> O <sub>3</sub>	water / EG	3.00–5.50 / 5.00–8.00	28	16 / 41	Room temperature
	Al <sub>2</sub> O <sub>3</sub>	EO/PO	2.25–7.40 / 5.00–7.10	28	30 / 20	
	CuO	water / EG	4.50–9.70 / 6.20–14.80	23	34 / 54	
<b>Eastman et al. [7]</b>	Cu	EG	0.01–0.56	< 10	41	Room temperature
<b>Xie et al. [51]</b>	SiC	water / EG	0.78–4.18 / 0.89–3.50	26 sphere	17 / 13	Effect of particle shape and size is examined.
	SiC	water / EG	1.00–4.00	600 cylinder	24 / 23	
<b>Xie et al. [40]</b>	Al <sub>2</sub> O <sub>3</sub>	water / EG	5.00	60.4	23 / 29	Room temperature
	Al <sub>2</sub> O <sub>3</sub>	PO/glycerol	5.00	60.4	38 / 27	
<b>Das et al. [11]</b>	Al <sub>2</sub> O <sub>3</sub>	water	1.00–4.00	38.4	24	21°C - 51°C
	CuO	water	1.00–4.00	28.6	36	
<b>Murshed et al. [33]</b>	TiO <sub>2</sub>	water	0.50–5.00	15 sphere	30	Room temperature
	TiO <sub>2</sub>	water	0.50–5.00	10x40 rod	33	

<sup>a</sup> EG: ethylene glycol, EO: engine oil, PO: pump oil, TO: transformer oil, PAO: polyalphaolefin

<sup>b</sup> The percentage values indicated are according to the expression  $100(k_{nf} - k_f) / k_f$

**Table 1 (continued).** Summary of experimental studies of thermal conductivity enhancement

	Particle Type	Base Fluid <sup>a</sup>	Particle Volume Fraction (%)	Particle Size (nm)	Maximum Enhancement (%) <sup>b</sup>	Notes
<b>Hong et al.</b> [58]	Fe	EG	0.10–0.55	10	18	Effect of clustering was investigated.
<b>Li and Peterson</b> [12]	Al <sub>2</sub> O <sub>3</sub>	water	2.00–10.00	36	29	27.5°C – 34.7°C
	CuO	water	2.00–6.00	29	51	28.9°C – 33.4°C
<b>Chopkar et al.</b> [35]	Al <sub>2</sub> Cu	water/EG	1.00–2.00	31/68/101	96/76/61	Effect of particle size was examined.
	Ag <sub>2</sub> Al	water/EG	1.00–2.00	33/80/120	106/93/75	
<b>Beck et al.</b> [27]	Al <sub>2</sub> O <sub>3</sub>	water	1.86–4.00	8 – 282	20	Effect of particle size was examined.
	Al <sub>2</sub> O <sub>3</sub>	EG	2.00–3.01	12 – 282	19	
<b>Mintsa et al.</b> [46]	Al <sub>2</sub> O <sub>3</sub>	water	0–18	36 / 47	31/31	20°C – 48°C
	CuO	water	0–16	29	24	
<b>Turgut et al.</b> [54]	TiO <sub>2</sub>	water	0.2–3.0	21	7.4	13°C – 55°C
<b>Choi et al.</b> [34]	MWCNT	PAO	0.04–1.02	25x50000	57	Room temperature
<b>Assael et al.</b> [36]	DWCNT	water	0.75–1.00	5 (diameter)	8	Effect of sonication time was examined.
	MWCNT	water	0.60	130x10000	34	
<b>Liu et al.</b> [42]	MWCNT	EG / EO	0.20–1.00 / 1.00–2.00	20~50 (diameter)	12/30	Room temperature
<b>Ding et al.</b> [24]	MWCNT	water	0.05–0.49	40 nm (diameter)	79	20°C – 30°C

<sup>a</sup> EG: ethylene glycol, EO: engine oil, PO: pump oil, TO: transformer oil, PAO: polyalphaolefin

<sup>b</sup> The percentage values indicated are according to the expression  $100(k_{nf} - k_f) / k_f$

An important issue regarding this discrepancy in experimental data is the debate about the measurement techniques. Li et al. [63] compared the transient hot-wire method and steady-state cut-bar method and showed that the results of thermal conductivity measurements conducted at room temperature do not differ

in these two measurement techniques. However, the authors noted that there is significant discrepancy in the data when measurements are conducted at higher temperatures. The authors explained this discrepancy by the fact that natural convection effect in the transient hot-wire method starts to deviate the results in a sense that higher values are measured by the method. At this point, the study of Ju et al. [30] should also be mentioned. They showed that transient hot-wire method can give erroneous results if the measurements are carried out just after the sonication since sonication results in an increase in the temperature of the sample. In their study, the effect of this temperature increase lasted for 50 min. In addition to this, they noted that the measurements made successively (in order to prevent random errors) can also create erroneous results if the interval between heating pulses is around 5 s. Therefore, although Li et al. [63] found nearly the same thermal conductivity values in their measurements, there might still be some erroneous results in the literature due to the abovementioned factors noted by Ju et al. [30].

Another important reason of discrepancy in experimental data is clustering of nanoparticles. Although there are no universally accepted quantitative values, it is known that the level of clustering affects the thermal conductivity of nanofluids [58]. The level of clustering depends on many parameters. It was shown that adding some surfactants and adjusting the pH value of the nanofluid provide better dispersion and prevent clustering to some extent [61]. As a consequence, two nanofluid samples with all of the parameters being the same can lead to completely different experimental results if their surfactant parameters and pH values are not the same [18]. Therefore, when performing experiments, researchers should also consider the type and amount of additives used in the samples and pH value of the samples.

A commonly utilized way of obtaining good dispersion and breaking the clusters is to apply ultrasonic vibration to the samples. The duration and the intensity of the vibration affect the dispersion characteristics. Moreover, immediately after the application of vibration, clusters start to form again and size of the clusters increases as time progresses [58]. Therefore, the time between the

application of vibration and measurement of thermal conductivity, duration of vibration, and intensity of vibration also affect the thermal conductivity of nanofluids, which creates discrepancy in experimental data in the literature [18].

In order to prevent such discrepancies in experimental data, future studies should be performed more systematically and the effects of the parameters associated with pH value, additives and application of vibration on thermal conductivity should be understood.

## 2.2.2. Theoretical Studies

### 2.2.2.1. Classical Models

More than a century ago, Maxwell derived an equation for calculating the effective thermal conductivity of solid-liquid mixtures consisting of spherical particles [37]:

$$k_{nf} = \frac{k_p + 2k_f + 2(k_p - k_f)\phi}{k_p + 2k_f - (k_p - k_f)\phi} k_f, \quad (1)$$

where  $k_{nf}$ ,  $k_p$ , and  $k_f$  are the thermal conductivity of the nanofluid, nanoparticles and base fluid, respectively.  $\phi$  is the volume fraction of particles in the mixture. As seen from the expression, the effect of the size and shape of the particles was not included in the analysis. It should be noted that the interaction between the particles was also neglected in the derivation.

Hamilton and Crosser [44] extended the Maxwell model in order to take the effect of the shape of the solid particles into account, in addition to the thermal conductivities of solid and liquid phases and particle volume fraction. The model is as follows:

$$k_{nf} = \frac{k_p + (n-1)k_f - (n-1)\phi(k_f - k_p)}{k_p + (n-1)k_f + \phi(k_f - k_p)} k_f, \quad (2)$$

where  $n$  is the empirical shape factor and it is defined as:

$$n = \frac{3}{\psi}, \quad (3)$$

where  $\psi$  is the sphericity. Sphericity is the ratio of the surface area of a sphere with a volume equal to that of the particle to the surface area of the particle. Therefore,  $n = 3$  for a sphere and in that case the Hamilton and Crosser model becomes identical to the Maxwell model [37].

Both Maxwell and Hamilton and Crosser models were originally derived for relatively larger solid particles that have diameters on the order of millimeters or micrometers. Therefore, it is questionable whether these models are able to predict the effective thermal conductivity of nanofluids. Nevertheless, these models are utilized frequently due to their simplicity in the study of nanofluids to have a comparison between theoretical and experimental findings [18].

Recently, many theoretical studies were made and several mechanisms were proposed in order to explain the anomalous thermal conductivity enhancement obtained with nanofluids. In the following sections, proposed mechanisms of thermal conductivity enhancement in nanofluids are discussed and thermal conductivity models based on those mechanisms are summarized.

#### **2.2.2.2. Enhancement Mechanisms**

In the following five sections, some mechanisms proposed to explain the anomalous thermal conductivity enhancement of nanofluids are discussed.

##### **2.2.2.2.1. Brownian Motion of Nanoparticles**

Brownian motion is the random motion of particles suspended in a fluid. When nanofluids are considered, this random motion transports energy directly by nanoparticles. In addition, a micro-convection effect, which is due to the fluid mixing around nanoparticles, is also proposed to be important. There are many studies in the literature regarding the effect of Brownian motion on the thermal conductivity of nanofluids. Bhattacharya et al. [64] used Brownian dynamics simulation to determine the effective thermal conductivity of nanofluids, by considering the Brownian motion of the nanoparticles. Effective thermal conductivity of the nanofluid was defined as:

$$k_{nf} = \phi k_p + (1 - \phi)k_f, \quad (4)$$

where  $k_p$  is not simply the bulk thermal conductivity of the nanoparticles, but it also includes the effect of the Brownian motion of the nanoparticles on the thermal conductivity. A method called the Brownian dynamics simulation was developed, the expressions were provided to calculate  $k_p$ , then the effective thermal conductivity of Cu/ethylene glycol and Al<sub>2</sub>O<sub>3</sub>/ethylene glycol nanofluids were calculated for different particle volume fractions. The results were compared with previous experimental data [43,60] and they were found to be in agreement. The prediction of the Hamilton and Crosser [44] model (Eqs. 2, 3) for these two nanofluids was also included in the comparison. It was found that conduction-based Hamilton and Crosser model underpredicted the effective thermal conductivity of the nanofluid, since it does not take into account the Brownian motion of the particles within the base fluid.

Prasher et al. [65] compared the effect of translational Brownian motion and convection induced by Brownian motion. They also considered the existence of an interparticle potential. By making an order-of-magnitude analysis, the authors concluded that convection in the liquid induced by Brownian motion of nanoparticles was mainly responsible for the anomalous thermal conductivity enhancement of nanofluids. It should be noted that in their work, the authors did not analyze the effect of clustering of nanoparticles.

Another study was made by Li and Peterson [66] who investigated the effect of mixing due to the Brownian motion of nanoparticles on the effective thermal conductivity of nanofluids numerically. Velocity, pressure, and temperature distribution around the nanoparticles were investigated for a single nanoparticle, for two nanoparticles, and for numerous nanoparticles. It was seen that improvement in thermal conduction capability of the nanofluid induced by two nanoparticles that were close to each other was more than twice the improvement observed for a single nanoparticle. A similar behavior was also observed for the simulation of several nanoparticles. As a result, it was concluded that the mixing effect created by the Brownian motion of the nanoparticles is an important reason for the large thermal conductivity enhancement of nanofluids. It

should be noted that in this study, the flow around the nanoparticles was solved as if the nanoparticles are macroscale objects. Slip boundary condition and wettability of particles were not considered.

There are also some studies which propose that Brownian motion is not very effective in thermal conductivity enhancement. For example, Evans et al. [67] theoretically showed that the thermal conductivity enhancement due to Brownian motion is a very small fraction of the thermal conductivity of the base fluid. This fact was also verified by molecular dynamics simulations. As a result, it was concluded that Brownian motion of nanoparticles could not be the main cause of anomalous thermal conductivity enhancement with nanofluids.

#### 2.2.2.2. Clustering of Nanoparticles

Nanoparticles are known to form clusters [49,68]. These clusters can be handled by using fractal theory [1]. Evans et al. [69] proposed that clustering can result in fast transport of heat along relatively large distances since heat can be conducted much faster by solid particles when compared to liquid matrix. This phenomenon is illustrated schematically in Fig. 1.

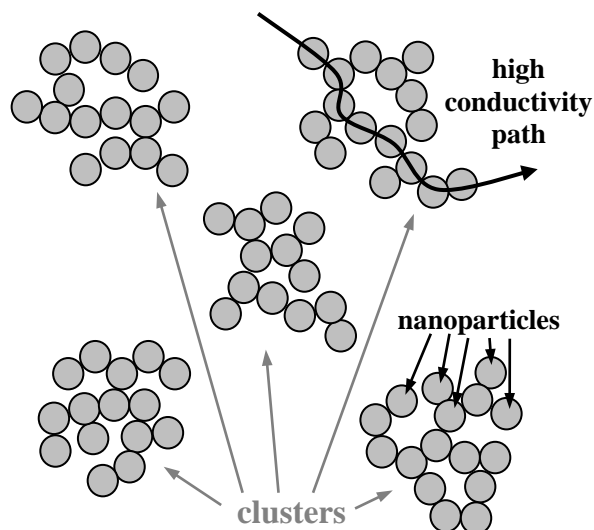


**Figure 1.** Schematic illustration representing the clustering phenomenon [49]. High conductivity path results in fast transport of heat along large distances.



Evans et al. [69] also investigated the dependence of thermal conductivity of nanofluids on clustering and interfacial thermal resistance. Effect of clusters was analyzed in three steps by using Bruggeman model [49], the model by Nan et al. [70], and Maxwell–Garnett (M–G) model [49,1]. The resulting thermal conductivity ratio expression is

$$\frac{k_{nf}}{k_f} = \frac{(k_{cl} + 2k_f) + 2\phi_{cl}(k_{cl} - k_f)}{(k_{cl} + 2k_f) - \phi_{cl}(k_{cl} - k_f)}, \quad (5)$$

where  $k_{cl}$  is the thermal conductivity of the clusters and  $\phi_{cl}$  is the particle volume fraction of the clusters, which are defined in the study and the related expressions are also given therein to calculate effective thermal conductivity theoretically. In addition to the theoretical work, Evans et al. [69] also determined the effective thermal conductivity of the nanofluid by utilizing a Monte Carlo simulation. The results of the theoretical approach and the computer simulation were compared and they were found to be in good agreement. It was shown that the effective thermal conductivity increased with increasing cluster size. However, as particle volume fraction increased, the nanofluid with clusters showed relatively smaller thermal conductivity enhancement. When it comes to interfacial resistance, it was found that interfacial resistance decreases the enhancement in thermal conductivity, but this decrease diminishes for nanofluids with large clusters. Another conclusion was that fiber shaped nanoparticles are more effective in thermal conductivity enhancement when compared to spherical particles. However, it was also noted that such fiber shaped particles or clusters increase the viscosity of the nanofluids significantly. At this point, it should be noted that excessive clustering of nanoparticles may result in sedimentation, which adversely affects the thermal conductivity [49]. Therefore, there should be an optimum level of clustering for maximum thermal conductivity enhancement [18].

Another study that proposes the clustering effect as the main reason of thermal conductivity enhancement was made by Koblinski et al. [71]. They analyzed the experimental data for thermal conductivity of nanofluids and examined the potential mechanisms of anomalous enhancement. Enhancement mechanisms such as microconvection created by Brownian motion of

nanoparticles, nanolayer formation around particles, and near field radiation were concluded not to be the major cause of the enhancement. It was noted that effective medium theories can predict the experimental data well when the effect of clustering is taken into account. Feng et al. [50] modeled the effect of clustering by taking the effect of particle size into account. It was found that clustering improves thermal conductivity enhancement and formation of clusters is more pronounced in nanofluids with smaller nanoparticles since distances between nanoparticles are smaller in those nanofluids, which increases the importance of van der Waals forces attracting particles to each other.

### 2.2.2.2.3. Liquid Layering around Nanoparticles

A recent study showed that liquid molecules form layered structures around solid surfaces [72] and it is expected that those nanolayers have a larger effective thermal conductivity than the liquid matrix [73]. As a result of this observation, the layered structures that form around nanoparticles are proposed to be responsible for the thermal conductivity enhancement of nanofluids [73]. This phenomenon is illustrated schematically in Fig. 2.

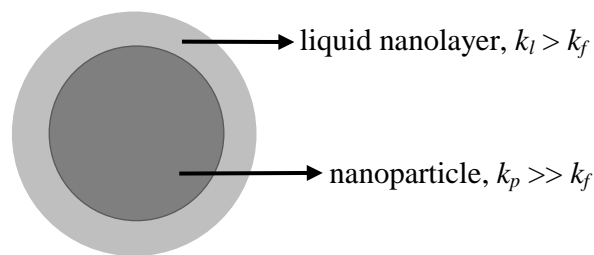


**Figure 2.** Schematic illustration representing the liquid layering around nanoparticles.  $k_l$ ,  $k_f$ , and  $k_p$  are the thermal conductivity of nanolayer, base fluid, and nanoparticle, respectively.

The fact that there is no experimental data regarding the thickness and thermal conductivity of these nanolayers is an important drawback of the proposed mechanism [18]. Some researchers develop a theoretical model by

considering liquid layering around nanoparticles and illustrate the predictions of their model by just assuming some values for the thermal conductivity and thickness of the nanolayer [73]. Some others model the thermal conductivity of the nanolayer so that it linearly varies across the radial direction [74] and there are also some researchers that take the temperature dependence of the thermal conductivity of these layers into account [75]. By choosing the parameters of the nanolayer accordingly, it is possible to produce results which are consistent with experimental data but this does not prove the validity of the proposed mechanism.

Recently, Lee [39] proposed a way of calculating the thickness and thermal conductivity of the nanolayer by considering the formation of electric double layer around the nanoparticles. According to the study, thickness of nanolayer depends on the dielectric constant, ionic strength, and temperature of the nanofluid. When it comes to the thermal conductivity of the nanolayer, the parameters are total charged surface density, ion density in the electric double layer, pH value of the nanofluid, and thermal conductivities of base fluid and nanoparticles. Another theoretical way to calculate the thickness and thermal conductivity of the nanolayer is proposed by Tillman and Hill [76]. They used the classical heat conduction equation together with proper boundary conditions to obtain a relation between the radial distribution of thermal conductivity in the nanolayer and nanolayer thickness. The relation requires an initial guess about the function that defines radial variation of thermal conductivity inside the nanolayer. According to the guess, it is possible to determine the thickness of the nanolayer and check the validity of the associated assumption. There are also some investigations which show that nanolayers are not the main cause of thermal conductivity enhancement with nanofluids. Among those studies, Xue et al. [77] examined the effect of nanolayer by molecular dynamics simulations and showed that nanolayers have no effect on the thermal transport. In the simulations, a simple monoatomic liquid was considered and the authors noted that in case of water, results might be different.

#### **2.2.2.2.4. Ballistic Phonon Transport in Nanoparticles**

In solids, diffusive heat transport is valid if the mean-free path of phonons is smaller than the characteristic size of the particle in consideration. Koblinski et al. [2] estimated the phonon mean-free path of  $\text{Al}_2\text{O}_3$  nanoparticles at room temperature according to the theory developed by Debye (Geiger and Poirier [78]) as 35 nm. In a particle with a diameter smaller than 35 nm, the heat transport is not diffusive, but heat is transported ballistically. Although this fact prevents the application of conventional theories for the modeling of thermal conductivity of nanofluids, Koblinski et al. noted that ballistic heat transport still cannot explain the anomalous thermal conductivity enhancements, because the temperature inside the nanoparticles is nearly constant and this fact does not depend on whether heat is transported by diffusion or ballistically. Therefore, the boundary conditions for the base fluid are the same in both cases, and this results in identical thermal conductivity values for the nanofluid. On the other hand, Koblinski et al. indicated that ballistic heat transport can create a significant effect on thermal conductivity of nanofluids if it enables efficient heat transport between nanoparticles. This is only possible if the nanoparticles are very close to each other (a few nanometers separated) and they note that this is the case for nanofluids with very small nanoparticles. Furthermore, the authors stress on the fact that the particles may become closer to each other due to the Brownian motion.

Another study regarding this subject was made by Nie et al. [79]. They investigated the possibility of a change in the phonon mean-free path of the liquid phase of nanofluids due to the presence of nanoparticles theoretically. The authors found that the layering structure, in which there is significant change in phonon mean-free path, is confined to a distance around 1 nm. As a result, it was concluded that such a highly localized effect cannot be responsible for the anomalous thermal conductivity enhancement with nanofluids. Furthermore, change of phonon transport speed in the liquid phase due to the presence of

nanoparticles was also investigated and the associated effect was found to be negligible.

#### **2.2.2.2.5. Near Field Radiation**

Domingues et al. [80] studied the effect of near field radiation on the heat transport between two nanoparticles. They analyzed the problem by utilizing molecular dynamics simulation and found that when the distance between the nanoparticles is smaller than the diameter of the particles, the heat conductance is two to three orders of magnitudes higher than the heat conductance between two particles that are in contact. This finding can be considered as a heat transfer enhancement mechanism for nanofluids since the separation between nanoparticles can be very small in nanofluids with nanoparticles smaller than 10 nm. Furthermore, Brownian motion of nanoparticles can also improve that mechanism since the distance between nanoparticles changes rapidly due to the random motion. An important study regarding this subject was made by Ben-Abdallah [81]. In that study, near field interactions between nanoparticles were analyzed numerically for the case of Cu/ethylene glycol nanofluid, and it was shown that the near field interactions between nanoparticles do not significantly affect the thermal conductivity of the nanofluid. It was noted that the results are valid also for other nanoparticle types; metals, metal oxides, and polar particles.

#### **2.2.2.3. Models of Nanofluid Thermal Conductivity**

In the following three sections, some theoretical models based on the aforementioned thermal conductivity enhancement mechanisms are discussed.

##### **2.2.2.3.1. Models Based on Brownian Motion**

Many models were developed for the determination of thermal conductivity of nanofluids based on the Brownian motion of nanoparticles. Three of these models are explained below. Additionally, an empirical model, which provides

information about the effect of Brownian motion on thermal conductivity of nanofluids, is also discussed.

Jang and Choi [82] modeled the thermal conductivity of nanofluids by considering the effect of Brownian motion of nanoparticles. The proposed model is a function of not only thermal conductivities of the base fluid and nanoparticles, but it also depends on the temperature and size of the nanoparticles. Energy transport in nanofluids was considered to consist of four modes; heat conduction in the base fluid, heat conduction in nanoparticles, collisions between nanoparticles (due to Brownian motion), and micro-convection caused by the random motion of the nanoparticles. Among these, the collisions between nanoparticles were found to be negligible when compared to other modes. As a result of the consideration of the three remaining modes, the following expression was presented:

$$k_{nf} = k_f(1 - \phi) + k_p^* \phi + 3C_l \frac{d_f}{d_p} k_f \text{Re}_d^2 \text{Pr}_f \phi, \quad (6)$$

where  $C_l$  is a proportionality constant,  $d_f$  the diameter of the fluid molecules,  $d_p$  the diameter of the nanoparticles,  $\text{Pr}_f$  Prandtl number of base fluid, and  $k_p^*$  is defined so that it also includes the effect of the Kapitza resistance,

$$k_p^* = \beta k_p, \quad (7)$$

where  $\beta$  is a constant. Reynolds number is defined as:

$$\text{Re}_d = \frac{\overline{C_{R.M.}} d_p}{\nu_f}, \quad (8)$$

where  $\overline{C_{R.M.}}$  is the random motion velocity of the nanoparticles and  $\nu_f$  is the kinematic viscosity of the base fluid.  $\overline{C_{R.M.}}$  can be determined by using

$$\overline{C_{R.M.}} = \frac{D_o}{\lambda_f}, \quad (9)$$

where  $\lambda_f$  is the mean-free path of the base fluid molecules.  $D_o$  is nanoparticle diffusion coefficient and it can be calculated by using the following expression [83]:

$$D_o = \frac{\kappa_B T}{3\pi\mu_f d_p}. \quad (10)$$

$\kappa_B$  is the Boltzmann constant,  $T$  the temperature in K, and  $\mu_f$  the dynamic viscosity of base fluid. When the model's dependence on nanoparticle size is considered, it is seen that nanofluid thermal conductivity increases with decreasing particle size, since decreasing particle size increases the effect of Brownian motion. In the derivation of this model, thickness of the thermal boundary layer around the nanoparticles was taken to be equal to  $3d_f / Pr$ , where  $d_f$  is the diameter of the base fluid molecule. Furthermore, the volume fraction of the liquid layer around nanoparticles was assumed to be equal to the nanoparticle volume fraction. These assumptions and some others were criticized by Prasher et al. [49] since they were not verified by any means.

Koo and Kleinstreuer [84] considered the thermal conductivity of nanofluids to be composed of two parts:

$$k_{nf} = k_{static} + k_{Brownian}, \quad (11)$$

where  $k_{static}$  represents the thermal conductivity enhancement due to the higher thermal conductivity of the nanoparticles and  $k_{Brownian}$  takes the effect of Brownian motion into account. For the static part, the classical Maxwell model [37] was proposed:

$$\frac{k_{nf}}{k_f} = \frac{k_p + 2k_f + 2(k_p - k_f)\phi}{k_p + 2k_f - (k_p - k_f)\phi}. \quad (12)$$

For  $k_{Brownian}$ , Brownian motion of particles was considered together with the effect of fluid particles moving with nanoparticles around them. As a result, the following expression was proposed:

$$k_{Brownian} = 5 \times 10^4 \beta \phi \rho_f c_{p,f} \sqrt{\frac{\kappa_B T}{\rho_p d_p}} f, \quad (13)$$

where  $\rho_p$  and  $\rho_f$  are the density of nanoparticles and base fluid, respectively, and  $T$  the temperature in K.  $c_{p,f}$  is specific heat capacity of base fluid. In the analysis, the interactions between nanoparticles and fluid volumes moving around them were not considered and an additional term,  $\beta$ , was introduced in order to take that

effect into account. Koo and Kleinstreuer indicated that this term becomes more effective with increasing volume fraction. Another parameter,  $f$ , was introduced to the model in order to increase the temperature dependency of the model. Both  $f$  and  $\beta$  were determined by utilizing available experimental data:

$$f = (-134.63 + 1722.3\phi) + (0.4705 - 6.04\phi)T, \quad (14)$$

which is obtained by using the results of the study of Das et al. [11] for CuO nanofluids. For other nanofluids,  $f$  can be taken as 1 due to lack of experimental data. Associated  $\beta$  values are listed in Table 2. It is difficult to determine theoretical expressions for  $f$  and  $\beta$  due to the complexities involved and this can be considered as a drawback of the model [18].

**Table 2.**  $\beta$  values for different nanoparticles to be used in Eq. (13) [84]

Type of particles	$\beta$	Remarks
Au-citrate, Ag-citrate and CuO	$0.0137(100\phi)^{-0.8229}$	$\phi < 1\%$
CuO	$0.0011(100\phi)^{-0.7272}$	$\phi > 1\%$
Al <sub>2</sub> O <sub>3</sub>	$0.0017(100\phi)^{-0.0841}$	$\phi > 1\%$

Xu et al. [85] proposed another thermal conductivity model for nanofluids, based on the Brownian motion of nanoparticles. Thermal conductivity was modeled to be composed of a static and a dynamic part, similar to the aforementioned study of Koo and Kleinstreuer [84]:

$$k_{nf} = k_{static} + k_{dynamic}. \quad (15)$$

The static part can be determined from the Hamilton and Crosser [44] model (Eqs. 2, 3). The dynamic part was modeled by considering the flow over the nanoparticles and taking the fractal distribution of the nanoparticle sizes into account:



$$k_{dynamic} = k_f c \frac{Nu \cdot d_f}{Pr} \frac{(2 - D_f) D_f}{(1 - D_f)^2} \frac{\left[ \left( \frac{d_{p,max}}{d_{p,min}} \right)^{1-D_f} - 1 \right]^2}{\left( \frac{d_{p,max}}{d_{p,min}} \right)^{2-D_f} - 1} \frac{1}{\bar{d}_p}, \quad (16)$$

where

$$D_f = 2 - \frac{\ln \phi}{\ln \left( \frac{d_{p,min}}{d_{p,max}} \right)}. \quad (17)$$

Here,  $c$  is an empirical constant,  $\bar{d}_p$  is the average diameter of nanoparticles, and  $d_{p,min}$  and  $d_{p,max}$  are the minimum and maximum diameters of nanoparticles. It was noted that  $d_{p,min} / d_{p,max}$  can be taken as 0.001. Nusselt number for liquid flow over a sphere is [86]

$$Nu = 2.0 + 0.5 Re Pr + O(Re^2 Pr^2), \quad (18)$$

where

$$Pr = \frac{\mu_f c_{p,f}}{k_f}, \quad (19)$$

and

$$Re = \frac{d_p u_p}{\nu_f}, \quad (20)$$

where  $u_p$  is the velocity of nanoparticles. Since  $Re \ll 1$  and  $Pr$  is of the order of 1,  $Nu \approx 2$ . Constant  $c$  comes from the fact that the thermal boundary layer around the nanoparticle due to the Brownian motion of the particle is not known. The proposed model was compared with experimental data and it was shown that  $c$  is a function of the type of base fluid and it does not depend on the type of nanoparticles.  $c$  is found to be 85.0 for deionized water and 280.0 for ethylene glycol. Thermal conductivity enhancement predicted by the model decreases with increasing particle size. It was noted that this is due to the fact that the effect of Brownian motion diminishes with increasing particle size. It should also be noted that the expression used for the Nusselt number is for macroscale flows and it

does not consider microscale effects such as slip flow at the surface of the nanoparticles [18].

Chon et al. [10] investigated the thermal conductivity of Al<sub>2</sub>O<sub>3</sub>/water nanofluid experimentally and proposed a correlation for the determination of the thermal conductivity of Al<sub>2</sub>O<sub>3</sub> nanofluids based on the experimental data. Three different nanopowders were used in the experiments with nominal diameters of 11, 47, and 150 nm. Experimental data showed that thermal conductivity increases with increasing temperature and decreasing particle size. Dependence on temperature becomes more pronounced at higher temperatures. The correlation provided is

$$\frac{k_{nf}}{k_f} = 1 + 64.7\phi^{0.7460} \left(\frac{d_f}{d_p}\right)^{0.3690} \left(\frac{k_p}{k_f}\right)^{0.7476} \text{Pr}^{0.9955} \text{Re}^{1.2321}, \quad (21)$$

where Prandtl number and Reynolds number are defined as:

$$\text{Pr} = \frac{\mu_f}{\rho_f \alpha_f}, \quad (22)$$

and

$$\text{Re} = \frac{\rho_f V_{Br} d_p}{\mu_f} = \frac{\rho_f \kappa_B T}{3\pi\mu_f^2 \lambda_f}. \quad (23)$$

$\alpha_f$  is the thermal diffusivity of the base fluid. The dynamic viscosity of the base fluid is

$$\mu_f = A \cdot 10^{B/(T-C)}, \quad (24)$$

where  $A$ ,  $B$ , and  $C$  are constants, which are equal to  $2.414 \times 10^{-5}$  Pa·s, 247.8 K, and 140 K, respectively, for water.  $T$  is in K.  $V_{Br}$  is the Brownian velocity of nanoparticles [83],

$$V_{Br} = \frac{\kappa_B T}{3\pi\mu d_p \lambda_f} = \frac{\kappa_B}{3\pi d_p \lambda_f} \cdot \frac{T}{A \cdot 10^{B/(T-C)}}, \quad (25)$$

where  $\lambda_f$  is the mean-free path and it was taken as 0.17 nm for water. In the correlation provided, effects of the base fluid thermal conductivity, Prandtl number, and Reynolds number were investigated and it was seen that Reynolds number, which is a measure of the mobility of particles, is the dominant factor in

determining the amount of thermal conductivity enhancement. Then, it was concluded that Brownian motion is mainly responsible for the anomalous enhancement in thermal conductivity. Brownian velocity of nanoparticles were also examined through the expression given for  $V_{Br}$  and it was stressed that temperature increases the Brownian motion, whereas increasing particle size slows down the particles dramatically. The correlation provided is valid for nanoparticle sizes ranging between 11 and 150 nm. For temperature, the associated validity range is 21–71°C.

### 2.2.2.3.2. Models Based on Clustering

The following paragraphs explain two theoretical models that are based on the clustering of nanoparticles. The first model also considers the effect of Brownian motion.

Xuan et al. [38] studied the thermal conductivity of nanofluids by considering Brownian motion and clustering of nanoparticles. An equation was proposed to predict the thermal conductivity of nanofluids:

$$\frac{k_{nf}}{k_f} = \frac{k_p + 2k_f - 2\phi(k_f - k_p)}{k_p + 2k_f + \phi(k_f - k_p)} + \frac{\rho_p \phi c_{p,p}}{2k_f} \sqrt{\frac{\kappa_B T}{3\pi r_{cl} \mu_f}} \quad (26)$$

Here,  $r_{cl}$  is the apparent radius of the nanoparticle clusters, which should be determined by experiment.  $T$  is temperature in K.  $\mu_f$  is the dynamic viscosity of the base fluid and it can be calculated from the study of Li and Xuan [87]. The first term on the right-hand side of Eq. (26) is the Maxwell model [37] for thermal conductivity of suspensions of solid particles in fluids. The second term on the right-hand side of Eq. (26) adds the effect of the random motion of the nanoparticles into account. For the contribution of this term, the following values were presented for Cu (50 nm)/water nanofluid: For  $\phi = 0.03\%$ , contribution of the second term is 11% when clustering occurs and 17% when clustering does not occur. For  $\phi = 0.04\%$ , contribution of the second term is 14% when clustering occurs and 24% when clustering does not occur. It was indicated that Brownian motion of nanoparticles becomes more effective with increasing temperature. On

the other hand, as nanoparticles (or clusters) become larger, their random motion becomes slower and this decreases the enhancement in thermal conductivity. It should be noted that the second term on the right-hand side of the equation is not nondimensional, which is an indication of a mistake in the analysis [18].

Chen et al. [88] measured the viscosity of TiO<sub>2</sub>/water and TiO<sub>2</sub>/ethylene glycol nanofluids and proposed a way of calculating the thermal conductivity of nanofluids by using the data. Two types of nanoparticles were used; spherical particles (25 nm) and cylindrical particles (10 nm in diameter and 100 nm in length). A model for the determination of the viscosity of the suspensions given by Krieger and Dougherty [89] was modified in order to take the effect of clustering into account. The modified model became a function of cluster radius, and cluster radius values of the sample nanofluids were determined by matching the predictions of the modified model with experimental data. Then, the determined cluster radius values were used in the thermal conductivity model proposed, which is a modification of Hamilton and Crosser [44] model (Eqs. 2, 3):

$$\frac{k_{nf}}{k_f} = \frac{k_{cl} + (n-1)k_f - (n-1)\phi_{cl}(k_f - k_{cl})}{k_{cl} + (n-1)k_f + \phi_{cl}(k_f - k_{cl})}, \quad (27)$$

where  $k_{cl}$  and  $\phi_{cl}$  are the thermal conductivity and volume fraction of the clusters, respectively.  $n$  was taken as 3 for the spheres and 5 for the cylinders in this work.

$$\phi_{cl} = \phi(r_{cl} / r_p)^{3-D}, \quad (28)$$

where  $r_{cl}$  and  $r_p$  are the radii of the clusters and nanoparticles, respectively.  $D$  is the fractal index, which was taken as 1.8 in the viscosity model and the same value might be used here.  $r_{cl} / r_p$  values are equal to 2.75 and 3.34, for TiO<sub>2</sub>/water (spherical) and TiO<sub>2</sub>/ethylene glycol (spherical) nanofluids, respectively. For the estimation of  $k_{cl}$ , the following expression was proposed for spherical particles [90]:

$$\frac{k_{cl}}{k_f} = \frac{1}{4} \left\{ \begin{array}{l} (3\phi_m - 1) \frac{k_p}{k_f} + (3(1 - \phi_m) - 1) \\ + \left[ ((3\phi_m - 1) \frac{k_p}{k_f} + (3(1 - \phi_m) - 1))^2 + 8 \frac{k_p}{k_f} \right]^{1/2} \end{array} \right\}, \quad (29)$$

where  $\phi_{in}$  is the solid volume fraction of clusters and it is defined as

$$\phi_{in} = \phi(r_{cl} / r_p)^{D-3}. \quad (30)$$

For the estimation of  $k_{cl}$ , the following expression was proposed for nanotubes [91].

$$\frac{k_{cl}}{k_f} = \frac{3 + \phi_{in}[2\beta_x(1-L_x) + \beta_z(1-L_z)]}{3 - \phi_{in}[2\beta_x L_x + \beta_z L_z]}, \quad (31)$$

where

$$\beta_x = (k_x - k_f) / [k_f + L_x(k_t - k_f)], \quad (32)$$

and

$$\beta_z = (k_z - k_f) / [k_f + L_z(k_t - k_f)]. \quad (33)$$

$k_x$  and  $k_z$  are the thermal conductivity of nanotubes along transverse and longitudinal directions, respectively.  $k_t$  is the isotropic thermal conductivity of the nanotube.  $k_x$ ,  $k_z$  and  $k_t$  can be taken to be equal to  $k_p$  as an approximation.  $L_x$  and  $L_z$  are defined as:

$$L_x = \frac{p^2}{2(p^2 - 1)} - \frac{p}{2(p^2 - 1)^{3/2}} \cosh^{-1}(p) \quad (34)$$

and

$$L_z = 1 - 2L_x. \quad (35)$$

$r_{cl} / r_p$  values are equal to 5.40 and 12.98 for TiO<sub>2</sub>/ethylene glycol (nanotube) and TiO<sub>2</sub>/water (nanotube) nanofluids, respectively.  $p$  is the aspect ratio of the nanotubes defined as length of nanotube divided by diameter of nanotube. The modified Hamilton and Crosser [44] model (Eqs. 2, 3) was compared with experimental data for both spherical particles and nanotubes, and a good agreement was observed.

### 2.2.2.3.3. Models Based on Liquid Layering

There are many theoretical models that take the effect of liquid layering around nanoparticles into account. Six of them are explained below. Some models

discussed below also take the effect of Brownian motion and clustering into account.

Yu and Choi [73] presented a model for the determination of the effective thermal conductivity of nanofluids by modifying the Maxwell model [37]. In the modification, the effect of the liquid nanolayers formed around nanoparticles was taken into account. The nanoparticle and the layer around it were considered as a single particle and the thermal conductivity of this particle was determined by using effective medium theory [92]. The result was substituted into the Maxwell model and the following expression was obtained.

$$k_{nf} = \frac{k_{pe} + 2k_f + 2(k_{pe} - k_f)(1 + \beta)^3 \phi}{k_{pe} + 2k_f - (k_{pe} - k_f)(1 + \beta)^3 \phi} k_f, \quad (36)$$

where  $k_{pe}$  is the thermal conductivity of the equivalent nanoparticle;

$$k_{pe} = \frac{[2(1 - \gamma) + (1 + \beta)^3(1 + 2\gamma)]\gamma}{-(1 - \gamma) + (1 + \beta)^3(1 + 2\gamma)} k_p, \quad (37)$$

where

$$\gamma = \frac{k_l}{k_p}, \quad (38)$$

and  $k_l$  is thermal conductivity of the nanolayer.  $\beta$  is defined as:

$$\beta = \frac{t}{r_p}, \quad (39)$$

where  $t$  is nanolayer thickness and  $r_p$  the nanoparticle radius.

Yu and Choi later applied the same idea to the Hamilton and Crosser [44] model (Eqs. 2, 3) and proposed a model for nonspherical particles [93]. Another model that considers non-spherical particles was developed by Xue [94].

Wang et al. [1] proposed an equation for the determination of the thermal conductivity of nanofluids by considering the effect of nanoparticle clustering and surface adsorption. Bruggeman model [90] and fractal theory were utilized in the analysis. The resulting thermal conductivity ratio expression is:

$$\frac{k_{nf}}{k_f} = \frac{(1-\phi) + 3\phi \int_0^\infty \frac{k_{cl}(r)n(r)}{k_{cl}(r) + 2k_f} dr}{(1-\phi) + 3\phi \int_0^\infty \frac{k_f n(r)}{k_{cl}(r) + 2k_f} dr}. \quad (40)$$

$k_{cl}$  is the equivalent thermal conductivity of the cluster determined by the Bruggeman model,

$$k_{cl} = (3\phi^* - 1)k_p + [3(1 - \phi^*) - 1]k_f + \sqrt{\Delta}, \quad (41)$$

where

$$\Delta = (3\phi^* - 1)^2 k_p^2 + [3(1 - \phi^*) - 1]^2 k_f^2 + 2[2 + 9\phi^*(1 - \phi^*)]k_p k_f, \quad (42)$$

and for  $\phi^*$ , following expression should be substituted.

$$\phi^* = (r_{cl} / r_p)^{D_{fl}-3}, \quad (43)$$

where  $r_{cl}$  is the radius of nanoparticle clusters,  $r_p$  the radius of a single nanoparticle, and  $D_{fl}$  the fractal dimension.  $D_{fl}$  was determined as 1.66 for 6.5 wt% SiO<sub>2</sub>/ethanol nanofluid, 1.73 for 0.13 vol.% CuO/water nanofluid, 1.76 for 0.25 vol.% CuO/water nanofluid, and 1.81 for 0.38 vol.% CuO/water nanofluid. CuO particles were 50 nm in size.  $n(r)$  is defined as

$$n(r) = \frac{1}{r_{cl} \sqrt{2\pi} \ln \sigma} \exp \left\{ - \left[ \frac{\ln(r_{cl} / \bar{r}_{cl})}{\sqrt{2\pi} \ln \sigma} \right]^2 \right\}, \quad (44)$$

where  $\bar{r}_{cl}$  is the geometric mean radius of nanoparticle clusters (which was recommended to be replaced by average particle radius) and  $\sigma$  is the standard deviation, which can be taken as 1.5. Surface adsorption was also considered and it was proposed that the thickness of the adsorption layer can be found by using the formula

$$t = \frac{1}{\sqrt{3}} \left( \frac{4M_f}{\rho_f N_A} \right)^{1/3}, \quad (45)$$

where  $M_f$  and  $\rho_f$  are the molecular weight and density of base liquid, respectively, and  $N_A$  the Avogadro constant (6.023x10<sup>23</sup>/mol). Then, thermal conductivity of nanoparticles, by taking surface adsorption into account, can be written as

$$k_{cp} = k_l \frac{(k_p + 2k_l) + 2A^3(k_p - k_l)}{(k_p + 2k_l) - A^3(k_p - k_l)}, \quad (46)$$

where  $A = 1 - t/(t + r_p)$  and  $k_l$  the effective thermal conductivity of the adsorption layer. It should be noted that in Eqs. (40–43, 46);  $(r_p + t)$ ,  $[(r_p + t)/r_p]^3 \phi$  and  $k_{cp}$  should be substituted for  $r_p$ ,  $\phi$ , and  $k_p$ , respectively, when surface adsorption is taken into account. Since  $k_l$  is difficult to predict, this model can be used as an upper bound for the determination of effective thermal conductivity by letting  $k_l = k_p$ .

The validity of the model was checked with the results of a previous experimental study [95] of CuO/water nanofluids.  $D_f$  values were determined by using transmission electron microscopy (TEM) photos of CuO/water nanofluids of different particle volume fraction. It was seen that the model predicts the thermal conductivity well as long as the effect of adsorption is taken into account. Smaller values were calculated when adsorption was neglected.

Xie et al. [74] also studied the effect of the interfacial nanolayer on the enhancement of thermal conductivity with nanofluids. A nanolayer was modeled as a spherical shell with thickness  $t$  around the nanoparticle. This is similar to the approach made by Yu and Choi [73], but Yu and Choi assumed the nanolayer thermal conductivity to be a constant, whereas here the thermal conductivity was assumed to change linearly across the radial direction, so that it is equal to thermal conductivity of base liquid at the nanolayer–liquid interface and equal to thermal conductivity of the nanoparticle at the nanolayer–nanoparticle interface. The associated expression for the determination of the thermal conductivity of nanofluid was given as

$$\frac{k_{nf} - k_f}{k_f} = 3\Theta \phi_T + \frac{3\Theta^2 \phi_T^2}{1 - \Theta \phi_T}, \quad (47)$$

where

$$\Theta = \frac{\beta_{lf} \left[ (1 + \gamma)^3 - \frac{\beta_{pl}}{\beta_{fl}} \right]}{(1 + \gamma)^3 + 2\beta_{lf} \beta_{pl}}, \quad (48)$$

and



$$\beta_{yf} = \frac{k_l - k_f}{k_l + 2k_f}, \quad (49)$$

$$\beta_{pl} = \frac{k_p - k_l}{k_p + 2k_l}, \quad (50)$$

$$\beta_{fl} = \frac{k_f - k_l}{k_f + 2k_l}, \quad (51)$$

where  $\phi_T$  is the total volume fraction of nanoparticles and nanolayers.  $k_l$  is the thermal conductivity of the nanolayer.  $\phi_T$  can be determined using

$$\phi_T = \phi(1 + \gamma)^3, \quad (52)$$

where

$$\gamma = t / r_p. \quad (53)$$

$k_l$  was defined as:

$$k_l = \frac{k_f M^2}{(M - \gamma) \ln(1 + M) + \gamma M}, \quad (54)$$

where

$$M = \varepsilon_p (1 + \gamma) - 1 \quad (55)$$

$$\varepsilon_p = k_p / k_f. \quad (56)$$

When the thermal conductivity of the nanolayer is taken as a constant, this model gives the same results as Yu and Choi [73] model. It was shown that for a chosen nanolayer thickness, the model is in agreement only with some of the experimental data. As a result, it was concluded that liquid layering around nanoparticles is not the only mechanism that affects the thermal conductivity of nanofluids.

Xue and Xu [96] presented another theoretical study for the effective thermal conductivity of nanofluids. In their derivation, nanoparticles were assumed to have a liquid layer around them with a specific thermal conductivity. First, an expression for the effective thermal conductivity of the “complex particle,” which was defined as the combination of the nanoparticle and nanolayer, was determined. Then, by using Bruggeman’s effective media theory

[90], the effective thermal conductivity of the nanofluid was determined. The resulting implicit expression for thermal conductivity of nanofluids is

$$\left(1 - \frac{\phi}{\alpha}\right) \frac{k_{nf} - k_f}{2k_{nf} + k_f} + \frac{\phi}{\alpha} \frac{(k_{nf} - k_l)(2k_l + k_p) - \alpha(k_p - k_l)(2k_l + k_{nf})}{(2k_{nf} + k_l)(2k_l + k_p) + 2\alpha(k_p - k_l)(k_l - k_{nf})} = 0, \quad (57)$$

where subscript  $l$  refers to nanolayer.  $\alpha$  is defined as

$$\alpha = \left(\frac{r_p}{r_p + t}\right)^3, \quad (58)$$

where  $t$  is the thickness of the nanolayer.

Li et al. [63] considered the effect of Brownian motion, liquid layering around nanoparticles, and clustering together. The effect of temperature on average cluster size, Brownian motion, and nanoparticle thermal conductivity was taken into account. Nanoparticle thermal conductivity is calculated by using the following expression [97]:

$$k_p = \frac{3r^* / 4}{3r^* / 4 + 1} k_b. \quad (59)$$

Here,  $k_b$  is thermal conductivity of the bulk material and  $r^* = r_p / \lambda$ , where  $\lambda$  is the mean-free path of phonons. Mean-free path of phonons can be calculated according to the following expression:

$$\lambda = \frac{10aT_m}{\gamma T} \quad (60)$$

Here,  $a$  is crystal lattice constant of the solid,  $\gamma$  Gruneisen constant,  $T$  temperature, and  $T_m$  the melting point (in K). Thickness of nanolayer around nanoparticles is calculated according to Eq. (45). It is assumed that thermal conductivity of the nanolayer is equal to the thermal conductivity of nanoparticles. As a result, particle volume fraction is modified according to the expression:

$$\phi_{eff} = (1 + t / r_p)^3 \phi. \quad (61)$$

$r_p$  is particle radius in this equation. The expressions presented above are substituted into the Xuan et al. [38] model (Eq. 26) to obtain:

$$\frac{k_{nf}}{k_f} = \frac{k_p + 2k_f - 2\phi(k_f - k_p)}{k_p + 2k_f + \phi(k_f - k_p)} + \frac{\rho_p \phi c_{p,p}}{2k_f} \sqrt{\frac{k_B T}{3\pi r_{cl} \mu_f}}. \quad (62)$$

Here,  $r_{cl}$  is the apparent radius of the nanoparticle clusters, which should be determined by experiment. The authors introduced the effect of temperature on clustering according to the fact that decreasing temperature results in a decrease in particle surface energy, which decreases the severity of clustering. As a result, the average cluster size was proposed to be calculated by:

$$r_{cl} = r_{cl0}(1 + b\Delta T). \quad (63)$$

Here,  $r_{cl0}$  is the average cluster size at the reference temperature and  $\Delta T$  is defined as the difference between the nanofluid temperature and reference temperature.  $b$  is a negative constant. Finally, nanofluid viscosity is calculated according to the expression proposed by Einstein [98]:

$$\mu_{nf} = (1 + 2.5\phi)\mu_f. \quad (64)$$

Another study regarding the effect of nanolayers was made by Sitprasert et al. [75]. They modified the model proposed by Leong et al. [99] by taking the effect of temperature on the thermal conductivity and thickness of nanolayer into account. Leong et al.'s static model is as follows:

$$k_{nf} = \frac{(k_p - k_l)\phi k_l [2\beta_1^3 - \beta^3 + 1] + (k_p + 2k_l)\beta_1^3 [\phi\beta^3(k_l - k_f) + k_f]}{\beta_1^3(k_p + 2k_l) - (k_p - k_l)\phi[\beta_1^3 + \beta^3 - 1]}. \quad (65)$$

Here, subscript  $l$  refers to nanolayer.  $\beta$  and  $\beta_1$  are defined as:

$$\beta = 1 + \frac{t}{r_p} \quad (66)$$

$$\beta_1 = 1 + \frac{t}{2r_p} \quad (67)$$

$t$  is the thickness of the nanolayer and  $r_p$  is the radius of the nanoparticles. This model was modified by providing the following relation for the determination of nanolayer thickness:

$$t = 0.01(T - 273)r_p^{0.35}, \quad (68)$$

where  $T$  is temperature in K and  $r_p$  the particle radius in nanometers. After the determination of nanolayer thickness, thermal conductivity of the nanolayer should be found according to the expression:

$$k_l = C \frac{t}{r_p} k_f, \quad (69)$$

where  $C$  is 30 and 110 for  $\text{Al}_2\text{O}_3$  and  $\text{CuO}$  nanoparticles, respectively. It should be noted that the above expressions provided for the determination of the thickness and thermal conductivity of the nanolayer were determined by using experimental data (which is known to have great discrepancies and uncertainties) and no explanation was made regarding the physics of the problem.

When the theoretical models based on nanolayer formation around nanoparticles are considered, it is seen that the main challenge is finding the thermal conductivity and thickness of the nanolayer [18]. Therefore, the future studies should focus on that aspect of the problem.

### 2.3. Comparison of Thermal Conductivity Models with Experimental Data

#### 2.3.1. Particle Volume Fraction

Predictions of some of the aforementioned thermal conductivity models are compared with the experimental data of four research groups [32,11,100,101] for  $\text{Al}_2\text{O}_3$ /water nanofluid in Figs. 3 and 4. In the figures, markers are experimental data while continuous lines are model predictions.  $\text{Al}_2\text{O}_3$ /water nanofluid is selected, since it is one of the most commonly used nanofluids in thermal conductivity research. All of the experimental data were obtained around room temperature. Average particle diameter is taken as 40 nm in the models since the particle sizes in the experiments are close to that value, as indicated in the figures. Nanoparticle size varies in the study of Wen and Ding [101], but its average value is 41.5 nm. Thermal conductivities of nanoparticles are calculated by using Eq. (59). That expression is valid for nonmetallic substances. For metallic nanoparticles, the following equation can be used when the relaxation times of electrons and phonons are comparable [102]:

$$k_p = \left( \frac{2r_p}{5 \times 10^{-6}} \right)^3 k_b \quad (70)$$

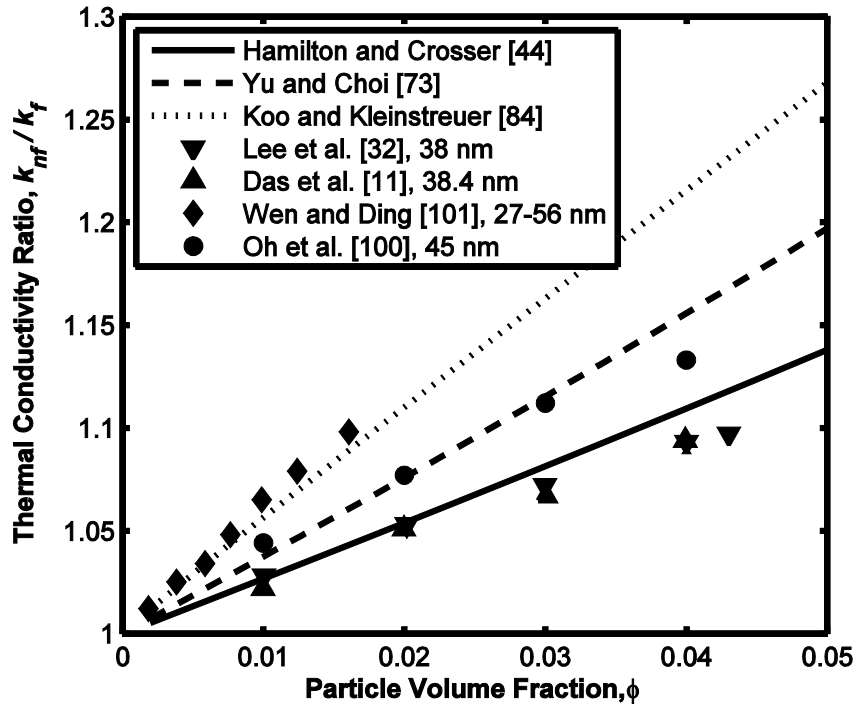


**Figure 3.** Comparison of the experimental results of the thermal conductivity ratio for  $\text{Al}_2\text{O}_3/\text{water}$  nanofluid with theoretical models as a function of particle volume fraction at a particle size around 40 nm

As seen in the figures, there exists significant discrepancy between experimental data. This discrepancy can be explained by the fact that parameters such as pH of the nanofluid, severity of clustering, and method of production of nanofluids usually differ in each experiment [18]. Experimental results of Wen and Ding [101] are relatively higher than the results of other research groups and they are predicted best by the model of Koo and Kleinstreuer [84]. However, since the size distribution of particles is not known in detail, it is difficult to reach a conclusion about the validity of the models. Dependency of the data of Lee et al. [32] on particle volume fraction is somewhat low and none of the models have such a small slope in the figures. Hamilton and Crosser [44] model (Eqs. 2, 3) is relatively closer to the experimental data of Lee et al. [32] and Das et al. [11]. It was noted that clusters as large as 100 nm were observed in the study of Lee et al. [32]. Therefore, it may be suggested that those samples are closer to the validity

range of the Hamilton and Crosser model. However, Das et al. [11] also considered the effect of temperature in their study and indicated that this agreement is just a coincidence.

It should also be noted that all of the experimental results presented here show nearly linear variation of thermal conductivity with particle volume fraction and theoretical models are in agreement with experimental results in that aspect [18].

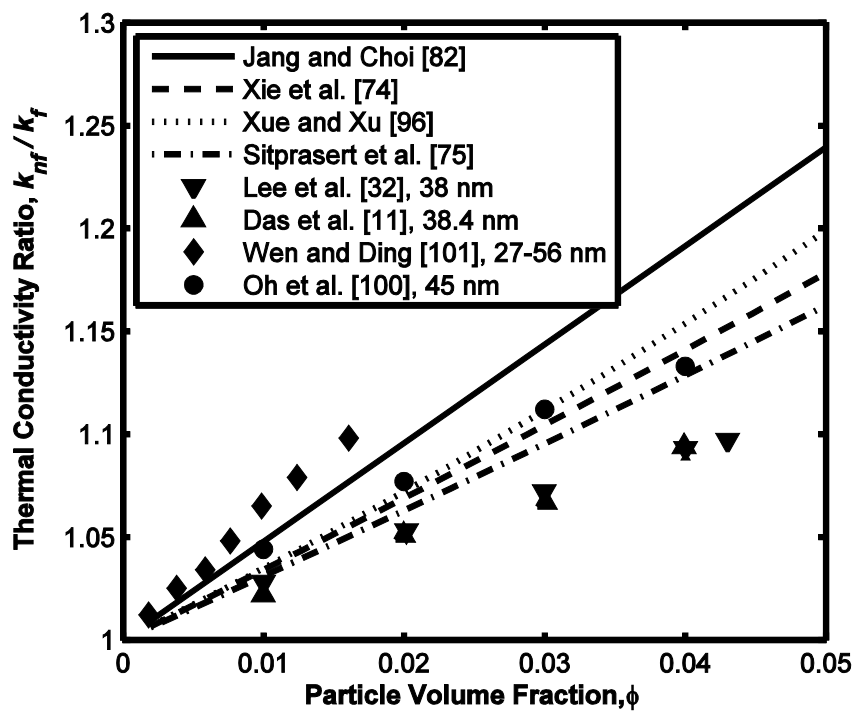


**Figure 4.** Comparison of the experimental results of the thermal conductivity ratio for  $\text{Al}_2\text{O}_3/\text{water}$  nanofluid with theoretical models as a function of particle volume fraction at a particle size around 40 nm

### 2.3.2. Particle Size

Dependence of theoretical models on particle size is compared with experimental data in Figs. 5-8, for  $\text{Al}_2\text{O}_3/\text{water}$  nanofluids. In the figures, markers are experimental data while continuous lines are model predictions. Experimental

data are around room temperature, and room temperature is substituted for model calculations. Linear interpolation was applied to some of the experimental data for determining thermal conductivity ratio at integer values of particle volume fraction. Since a nearly linear relationship exists between thermal conductivity ratio and particle volume fraction, associated errors are not expected to be large.

In Figs. 5 and 6, an experimental data set prepared by combining the results of five different research groups [27,32,40,11,100] is compared with the predictions of two theoretical models. As seen from the figures, there is significant discrepancy in experimental data. Nevertheless, the general trend is increasing thermal conductivity with increasing particle size. As mentioned in Section 2.2.1.2.4, although this trend is the case for nanofluids with  $\text{Al}_2\text{O}_3$  nanoparticles, when overall trend is considered for different types of nanofluids, it is seen that thermal conductivity generally increases with decreasing particle size. At this point, it should be noted that thermal conductivity increases with decreasing particle size when Brownian motion is considered as the main mechanism of thermal conductivity enhancement, because the effect of Brownian motion increases with decreasing particle size, which improves micro-convection around nanoparticles. Same is true for the formation of liquid layers around nanoparticles as an enhancement mechanism, because the enhancement effect of nanolayers increases with increasing specific surface area of nanoparticles. Since specific surface area of nanoparticles is higher in case of smaller particles, decreasing particle size increases the thermal conductivity enhancement according to the models, which are based on liquid layering. It is thought that the contradictory trend in the results of nanofluids with  $\text{Al}_2\text{O}_3$  nanoparticles might be due to the uncontrolled clustering of nanoparticles and such trends do not prove that these proposed mechanisms of thermal conductivity enhancement are incorrect [18].

When Fig. 5 is observed, it is seen that Hamilton and Crosser [44] model (Eqs. 2, 3) predicts increasing thermal conductivity with increasing particle size. The Hamilton and Crosser model does not take the effect of particle size on thermal conductivity into account, but it becomes slightly dependent on particle

size due to the fact that particle thermal conductivity increases with increasing particle size according to Eq. (59). However, the model still fails to predict experimental data for particle sizes larger than 40 nm since particle size dependence diminishes with increasing particle size.

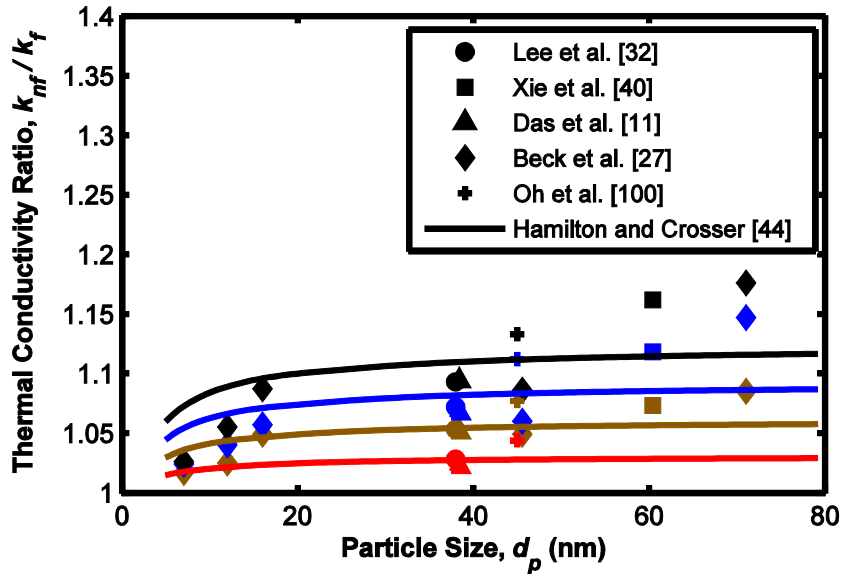


**Figure 5.** Comparison of the experimental results of the thermal conductivity ratio for  $\text{Al}_2\text{O}_3$ /water nanofluid with Hamilton and Crosser model [44] as a function of the particle size at various values of the particle volume fraction. Colors indicate different values of particle volume fraction; red 1%, brown 2%, blue 3%, and black 4%.

Predictions of six other models, which are analyzed in the previous section, are also examined and it was seen that all of them predict increasing thermal conductivity with decreasing particle size. Since the associated plots are very similar to each other qualitatively, only the model of Xue and Xu [96] is presented in Fig. 6. This trend of increasing thermal conductivity with decreasing particle size is due to the fact that these models are either based on Brownian motion (Koo and Kleinstreuer [84] and Jang and Choi [82] models) or based on liquid layering around nanoparticles (Yu and Choi [73], Xie et al. [74], Xue and Xu [96], and Sitprasert et al. [75] models).



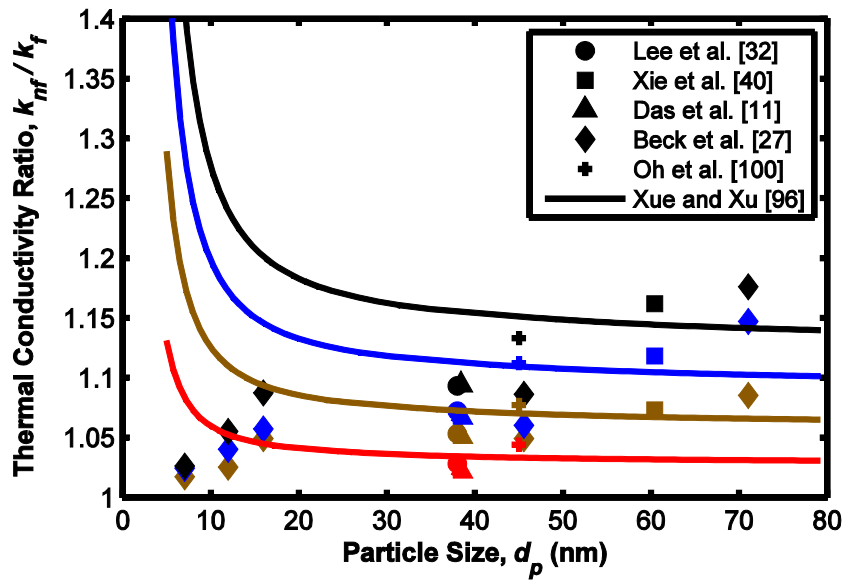


**Figure 6.** Comparison of the experimental results of the thermal conductivity ratio for  $\text{Al}_2\text{O}_3/\text{water}$  nanofluid with Xue and Xu model [96] as a function of the particle size at various values of the particle volume fraction. Colors indicate different values of particle volume fraction; red 1%, brown 2%, blue 3%, and black 4%.

Although the general trend for  $\text{Al}_2\text{O}_3/\text{water}$  nanofluids is as presented in Figs. 5 and 6, there is also experimental data for  $\text{Al}_2\text{O}_3/\text{water}$  nanofluids, which shows increasing thermal conductivity with decreasing particle size [3,28,40,10,47,103,104,100]. In Figs. 7 and 8, those experimental results are combined in order to provide some meaningful comparison with theoretical models. Due to the limited data, results are only plotted for 1 and 3 vol.% nanofluids. When the experimental results are observed, it is seen that the discrepancy in the data is somewhat larger for the 3 vol.% case. This might be due to the fact that at higher particle volume fractions, clustering of particles is more pronounced, which affects the thermal conductivity of nanofluids [18]. It should be noted that clustering may increase or decrease the thermal conductivity enhancement. If a network of nanoparticles is formed as a result of clustering, this may enable fast heat transport along nanoparticles. On the other hand, excessive clustering may result in sedimentation, which decreases the effective particle volume fraction of the nanofluid.

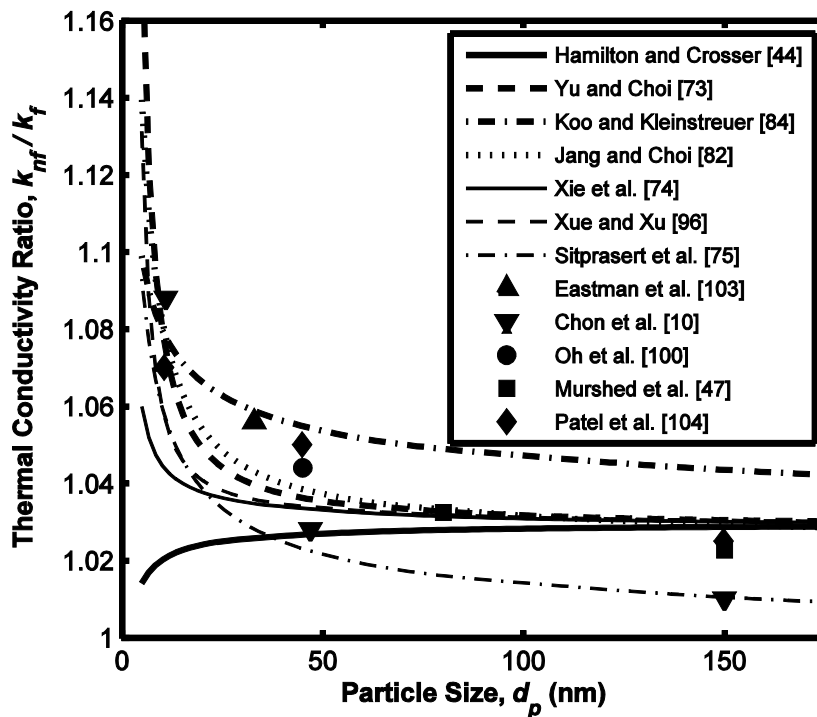


**Figure 7.** Comparison of the experimental results of the thermal conductivity ratio for 1 vol.%  $\text{Al}_2\text{O}_3$ /water nanofluid with theoretical models as a function of particle size

When the predictions of the models are compared (Figs. 7, 8), it is seen that Yu and Choi model [73], Jang and Choi model [82], and Xue and Xu model [96] provide very close results. All of these three models generally predict the experimental data well, and it is interesting to note that two of these models are based on nanolayer formation around nanoparticles (Yu and Choi [73] and Xue and Xu [96] models), whereas Jang and Choi model [82] is based on Brownian motion. Therefore, it is possible to obtain similar results by considering different mechanisms of thermal conductivity enhancement and more systematic experimental data sets are required in order to differentiate these models. For example, it is known that the effect of Brownian motion diminishes with increasing viscosity of base fluid. By preparing different nanofluids by using two base fluids with significantly different viscosities and measuring the thermal conductivities, Tsai et al. [105] showed that Brownian motion has a significant

effect on thermal conductivity enhancement especially for nanofluids with low viscosity base fluids.

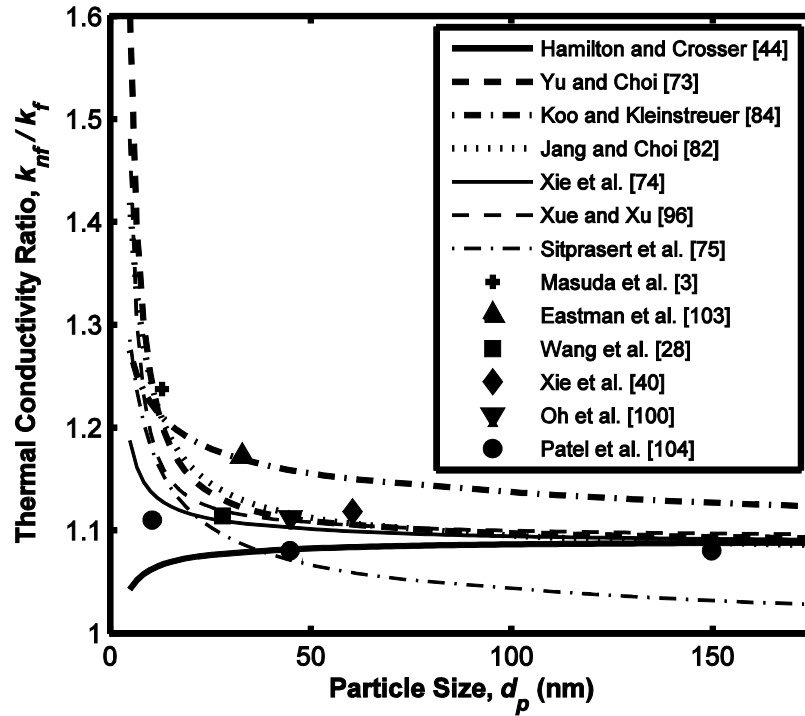


**Figure 8.** Comparison of the experimental results of the thermal conductivity ratio for 3 vol.%  $\text{Al}_2\text{O}_3$ /water nanofluid with theoretical models as a function of particle size.

It is also seen that Sitprasert et al. [75] model underpredicts the experimental data for large nanoparticles. In that model, the relation between the nanolayer thickness and particle size was found empirically by utilizing experimental data. There is not much data in the literature that considers spherical particles larger than 100 nm and this might be the reason behind such a result. On the other hand, Koo and Kleinstreuer model [84] overpredicts the experimental data for large nanoparticles. It should be noted that Koo and Kleinstreuer model includes an empirical term ( $f$ ), which is a function of temperature and particle volume fraction. It is taken as 1 since the authors did not provide an expression for nanofluids with  $\text{Al}_2\text{O}_3$  nanoparticles. By choosing a proper function for that

term accordingly, it might be possible to prevent the associated overprediction. However, since that term is not a function of particle size, a modification in  $f$  will also affect the results for smaller particle sizes. Finally, when the results of Xie et al. [74] model is considered, it is seen that the model does not predict significant increase in thermal conductivity enhancement with decreasing particle size up to 20 nm. It is thought that this is mainly due to the fact that the thermal conductivity of nanolayer is modeled to vary linearly in radial direction which diminishes the associated effect of nanolayer [18].

### **2.3.3. Temperature**

In this section, dependence of the theoretical models on temperature is compared with experimental data (Figs. 9-11). In the figures, markers are experimental data while continuous lines are model predictions. It should be noted that the presented data of Li and Peterson [12] is obtained by using the line fit provided by the authors since data points create ambiguity due to fluctuations. In determining the thermal conductivity ratio, thermal conductivity of the nanofluid is divided by the thermal conductivity of water at that temperature. In the models, particle size is selected as 40 nm since most of the experimental data is close to that value, as explained in the previous sections.

Although there is no agreement in the quantitative values, experimental results generally suggest that thermal conductivity ratio increases with temperature. It is seen that the temperature dependence of the data of Li and Peterson [12] is much higher than the results of other two research groups. On the other hand, the results of Chon et al. [10] show somewhat weaker temperature dependence. This might be explained by the fact that the average size of nanoparticles in that study is larger when compared to others, since increasing particle size decreases the effect of both Brownian motion and nanolayer formation. It should also be noted that dependence on particle volume fraction becomes more pronounced with increasing temperature in all of the experimental studies [18].

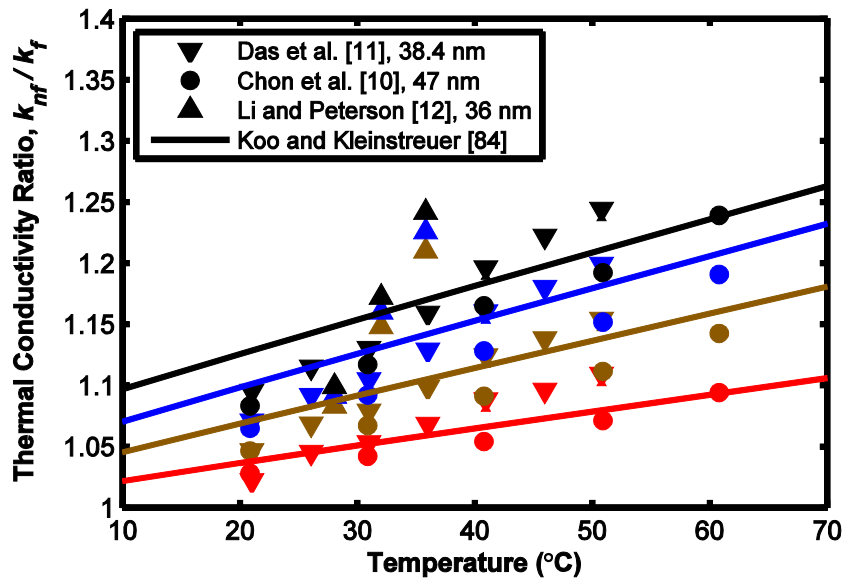


**Figure 9.** Comparison of the experimental results of the thermal conductivity ratio for  $\text{Al}_2\text{O}_3/\text{water}$  nanofluid with Koo and Kleinstreuer model [84] as a function of temperature at various values of particle volume fraction. Colors indicate different values of particle volume fraction; red 1%, brown 2%, blue 3%, and black 4%.

When it comes to theoretical models, predictions of Hamilton and Crosser model [44], Yu and Choi model [73], Xue and Xu model [96], and Xie et al. [74] model do not depend on temperature except for a very slight decrease in thermal conductivity ratio with temperature due to the increase in the thermal conductivity of water with temperature. Therefore, these models fail to predict the aforementioned trends of experimental data. Since the predictions of these four models with respect to temperature do not provide any additional information; associated plots are not shown here.

The model proposed by Koo and Kleinstreuer [84] considers the effect of Brownian motion on the thermal conductivity and the predictions of this model are presented in Fig. 9. In the model, temperature dependence of thermal conductivity is taken into account by an empirical factor  $f$ , which is a function of particle volume fraction and temperature. The authors did not provide the associated function for nanofluids with  $\text{Al}_2\text{O}_3$  nanoparticles. Because of this, the function provided for CuO nanoparticles is used in the calculations (Eq. 14). A multiplicative constant is introduced into the associated expression in order to

match experimental data. As seen from Fig. 9, model of Koo and Kleinstreuer generally predicts the trend in the experimental data correctly. Since  $f$  is a function of both particle volume fraction and temperature, one can make further adjustments in the associated parameters to predict a specific data set with high accuracy. It is interesting to note that the relation between particle volume fraction and thermal conductivity ratio is not linear at high temperatures. This is mainly due to the second term on the right-hand side of Eq. (14), which creates a reduction in the effect of particle volume fraction with increasing temperature. By using a different function for  $f$  and finding the associated constants, it is possible to eliminate such effects.

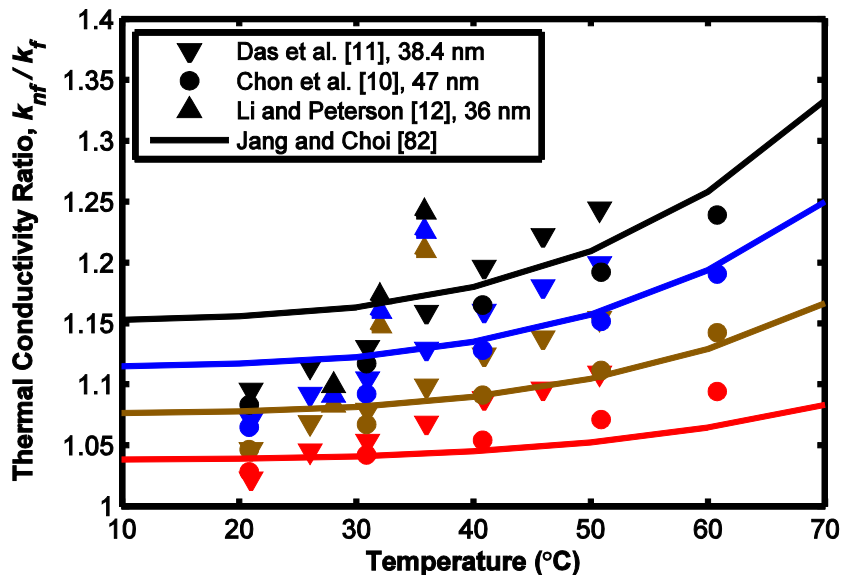


**Figure 10.** Comparison of the experimental results of the thermal conductivity ratio for  $\text{Al}_2\text{O}_3/\text{water}$  nanofluid with Jang and Choi model [82] as a function of temperature at various values of particle volume fraction. Colors indicate different values of particle volume fraction; red 1%, brown 2%, blue 3%, and black 4%.

In Fig. 10, results of Jang and Choi [82] model is presented. It is important to note that this model predicts nonlinear temperature dependence of thermal conductivity, whereas other two models predict linear behavior. Experimental results of Das et al. [11] and Li and Peterson [12] show nearly linear variation of

thermal conductivity ratio with temperature, which is contradictory with the model. On the other hand, result of Chon et al. [10] suggests nonlinear variation and the associated trend is somewhat in agreement with the model of Jang and Choi.

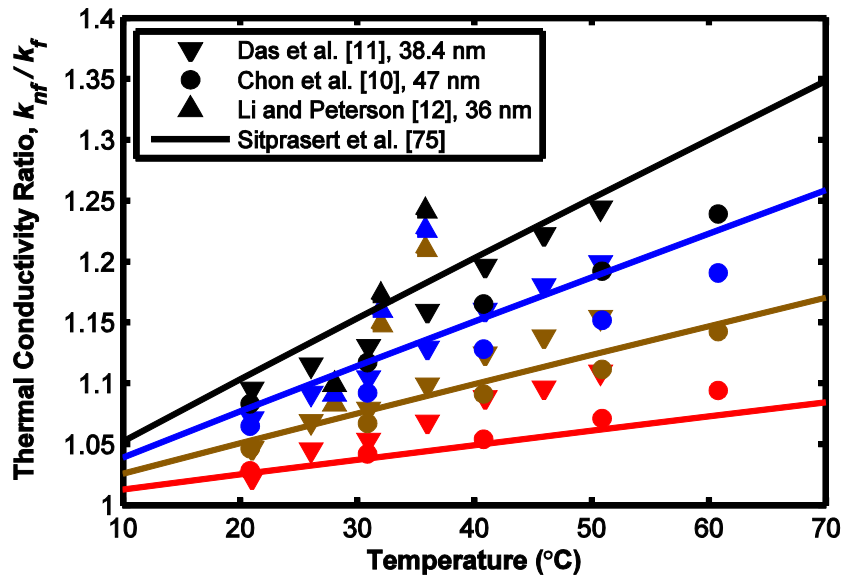


**Figure 11.** Comparison of the experimental results of the thermal conductivity ratio for  $\text{Al}_2\text{O}_3/\text{water}$  nanofluid with Sitprasert et al. model [75] as a function temperature at various values of particle volume fraction. Colors indicate different values of particle volume fraction; red 1%, brown 2%, blue 3%, and black 4%.

Predictions of Sitprasert et al. model [75] is shown in Fig. 11. The model predicts linear variation of thermal conductivity ratio with increasing temperature. It should be noted that the effect of particle volume fraction dramatically increases with temperature and starts to overpredict the rate of thermal conductivity increase with particle volume fraction. Since the temperature dependence of thermal conductivity is introduced to the model empirically, it is possible to modify the associated expression in order to predict experimental data better [18].

## 2.4. Concluding Remarks

This chapter summarized the research in nanofluid thermal conductivity. Both experimental and theoretical investigations were reviewed and theoretical models were compared with the experimental findings.

Results show that there exists significant discrepancy in the experimental data. Effect of particle size on the thermal conductivity of nanofluids has not been completely understood yet. It is expected that Brownian motion of nanoparticles results in higher thermal conductivity enhancement with smaller particle size. However, some of the experiments show that the thermal conductivity decreases with decreasing particle size. This contradiction might be due to the uncontrolled clustering of nanoparticles resulting in larger particles [18]. Particle size distribution of nanoparticles is another important factor and it is suggested that average particle size is not sufficient to characterize a nanofluid due to the nonlinear relations involved between particle size and thermal transport. It is also known that particle shape is effective on the thermal conductivity. Since cylindrical and rod-shaped particles offer higher enhancement when compared to spherical particles, more research should be made for the investigation of the performance of such particles when compared to spherical particles [18].

An important reason of discrepancy in experimental data is the clustering of nanoparticles. Although there are no universally accepted quantitative values, it is known that the level of clustering affects the thermal conductivity of nanofluids [58]. Since level of clustering is related to the pH value and the additives used, two nanofluid samples with all of the parameters being the same can lead to completely different experimental results if their surfactant parameters and pH values are not the same [18]. Therefore, the researchers providing experimental results should give detailed information about the additives utilized and pH values of the samples.

In addition to these, the duration and the intensity of the vibration applied to the nanofluid samples significantly affect thermal conductivity. Therefore, in order to prevent associated complications about the experimental results,



researchers should clearly specify the procedures associated with the application of vibration to the samples.

Temperature dependence is an important parameter in the thermal conductivity of nanofluids. Limited study has been done about this aspect of the thermal conductivity of nanofluids up to now. Investigation of the thermal performance of nanofluids at high temperatures may widen the possible application areas of nanofluids.

When the application of nanofluids is considered, two important issues are erosion and settling. Before commercialization of nanofluids, possible problems associated with these issues should be investigated and solved. It should also be noted that, increase in viscosity by the use nanofluids is an important drawback due to the associated increase in pumping power. Therefore, further experimental research is required in that area in order to determine the feasibility of nanofluids.

In order to predict the thermal conductivity of nanofluids, many theoretical models have been developed recently. However, there is still controversy about the underlying mechanisms of the thermal conductivity enhancement of nanofluids. As a result of this, none of the theoretical models are able to completely explain the thermal conductivity enhancement in nanofluids [18]. On the other hand, some researchers report experimental data of thermal conductivity that is consistent with the predictions of the classical models (such as Hamilton and Crosser model [44]). Consequently, further work is required in theoretical modeling of heat transport in nanofluids as well.

## CHAPTER 3

### CONVECTIVE HEAT TRANSFER WITH NANOFLUIDS – LITERATURE SURVEY AND THEORETICAL ANALYSIS

#### 3.1. Introduction

Nanofluids are promising heat transfer fluids due to the high thermal conductivity enhancements obtained. Thermal conductivity of nanofluids has been discussed in Chapter 2 in detail. In order to utilize nanofluids in practical applications, their convective heat transfer characteristics need to be understood. For that purpose, many researchers investigate the convective heat transfer performance of nanofluids. In this chapter, the discussion is focused on forced convection of nanofluids inside circular tubes.

In the first part of the chapter, a literature survey of the studies about the forced convection heat transfer with nanofluids is presented. Experimental, theoretical and numerical studies are presented in separate sections.

In the second part of the chapter, the validity of the application of classical heat transfer correlations for the analysis of nanofluid convective heat transfer is examined by comparing the associated results with the experimental data in the literature. In the analysis, laminar flow of the nanofluid inside a straight circular tube under both constant wall temperature and constant wall heat flux boundary conditions is considered. In addition, the effect of thermal conductivity of nanofluids on fully developed heat transfer is discussed.

#### 3.2. Literature Survey

There are many studies in the literature regarding the convective heat transfer with nanofluids. In this literature survey, the discussion focuses on forced convection of nanofluids in circular tubes.

### 3.2.1. Experimental Studies

Pak and Cho [13] investigated the convective heat transfer of  $\text{Al}_2\text{O}_3$ (13 nm)/water and  $\text{TiO}_2$ (27 nm)/water nanofluids in the turbulent flow regime (values in parenthesis indicate particle diameter). Constant wall heat flux boundary condition was considered in the analysis. Heat transfer enhancement as high as 75% was obtained by using  $\text{Al}_2\text{O}_3$ /water nanofluid with a particle volume fraction of 2.78%. It was indicated that the heat transfer enhancement obtained with  $\text{Al}_2\text{O}_3$  particles is higher than that obtained with  $\text{TiO}_2$  particles.

Li and Xuan [106] examined the heat transfer performance of Cu/water nanofluid in both laminar and turbulent flow regimes by utilizing constant wall heat flux boundary condition and observed enhancements up to 60%. It was seen that the heat transfer coefficient enhancement ratio (heat transfer coefficient of nanofluid divided by the heat transfer coefficient of base fluid) increases with increasing Reynolds number. The researchers related this increase to the thermal dispersion phenomenon which is explained in the following section.

Chen et al. [107] used  $\text{TiO}_2$  nanotubes in their investigation. The diameter of the nanotubes was about 10 nm whereas their length was around 100 nm. Water was used as the base fluid. Laminar flow in a circular tube under constant wall heat flux boundary condition was considered in the analysis. It was noted that the local convective heat transfer coefficient decreased in the axial direction and reached a nearly constant value around  $800 \text{ W/m}^2\text{K}$  for  $\text{Re} = 1700$ . There was not much change in this value for different particle weight fractions (0.5%, 1%, 2.5%).

Kulkarni et al. [108] performed experiments regarding the heat transfer performance of  $\text{SiO}_2$ /water-ethylene glycol mixture nanofluid in turbulent flow regime under constant wall heat flux boundary condition. The researchers examined the effect of particle size, and they indicated that heat transfer enhancement increases with increasing particle size.

$\text{Al}_2\text{O}_3$ /water nanofluids are widely utilized for the experimental investigations of heat transfer of nanofluids due to their relatively easier

production and low cost. Wen and Ding [101], Hwang et al. [14], Anoop et al. [109] and Kim et al. [110] investigated these nanofluids for the case of laminar flow under constant wall heat flux boundary condition. Wen and Ding [101] performed the associated analysis by varying the particle volume fraction between 0.6% and 1.6%. Nanofluids used in the analysis had a particle size distribution between 27 and 56 nm. The researchers obtained increasing heat transfer enhancement with increasing particle volume fraction and Reynolds number. It was noted that local heat transfer coefficient enhancement ratio is higher at the entrance of the tube. Another observation was that the nanofluids thermally develop more slowly when compared to pure fluids. Hwang et al. [14] investigated  $\text{Al}_2\text{O}_3$  (30 nm) nanofluids at relatively lower particle volume fractions (between 0.01% and 0.3%) and showed that heat transfer enhancement is still significant (8%) at low particle volume fractions (0.3%). Contrary to the results of other researchers, Hwang et al. did not observe an increase in heat transfer coefficient enhancement with increasing Reynolds number. Anoop et al. [109] also investigated  $\text{Al}_2\text{O}_3$ /water nanofluids but focused on the effect of particle size on heat transfer enhancement by considering 45 and 150 nm particles. They observed that higher enhancement can be obtained with 45 nm particles when compared to the 150 nm case. When analyzing the heat transfer of  $\text{Al}_2\text{O}_3$ /water nanofluids, Kim et al. [110] also considered the turbulent flow. 15% and 20% heat transfer coefficient enhancements were observed for 3 vol.%  $\text{Al}_2\text{O}_3$ /water nanofluid, for laminar and turbulent flow, respectively.

Heris et al. [15] investigated the laminar flow of  $\text{Al}_2\text{O}_3$ (20 nm)/water nanofluid and instead of the commonly analyzed constant wall heat flux boundary condition, they considered the constant wall temperature boundary condition. Similar to the findings of Li and Xuan [106] and Wen and Ding [101], they observed increasing heat transfer enhancement with increasing Peclet number. In addition, it was noted that the enhancement values increase with increasing particle volume fraction. In another study, Heris et al. [16] compared the heat transfer performance of  $\text{Al}_2\text{O}_3$ /water and  $\text{CuO}$ /water nanofluids. They observed that the heat transfer enhancement obtained with  $\text{Al}_2\text{O}_3$  nanoparticles is higher

than that obtained with CuO nanoparticles. For example, at a Peclet number of 5000, heat transfer coefficient enhancement ratio was 1.29 for 2.5 vol.% Al<sub>2</sub>O<sub>3</sub>/water nanofluid whereas it was 1.23 for CuO/water nanofluid for the same particle volume fraction. Maximum enhancement ratio was observed around  $Pe = 6000$  for 3 vol.% Al<sub>2</sub>O<sub>3</sub>/water nanofluid, which is 1.37.

There are many other experimental studies in the literature about the convective heat transfer of nanofluids. Two comprehensive reviews of these studies were performed by Kakaç and Pramuanjaroenkij [111] and Godson et al. [112]. When the experimental studies in the literature are examined, the general trend is that the heat transfer enhancement obtained with nanofluids exceeds the enhancement due to the thermal conductivity enhancement. This fact indicates that there should be additional mechanisms of heat transfer enhancement with nanofluids. There are numerous theoretical studies in the literature that propose such heat transfer enhancement mechanisms and some of these studies are summarized below.

### **3.2.2. Theoretical Studies**

Xuan and Roetzel [17] proposed two approaches for the heat transfer analysis of nanofluids. In the first method, it is assumed that the presence of nanoparticles in the flow affects the heat transfer only through the altered thermophysical properties. Then the governing equations of fluid flow and heat transfer for a pure fluid can be utilized for the analysis of nanofluids by substituting the associated thermophysical properties. This also means that the classical correlations of convective heat transfer for pure fluids can be used for nanofluids. In the second method, the nanofluid is still treated as a single phase fluid but the additional heat transfer enhancement obtained with nanofluids is considered by modeling the dispersion phenomenon. It was noted that thermal dispersion occurs in nanofluid flow due to the random motion of nanoparticles. By considering the fact that this random motion creates small perturbations in velocity and temperature, the

researchers showed that the effective thermal conductivity in the governing energy equation takes the following form.

$$k_{eff} = k_{nf} + k_d. \quad (71)$$

$k_{nf}$  is the thermal conductivity of the nanofluid.  $k_d$  is dispersed thermal conductivity and it was proposed that it can be calculated by using the following expression.

$$k_d = C(\rho c_p)_{nf} u_x \phi d_p r_0. \quad (72)$$

In this relation,  $\rho$  is density,  $c_p$  is specific heat,  $u_x$  is axial velocity,  $\phi$  is particle volume fraction,  $d_p$  is nanoparticle diameter, and  $r_0$  is tube radius.  $C$  is an empirical constant that should be determined by matching experimental data. Subscript  $nf$  indicates the nanofluid. In another study, based on this thermal dispersion model, following correlation was proposed by Li and Xuan [106] for the determination of Nusselt number.

$$Nu_{nf} = c_1 \left( 1 + c_2 \phi^{m_1} Pe_d^{m_2} \right) Re_{nf}^{m_3} Pr_{nf}^{0.4}. \quad (73)$$

It was noted that the provided correlation can be used for the heat transfer prediction of the forced convection of nanofluid flow inside circular tubes.  $Pe_d$  is particle Peclet number, which is defined as

$$Pe_d = \frac{u_m d_p}{\alpha_{nf}}. \quad (74)$$

$u_m$  is mean flow velocity and  $\alpha_{nf}$  is nanofluid thermal diffusivity.  $Re_{nf}$  and  $Pr_{nf}$  are the conventional Reynolds and Prandtl numbers, but the thermophysical properties of the nanofluid should be used in the associated calculations.  $c_1$ ,  $c_2$ ,  $m_1$ ,  $m_2$ , and  $m_3$  are empirical constants that should be determined by using experimental data.

Another theoretical analysis of nanofluid heat transfer was performed by Ding and Wen [113]. The researchers focused on the particle migration caused by shear, viscosity gradient and Brownian motion. They showed that the particle volume fraction decreases in radial direction for the flow of a nanofluid in a circular tube, which results in a nonuniform distribution of thermophysical properties in the radial direction. It was noted that this variation of thermophysical

properties in radial direction alters both temperature and velocity distribution in the flow and this fact was proposed to be an effective mechanism of heat transfer enhancement of nanofluids.

An important issue for the analysis of nanofluids is the slip motion between nanoparticles and fluid molecules. Buongiorno [114] analyzed the effect of thermal dispersion by considering seven slip mechanisms and indicated that the Brownian motion and thermophoresis are dominant among these mechanisms. Through a nondimensional analysis, Buongiorno also proposed that the slip motion of nanoparticles does not directly affect the thermal transport in the flow but it results in particle migration. It was noted that radial distribution of thermophysical properties in the flow changes due to this particle migration, and temperature gradients and thermophoresis further increase thermophysical property gradients in the flow. It was indicated that this phenomena might explain the extra heat transfer enhancement obtained with nanofluids. Buongiorno provided four partial differential equations for the analysis of nanofluid heat transfer by considering the problem as a two-phase flow. Associated equations are continuity equation for nanoparticles, continuity equation for nanofluid, momentum equation for nanofluid and energy equation for nanofluid. Similar to the findings of Buongiorno [114], Hwang et al. [14] noted that the change in the fully developed velocity profile in a circular tube due to the variation of viscosity in radial direction improves convective heat transfer of nanofluids.

For the proper analysis of nanofluid heat transfer, accurate estimation of thermophysical properties of the nanofluid is very important. In order to stress the importance of this issue, Mansour et al. [115] studied the effect of utilizing different correlations for the determination of the thermophysical properties of nanofluids on the results of the thermal performance analyses of nanofluids. Throughout the analysis, fully developed condition was examined for both laminar and turbulent flow cases and nanofluids were considered as single phase fluids. Different expressions used in the literature for the determination of specific heat, dynamic viscosity and thermal conductivity were presented and discrepancy between them was illustrated. Then the analyses of pressure drop and heat transfer

of a simple configuration were performed by utilizing two different sets of correlations for the determination of the aforementioned properties. Results were determined for different particle volume fractions, and it was shown that the two cases provided different results. For laminar flow condition, the results were contradictory not only quantitatively but also qualitatively. As a result of these observations, it was concluded that the choice of the correlations for the determination of the thermophysical properties is a key issue in nanofluid heat transfer analysis.

In this part of the literature survey, proposed mechanisms of heat transfer enhancement of nanofluids were discussed and a study that indicates the importance of accurate determination of thermophysical properties was summarized. It is seen that there are both single phase and two-phase models proposed for the analysis of nanofluid heat transfer. Numerical study is a proper tool in order to examine the validity of these models and as a consequence, many researchers investigated the heat transfer performance of nanofluids numerically. In the following section, some of the numerical studies are summarized.

### **3.2.3. Numerical Studies**

Maïga et al. [116] investigated laminar and turbulent nanofluid flow inside circular tubes.  $\text{Al}_2\text{O}_3/\text{water}$  and  $\text{Al}_2\text{O}_3/\text{ethylene glycol}$  nanofluids were considered under the constant wall heat flux boundary condition. In the analysis, they assumed nanofluids as single phase fluids and the effect of nanoparticles was taken into account only through the substitution of the thermophysical properties of the nanofluids into the governing equations. As a result of the analysis, it was concluded that  $\text{Al}_2\text{O}_3/\text{ethylene glycol}$  nanofluid provides higher enhancement when compared to  $\text{Al}_2\text{O}_3/\text{water}$  nanofluid.

Another single phase analysis of nanofluid heat transfer was made by Heris et al. [117]. They performed a numerical analysis that simulates their experimental study [15] by utilizing the thermal dispersion model proposed by Xuan and Roetzel [17]. In the analysis, they did not take the variation of thermal



conductivity with temperature into account. Furthermore, they assumed uniform thermal dispersion throughout the domain. The researchers considered the effect of particle volume fraction and particle size on heat transfer and concluded that increasing particle volume fraction and decreasing particle size increase the heat transfer enhancement.

There are also numerical studies that consider two-phase approach in the literature. Behzadmehr et al. [118] investigated the flow of a nanofluid in a circular tube at turbulent regime. A numerical solution was made for the constant wall heat flux boundary condition and the difference between the velocities of the nanoparticles and fluid molecules was taken into account. The results of the numerical solution were compared with a previous experimental study of Cu/water nanofluids [106] and good agreement was observed. The researchers also compared the results of single phase assumption with experimental data and it was seen that single phase approach failed to predict the associated Nusselt number values.

Bianco et al. [119] considered the laminar flow of  $\text{Al}_2\text{O}_3$ /water nanofluid. Under constant wall heat flux boundary condition, they analyzed the problem by using both single phase and two-phase approaches. They indicated that taking the variation of thermophysical properties with temperature into account results in higher enhancement values. Furthermore, they noted that the difference between the results of single phase and two-phase approaches is small, especially when temperature dependence of thermophysical properties is taken into account. This is an important result which can be considered as an indication of the fact that the single phase assumption provides acceptable results.

There are many other numerical studies about nanofluids in the literature. Wang and Mujumdar [120] provide a summary of those numerical studies and also review some theoretical studies regarding the convective heat transfer of nanofluids.

### 3.3. Thermophysical Properties of Nanofluids

In the analysis of convective heat transfer of nanofluids, accurate determination of the thermophysical properties is a key issue. Calculations of density and specific heat of nanofluids are relatively straightforward, but when it comes to viscosity and thermal conductivity, there is significant discrepancy in both experimental results and theoretical models available in the literature.

#### 3.3.1. Density

Density of nanofluids can be determined by using the following expression [13].

$$\rho_{nf} = \phi\rho_p + (1-\phi)\rho_f . \quad (75)$$

Here,  $\phi$  is particle volume fraction and subscripts  $nf$ ,  $p$ , and  $f$  correspond to nanofluid, particle, and base fluid, respectively. Pak and Cho [13] experimentally showed that Eq. (75) is an accurate expression for determining the density of nanofluids.

#### 3.3.2. Specific Heat

There are two expressions for determining the specific heat of nanofluids [13,17]:

$$c_{p,nf} = \phi c_{p,p} + (1-\phi)c_{p,f} , \quad (76)$$

and

$$(\rho c_p)_{nf} = \phi(\rho c_p)_p + (1-\phi)(\rho c_p)_f . \quad (77)$$

It is thought that Eq. (77) is theoretically more consistent since specific heat is a mass specific quantity whose effect depends on the density of the components of a mixture.

#### 3.3.3. Viscosity

Nanofluid viscosity is an important parameter for practical applications since it directly affects the pressure drop in forced convection. Therefore, for enabling the

usage of nanofluids in practical applications, the extent of viscosity increase of nanofluids with respect to pure fluids should be thoroughly investigated. At present, research on viscosity is limited in the literature when compared with the research related to the thermal conductivity of nanofluids. In the following two sections, experimental research activities regarding the viscosity of nanofluids are summarized and some theoretical models of nanofluid viscosity are discussed.

### **3.3.3.1. Experimental Studies**

Similar to the case of thermal conductivity, there is significant discrepancy in the experimental results regarding the viscosity of nanofluids. Nevertheless, the general trend is that the increase in the viscosity by the addition of nanoparticles to the base fluid is significant. For example, Wang et al. [28] considered the viscosity of Al<sub>2</sub>O<sub>3</sub>/ethylene glycol nanofluid at room temperature. For the particle volume fraction of 3.5%, 40% increase in viscosity was observed. Nguyen et al. [121] measured the viscosity of 4.0 vol.% Al<sub>2</sub>O<sub>3</sub>/water nanofluid and reported 60% and 50% increase at room temperature and at 60°C, respectively. For the nanofluids prepared by using carbon nanotubes, the associated increase in viscosity is even higher. Chen et al. [122] considered the viscosity of 1.0 vol.% CNT/water nanofluid at room temperature and indicated an increase of 34%.

It is known that nanofluid viscosity depends on many parameters such as; particle volume fraction, particle size, temperature, and extent of clustering. Increasing particle volume fraction increases viscosity and this was validated by many studies [47,121,123,124]. When it comes to the effect of particle size, there are different results in the literature. Prasher et al. [125] indicated that nanofluid viscosity does not change significantly with particle size. On the other hand, Nguyen et al. [121] observed increasing viscosity with increasing particle size whereas Pastoriza-Gallego et al. [126] reported decreasing viscosity with increasing particle size. Nguyen et al. also analyzed the effect of temperature on viscosity and observed a decrease in viscosity with increasing temperature. In

addition, they noted that the temperature dependence of viscosity significantly increases with particle volume fraction.

Two phenomena observed in nanofluid research should also be mentioned in this section. First phenomenon is the shear thinning of nanofluids, which was indicated by several researchers [24,123,124]. Shear thinning is advantageous for practical applications since shear rate is higher at the boundaries of a flow which results in decreased viscosity at the channel wall which decreases the associated pressure drop. However, there are also some researchers that observed Newtonian behavior of nanofluid viscosity. Further research is required in this area for obtaining a better understanding about the rheology of nanofluids.

Second phenomenon that needs clarification is the hysteresis phenomenon in nanofluid viscosity which is observed by Nguyen et al. [121]. Nguyen et al. showed that after exceeding some critical temperature, viscosity characteristics of nanofluids changes irreversibly. For example, viscosity of 7 vol.% Al<sub>2</sub>O<sub>3</sub>/water nanofluid at 55°C was measured, and the sample was heated up to 72°C, then it was cooled back to 55°C and it was observed that the viscosity was doubled. Since such a behavior may limit the practical application of nanofluids to a specific temperature range, further research is required also in this area.

The general trend in available experimental data is that the increase in viscosity with the addition of nanoparticles into the base fluid is larger than the theoretical predictions obtained by using conventional theoretical models. Some of these conventional models together with some recent expressions proposed for the determination of the viscosity of nanofluids are briefly discussed in the next section.

### 3.3.3.2. Theoretical Models

Einstein [98] proposed an expression for determining the dynamic viscosity of dilute suspensions that contain spherical particles. In the model, the interactions between the particles are neglected. The associated expression is as follows.

$$\mu_{nf} = (1 + 2.5\phi)\mu_f. \quad (78)$$

Some of the later research considered the fact that viscosity should increase unboundedly as particle volume fraction reaches its maximum. For example, Brinkman [127] suggested the following equation.

$$\mu_{nf} = \frac{1}{(1-\phi)^{2.5}} \mu_f . \quad (79)$$

In some studies, the interactions between particles were taken into account. These attempts widened the applicability range of the models in terms of particle volume fraction. An example of such an improvement is the study of Batchelor [128].

$$\mu_{nf} = (1 + 2.5\phi + 6.2\phi^2) \mu_f . \quad (80)$$

Although these models are frequently used in nanofluid research, it was shown that they underpredict the viscosity of nanofluids [121]. An empirical correlation proposed by Nguyen et al. [121] for Al<sub>2</sub>O<sub>3</sub>/water nanofluids is:

$$\mu_{nf} = (1 + 2.5\phi + 150\phi^2) \mu_f . \quad (81)$$

The above correlation is valid for the nanofluids with a particle size of 36 nm. Experimental studies show that particle size is an important parameter that affects the viscosity of nanofluids. However, at present, it is difficult to obtain a consistent set of experimental data for nanofluids that covers a wide range of particle size and particle volume fraction. Therefore, for the time being, Eq. (81) can be used as an approximation for Al<sub>2</sub>O<sub>3</sub>/water nanofluids with different particle sizes. When it comes to temperature dependence of viscosity, Nguyen et al. [121] showed that for particle volume fractions below 4%, viscosity enhancement ratio (viscosity of nanofluid divided by the viscosity of base fluid) does not significantly change with temperature.

Some recent theoretical formulations developed especially for nanofluids were listed by Yu et al. [129]. The equations are provided in Table 3 together with their applicable nanofluid type.

**Table 3.** Viscosity models for nanofluids [129]

Tseng and Lin [130], TiO <sub>2</sub> /water nanofluids
$\mu_{nf} = 13.47e^{35.98\phi} \mu_f$
Maïga et al. [116], Al <sub>2</sub> O <sub>3</sub> /water nanofluids
$\mu_{nf} = (1 + 7.3\phi + 123\phi^2) \mu_f$
Maïga et al. [116], Al <sub>2</sub> O <sub>3</sub> /ethylene glycol nanofluids
$\mu_{nf} = (1 - 0.19\phi + 306\phi^2) \mu_f$
Koo and Kleinstreuer (2005), CuO based nanofluids
$\mu_{eff} = \mu_f + 5 \times 10^4 \beta \rho_f \phi \sqrt{\frac{\kappa_B T}{2 \rho_p r_p}} [(-134.63 + 1722.3\phi) + (0.4705 - 6.04\phi)T]$
where
$\beta = \begin{cases} 0.0137(100\phi)^{-0.8229} & \text{for } \phi < 0.01 \\ 0.0011(100\phi)^{-0.7272} & \text{for } \phi > 0.01 \end{cases}$
$\kappa_B$ is Boltzmann constant, $T$ is temperature in K, $r_p$ is nanoparticle radius in m.
Kulkarni et al. [123], CuO/water nanofluids
$\mu_{nf} = \exp[-(2.8751 + 53.548\phi - 107.12\phi^2) + (1078.3 + 15857\phi + 20587\phi^2)(1/T)]$

### 3.3.4. Thermal Conductivity

Thermal conductivity of nanofluids is discussed in detail in Chapter 2. In the numerical analysis presented in Chapters 4 and 5, the model proposed by Chon et al. [10] is used for the determination of thermal conductivity of nanofluids. The model is an empirical correlation based on the experimental data of Al<sub>2</sub>O<sub>3</sub>/water nanofluids:

$$\frac{k_{nf}}{k_f} = 1 + 64.7\phi^{0.7460} \left(\frac{d_f}{d_p}\right)^{0.3690} \left(\frac{k_p}{k_f}\right)^{0.7476} \text{Pr}^{0.9955} \text{Re}^{1.2321}. \quad (82)$$

Here,  $d_f$  is the diameter of the fluid molecules. Prandtl number and Reynolds number are defined as follows.

$$\text{Pr} = \frac{\mu_f}{\rho_f \alpha_f}, \quad (83)$$

$$\text{Re} = \frac{\rho_f V_{Br} d_p}{\mu_f}. \quad (84)$$

$\alpha_f$  is the thermal diffusivity of the base fluid.  $V_{Br}$  is the Brownian velocity of the nanoparticles and it is calculated by using the following expression.

$$V_{Br} = \frac{\kappa_B T}{3\pi\mu_f d_p \lambda_f}. \quad (85)$$

$\kappa_B$  is Boltzmann constant and  $T$  is temperature in K.  $\lambda_f$  is mean-free path of the fluid molecules, and it is 0.17 nm for water. The validity range of the correlation is between 11 nm and 150 nm for particle diameter, 1% and 4% for particle volume fraction, and 21°C and 71°C for temperature.

### 3.4. Theoretical Analysis

#### 3.4.1. Introduction

Accurate theoretical analysis of convective heat transfer of nanofluids is very important for the practical application of nanofluids in thermal devices. One approach proposes that the analysis can be made by assuming the nanofluid flow as single phase since the nanoparticles are very small and they fluidize easily [116]. One may further assume that the presence of nanoparticles does not affect the convective heat transfer characteristics of the flow, which is defined by the dimensionless temperature distribution. Then the heat transfer performance of nanofluids can be analyzed by using classical correlations developed for the determination of Nusselt number for the flow of pure fluids. In the calculations, one should substitute the thermophysical properties of the nanofluid to the associated expressions. This approach is a very practical way of analyzing convective heat transfer of nanofluids. By comparing the results of such an analysis with the experimental data available in the literature, one can examine the validity of the approach. It should be noted that if the approach provides

sufficiently accurate results, it significantly eases the analysis of nanofluid heat transfer.

In the following two sections, Section 3.4.2.1 and 3.4.2.2, the above described approach of using classical correlations; such as Shah [131] and Sieder-Tate [132] correlations, for nanofluid heat transfer analysis is applied to the laminar nanofluid flow through a straight circular tube. In addition, a correlation by Li and Xuan [106] among those developed for the analysis of nanofluid convective heat transfer is also examined by comparing its predictions with experimental data.

Section 3.4.3 is focused on the effect of thermal conductivity of nanofluids on the fully developed heat transfer coefficient values. Both constant wall temperature and constant wall heat flux boundary conditions are considered in the analysis.

### 3.4.2. Heat Transfer Coefficient Enhancement

The theoretical study of heat transfer coefficient enhancement obtained with nanofluids is presented in two parts, according to the type of the boundary condition, namely; constant wall heat flux boundary condition and constant wall temperature boundary condition.

#### 3.4.2.1. Constant Wall Heat Flux Boundary Condition

One of the most commonly used empirical correlations for the determination of convective heat transfer in laminar flow regime inside circular tubes is the Shah correlation [131]. The associated expression for the calculation of local Nusselt number is as follows.

$$\begin{aligned}
 Nu_x &= 1.302x_*^{-1/3} - 1 && \text{for } x_* \leq 5 \times 10^{-5} \\
 &1.302x_*^{-1/3} - 0.5 && \text{for } 5 \times 10^{-5} < x_* \leq 1.5 \times 10^{-3} \\
 &4.364 + 0.263x_*^{-0.506} e^{-41x_*} && \text{for } x_* > 1.5 \times 10^{-3}
 \end{aligned} \tag{86}$$

$x_*$  is defined as follows.



$$x_* = \frac{x/d}{\text{Re Pr}} = \frac{x/d}{Pe} = \frac{1}{Gz_x}. \quad (87)$$

Re, Pr and  $Pe$  are Reynolds number, Prandtl number and Peclet number, respectively.  $d$  is tube diameter and  $x$  is axial position. At this point, it should be noted that for the same tube diameter and same flow velocity,  $Pe_f$  and  $Pe_{nf}$  are different.

$$\frac{Pe_{nf}}{Pe_f} = \frac{\alpha_f}{\alpha_{nf}} = \frac{k_f}{k_{nf}} \frac{\rho_{nf}}{\rho_f} \frac{c_{p,nf}}{c_{p,f}}. \quad (88)$$

Enhancement in density and specific heat increases  $Pe_{nf}$  whereas thermal conductivity increase results in a decrease in  $Pe_{nf}$ . Therefore, when the pure working fluid in a system is replaced with a nanofluid, the flow velocity should be adjusted in order to operate the system at the same Peclet number. In this part of the study, heat transfer enhancements obtained with nanofluids are calculated by comparing the associated results with the pure fluid case for the same flow velocity and tube diameter, so that the effect of the change in Peclet number is also examined.

In order to examine the heat transfer enhancement obtained with nanofluids for the same flow velocity, axial position, and tube diameter, one can use Eq. (86) and obtain the local Nusselt number enhancement ratio.

$$\begin{aligned} \frac{Nu_{x,nf}}{Nu_{x,f}} &= \frac{1.302x_{*,nf}^{-1/3} - 1}{1.302x_{*,f}^{-1/3} - 1} && \text{for } x_* \leq 5 \times 10^{-5} \\ &\frac{1.302x_{*,nf}^{-1/3} - 0.5}{1.302x_{*,f}^{-1/3} - 0.5} && \text{for } 5 \times 10^{-5} < x_* \leq 1.5 \times 10^{-3}. \\ &\frac{4.364 + 0.263x_{*,nf}^{-0.506} e^{-41x_{*,nf}}}{4.364 + 0.263x_{*,f}^{-0.506} e^{-41x_{*,f}}} && \text{for } x_* > 1.5 \times 10^{-3} \end{aligned} \quad (89)$$

It should be noted that the increases in the density and specific heat of the nanofluid increase values of the terms with  $x_{*,nf}$  in Eq. (89), which increases local Nusselt number enhancement ratio. On the other hand, increase in the thermal conductivity of the nanofluid decreases values of the terms with  $x_{*,nf}$ , and the local Nusselt number enhancement ratio decreases as a consequence. One can integrate the numerator and denominator of Eq. (89) along the tube and obtain the average

Nusselt number enhancement ratio for a specific case. The effects of thermophysical properties on average Nusselt number enhancement ratio are qualitatively the same as the local Nusselt number case. For a pure fluid, average heat transfer coefficient can be defined as follows.

$$h_f = \frac{Nu_f k_f}{d}. \quad (90)$$

For a nanofluid, average heat transfer coefficient becomes the following expression.

$$h_{nf} = \frac{Nu_{nf} k_{nf}}{d}. \quad (91)$$

By using Eqs. (90, 91), one can obtain the average heat transfer coefficient enhancement ratio as follows.

$$\frac{h_{nf}}{h_f} = \frac{k_{nf}}{k_f} \frac{Nu_{nf}}{Nu_f}. \quad (92)$$

One should use Eq. (89) and perform the associated integrations for calculating average Nusselt number enhancement ratio in Eq. (92). Although the increase in thermal conductivity of the nanofluid decreases Nusselt number enhancement ratio, due to the multiplicative effect of thermal conductivity in the definition of heat transfer coefficient, it is expected that the increase in the thermal conductivity of the nanofluid improves heat transfer coefficient enhancement ratio.

In order to examine the validity of the usage of the Shah correlation for the determination of nanofluid heat transfer in laminar flow, the average heat transfer coefficient enhancement ratio is calculated by using Eqs. (89, 92) and the results are compared with the experimental data of Li and Xuan [106]. For the determination of thermophysical properties, Eqs. (75, 77) and experimental data of Li and Xuan [87] are used. Li and Xuan [106] investigated the convective heat transfer of Cu/water nanofluids for different particle volume fractions between 0.3% and 2%. Reynolds number was varied between 800 and 2300 for laminar flow. Fig. 12 provides a comparison between the results of Shah correlation and the experimental results in terms of the variation of average heat transfer coefficient enhancement ratio with base fluid Reynolds number. In this figure, it is

seen that Shah correlation underpredicts the experimental data. Furthermore, it cannot predict the increasing enhancement of experimental data with Reynolds number and indicates nearly the same enhancement ratios for different Reynolds numbers. Therefore, for the determination of convective heat transfer of nanofluids, usage of such classical correlations seems to be not accurate for the present case.

For the constant wall heat flux boundary condition, another approach is to use a recent correlation proposed by Li and Xuan [106], which may predict the heat transfer enhancement of nanofluids better. The correlation they proposed for the determination of average Nusselt number for the forced convection of nanofluids inside circular tubes is based on the thermal dispersion model and it is in the following form.

$$Nu_{nf} = c_1 \left( 1 + c_2 \phi^{m_1} Pe_d^{m_2} \right) Re_{nf}^{m_3} Pr_{nf}^{0.4}. \quad (93)$$

$Pe_d$  is particle Peclet number which is defined as

$$Pe_d = \frac{u_m d_p}{\alpha_{nf}}. \quad (94)$$

$u_m$  is mean flow velocity.  $Re_{nf}$  and  $Pr_{nf}$  are the conventional Reynolds and Prandtl numbers, but the thermophysical properties of the nanofluid should be used. For constant wall heat flux boundary condition, Li and Xuan [106] provided the empirical constants  $c_1$ ,  $c_2$ ,  $m_1$ ,  $m_2$  and  $m_3$  based on their experimental study. The associated expression is the following.

$$Nu_{nf} = 0.4328 \left( 1 + 11.285 \phi^{0.754} Pe_d^{0.218} \right) Re_{nf}^{0.333} Pr_{nf}^{0.4}. \quad (95)$$

It can be said that Eq. (95) is valid in the range of the experimental data [106];  $800 < Re_{nf} < 2300$  and  $0.3\% < \phi < 2\%$ . It should also be noted that tube diameter is 1 cm and tube length is 0.8 m in the experiments. The predictions of Eq. (95) are also included in Fig. 12. In the figure, it is seen that Li and Xuan correlation correctly predicts the experimental data. This is mainly due to term with  $Pe_d$  in Eq. (95), which takes the thermal dispersion effect into account.

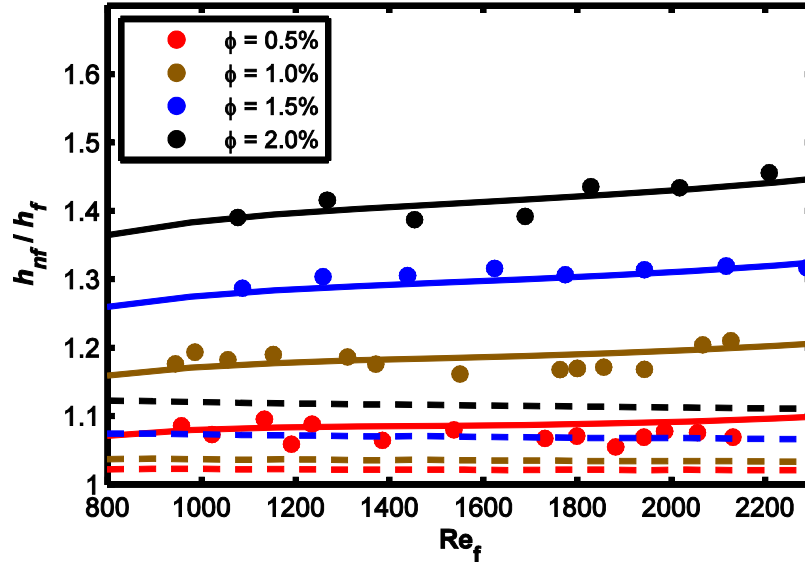


**Figure 12.** Variation of average heat transfer coefficient enhancement ratio with Reynolds number for different particle volume fractions of the Cu/water nanofluid. Markers: Experimental data of Li and Xuan [106]. Dashed lines: Predictions of Shah correlation [131] (integrated for determining average Nusselt number). Solid lines: Predictions of Li and Xuan correlation [106].  $Re_f$ : Reynolds number of the base fluid.

### 3.4.2.2. Constant Wall Temperature Boundary Condition

The approach followed in the previous section for constant wall heat flux boundary condition is repeated in this section for constant wall temperature boundary condition. For the determination of the average Nusselt number, one can use the classical Sieder-Tate correlation [132].

$$Nu = 1.86 \left( Pe \frac{d}{L} \right)^{1/3} \left( \frac{\mu_b}{\mu_w} \right). \quad (96)$$

Here  $L$  is tube length.  $\mu_w$  is dynamic viscosity at the wall temperature whereas  $\mu_b$  is dynamic viscosity at the bulk mean temperature which is defined as:

$$T_b = \frac{T_i + T_o}{2}. \quad (97)$$

$T_i$  is inlet temperature whereas  $T_o$  is outlet temperature. Neglecting the variation of viscosity enhancement ratio of the nanofluid ( $\mu_{nf} / \mu_f$ ) with temperature, and

applying Sieder-Tate correlation (Eq. 96) for a pure fluid and nanofluid, following expression can be obtained.

$$\frac{Nu_{nf}}{Nu_f} = \left( \frac{Pe_{nf}}{Pe_f} \right)^{1/3} = \left( \frac{k_f}{k_{nf}} \frac{\rho_{nf}}{\rho_f} \frac{c_{p,nf}}{c_{p,f}} \right)^{1/3}. \quad (98)$$

Using Eq. (92), heat transfer coefficient enhancement ratio becomes the following.

$$\frac{h_{nf}}{h_f} = \left( \frac{\rho_{nf}}{\rho_f} \frac{c_{p,nf}}{c_{p,f}} \right)^{1/3} \left( \frac{k_{nf}}{k_f} \right)^{2/3}. \quad (99)$$

By examining this expression, it can be observed that the enhancements in the thermophysical properties of the nanofluid; density, specific heat, and thermal conductivity, improve the heat transfer coefficient. It should be noted that the effect of thermal conductivity enhancement is more pronounced when compared to density and specific heat.

In order to examine the validity of Eq. (99) for the determination of heat transfer coefficient enhancement ratio of nanofluids, the predictions of this equation are compared with experimental data. There is very limited experimental data in the literature for laminar forced convection of nanofluids under the constant wall temperature boundary condition. Heris et al. [15] investigated constant wall temperature boundary condition for the flow of  $Al_2O_3$ /water nanofluid. Their test section consists of a straight circular tube with an inner diameter of 5 mm and length of 1 m. The nanoparticles used in the nanofluid have a diameter of 20 nm. Peclet number was varied between 2500 and 6500 and the heat transfer measurements were performed for different nanofluids with particle volumes fractions ranging between 0.2% and 2.5%. In Fig. 13, experimental results of Heris et al. [15] are provided in terms of the variation of average heat transfer coefficient enhancement ratio with base fluid Peclet number. In the figure, the predictions of the Sieder-Tate correlation are also included. For the determination of thermophysical properties, Eqs. (75, 77, 81, 82) are used. A sample calculation of the associated analysis is provided in Appendix A.1. It is observed that the Sieder-Tate correlation underpredicts the experimental data

significantly. Therefore, similar to the previous case of constant wall heat flux, direct application of such classical correlations for the analysis of nanofluid heat transfer seems to be not valid for constant wall temperature boundary condition. The associated underprediction shows that there should be additional enhancement mechanisms related to the convective heat transfer of nanofluids which further improve the heat transport.

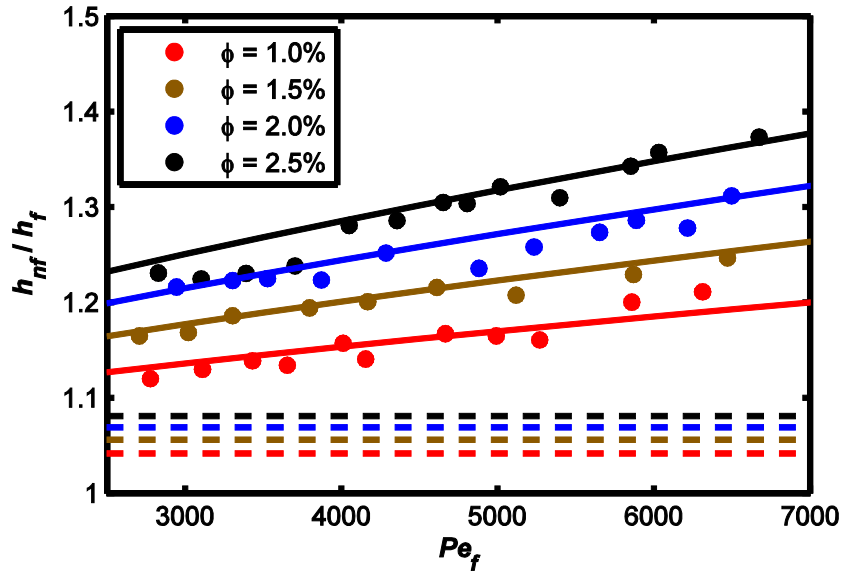


**Figure 13.** Variation of average heat transfer coefficient enhancement ratio with Pelet number for different particle volume fractions of the  $\text{Al}_2\text{O}_3/\text{water}$  nanofluid. Markers: Experimental data of Heris et al. [15]. Dashed lines: Predictions of Sieder-Tate correlation [132]. Solid lines: Predictions of Li and Xuan correlation [106].  $Pe_f$ : Pelet number of the base fluid.

The correlation proposed by Li and Xuan [106], which is discussed in the previous section (Eq. 93), was derived generally for forced convection of nanofluids inside circular tubes. Therefore, it can also be used to predict heat transfer of nanofluids when the boundary condition is constant wall temperature. However, Li and Xuan [106] did not provide the associated empirical constants for constant wall temperature boundary condition (see Eq. 93), since their experimental study only considers the constant wall heat flux boundary condition. For the present analysis, those constants are determined by fitting the

experimental data of Heris et al. [15]. Then the correlation becomes the following expression.

$$Nu_{nf} = 0.37(1 + 58\phi^{0.75} Pe_d^{0.72}) Re_{nf}^{0.333} Pr_{nf}^{0.4}. \quad (100)$$

The results of this correlation are provided in Fig. 13 as well. It is seen that the correlation correctly predicts the experimental data which indicates increasing enhancement with Peclet number. It can be said that Eq. (100) is valid in the range of the experimental data [15];  $2500 < Pe_{nf} < 3500$  and  $0.2\% < \phi < 2.5\%$ . It should also be noted that tube diameter is 5 mm and tube length is 1 m in the experiments.

### 3.4.3. Effect of Thermal Conductivity on Fully Developed Heat Transfer

In this additional section, effect of thermal conductivity of nanofluids on fully developed heat transfer coefficient values is investigated. Similar to the analysis in the previous sections, the nanofluid is treated as a pure fluid with enhanced thermophysical properties. Although this approach is shown to underestimate the experimental results in the previous sections, it can still be used to obtain a better understanding about the effect of thermal conductivity on heat transfer due to its simplicity.

As a result of the Graetz solution for parabolic velocity profile under constant wall temperature and constant wall heat flux boundary conditions, Nusselt number can be obtained as follows [133]:

$$Nu_x = \frac{h_x d}{k_{nf}} = \frac{\sum_{n=0}^{\infty} A_n e^{-\lambda_n^2 \xi}}{2 \sum_{n=0}^{\infty} \frac{A_n}{\lambda_n^2} e^{-\lambda_n^2 \xi}}, \text{ for constant wall temperature,} \quad (101)$$

$$Nu_x = \frac{h_x d}{k_{nf}} = \left[ \frac{11}{48} - \frac{1}{2} \sum_{n=1}^{\infty} \frac{e^{-\beta_n^2 \xi}}{A_n \beta_n^4} \right]^{-1}, \text{ for constant wall heat flux,} \quad (102)$$

where  $\xi = x / (r_0 Pe)$ .

These expressions are valid for the thermal entrance region of a circular pipe with hydrodynamically fully developed laminar nanofluid flow under the assumption

of treating nanofluids as pure fluids. Eigenvalues and coefficients in Eqs. (101, 102) are given in Kakaç and Yener [133]. Under the fully developed conditions, Nusselt number becomes:

$$Nu_{fd} = \frac{\lambda_0^2}{2} = \frac{(2.7043644)^2}{2} = 3.657, \text{ for constant wall temperature,} \quad (103)$$

$$Nu_{fd} = 4.364, \text{ for constant wall heat flux.} \quad (104)$$

In order to stress the importance of the accurate determination of the thermal conductivity of nanofluids, heat transfer coefficient of the laminar flow of Al<sub>2</sub>O<sub>3</sub>/water nanofluid inside a circular tube is investigated by using the abovementioned asymptotic values of Nusselt number. Nanoparticles are assumed to be spherical with a diameter of 38.4 nm. Two different temperatures are considered in the analysis; room temperature and 50°C. Flow is both hydrodynamically and thermally fully developed. Tube diameter is selected as 1 cm.

For the determination of the thermal conductivity of the nanofluids at room temperature, Hamilton and Crosser [44] model (Eqs. 2, 3) is utilized and fully developed heat transfer coefficients are determined. A sample calculation of this analysis is provided in Appendix A.2 for the 4 vol.% Al<sub>2</sub>O<sub>3</sub>/water nanofluid.

In Table 4, results of 1 and 4 vol.% Al<sub>2</sub>O<sub>3</sub>/water nanofluids are compared with pure water. As seen from the table, due to the definition of the Nusselt number ( $Nu = hd / k$ ), the enhancement in thermal conductivity by the use of nanofluids directly results in the enhancement in heat transfer coefficient.

At 50°C, thermal conductivity of the nanofluids is determined by using the model of Jang and Choi [82]. Additionally, experimental thermal conductivity data provided by Das et al. [11] is also included for comparison. The experimental data is also for Al<sub>2</sub>O<sub>3</sub>/water nanofluid with a particle size of 38.4 nm (spherical) at 50°C. In Table 5, results of 1 and 4 vol.% Al<sub>2</sub>O<sub>3</sub>/water nanofluids are compared with pure water. As seen in this table, there exists significant difference between the experimental and theoretical thermal conductivity data especially for the 1 vol.% case. This difference directly causes a discrepancy in the associated heat transfer coefficient values.



**Table 4.** Thermal conductivity and heat transfer coefficient values for pure water and Al<sub>2</sub>O<sub>3</sub>/water nanofluid, room temperature

	Pure Water	1 vol.% Al <sub>2</sub> O <sub>3</sub> /water	4 vol.% Al <sub>2</sub> O <sub>3</sub> /water
$k$ [W/mK]	0.6060	0.6223	0.6732
(Enhancement) <sup>a</sup>	(-)	(2.7%)	(11.1%)
$h_{fd}$ for Constant Wall Temperature [W/m <sup>2</sup> K]	221.6	227.6	246.2
(Enhancement)	(-)	(2.7%)	(11.1%)
$h_{fd}$ for Constant Wall Heat Flux [W/m <sup>2</sup> K]	264.5	271.6	293.8
(Enhancement)	(-)	(2.7%)	(11.1%)

<sup>a</sup> The percentage values indicated are according to the expression  $100(k_{nf} - k_f) / k_f$ .

**Table 5.** Thermal conductivity and heat transfer coefficient values for pure water and Al<sub>2</sub>O<sub>3</sub>/water nanofluid,  $T = 50^\circ\text{C}$

	Pure Water	Theoretical Model (Jang and Choi 2004)		Experimental Data (Das et al. 2003)	
		1 vol.% Al <sub>2</sub> O <sub>3</sub> /water	4 vol.% Al <sub>2</sub> O <sub>3</sub> /water	1 vol.% Al <sub>2</sub> O <sub>3</sub> /water	4 vol.% Al <sub>2</sub> O <sub>3</sub> /water
$k$ [W/mK]	0.6410	0.6750	0.7772	0.7109	0.7974
(Enhancement) <sup>a</sup>	(-)	(5.3%)	(21.2%)	(10.9%)	(24.4%)
$h_{fd}$ for Constant Wall Temperature [W/m <sup>2</sup> K]	234.4	246.9	284.2	260.0	291.6
(Enhancement)	(-)	(5.3%)	(21.2%)	(10.9%)	(24.4%)
$h_{fd}$ for Constant Wall Heat Flux [W/m <sup>2</sup> K]	279.7	294.6	339.2	310.2	348.0
(Enhancement)	(-)	(5.3%)	(21.2%)	(10.9%)	(24.4%)

<sup>a</sup> The percentage values indicated are according to the expression  $100(k_{nf} - k_f) / k_f$ .

When the thermal conductivity data of Murshed et al. [47] is considered, it is seen that at 60°C, 1 vol.% Al<sub>2</sub>O<sub>3</sub>(80 nm)/water nanofluid has a thermal conductivity enhancement around 12%. When the particle size of 80 nm is substituted to the Jang and Choi model [82], a thermal conductivity enhancement of 4.8% is obtained. As a result, using this data would cause an even larger discrepancy in the heat transfer coefficient values. On the other hand, Mintsa et al. [46] measured the thermal conductivity of 4 vol.% Al<sub>2</sub>O<sub>3</sub>(47 nm)/water nanofluid

at 48°C and reported 18% thermal conductivity enhancement (corresponding prediction of Jang and Choi model is 19.8%). Therefore, care must be taken when using the theoretical models of thermal conductivity in heat transfer calculations.

A more detailed convective heat transfer performance analysis of nanofluids, together with two additional cases (slug flow case and linear wall temperature boundary condition case) is provided by Kakaç and Pramuanjaroenkij [111].

#### **3.4.4. Concluding Remarks**

By considering the results of the analysis presented in Section 3.4.2.1 and 3.4.2.2, it can be concluded that the convective heat transfer analysis of nanofluids cannot be performed by using the classical correlations developed for pure fluids. It is also seen that the correlation proposed by Li and Xuan [106] correctly predicts the available experimental data. The accuracy of the correlation can be considered as an indication of the validity of the thermal dispersion model for the analysis of convective heat transfer of nanofluids. For further examination of the validity of thermal dispersion model, solution of governing energy equation with the modifications associated with the thermal dispersion model is required. For that purpose, a numerical analysis is performed which is discussed in Chapters 4 and 5.

The discussion presented in Section 3.4.3 shows that the heat transfer analysis of nanofluids heavily depends on the thermal conductivity values used in the calculations. Therefore, accurate determination of thermal conductivity of nanofluids is a key issue for the proper analysis of nanofluid heat transfer.

## CHAPTER 4

### CONVECTIVE HEAT TRANSFER WITH NANOFLUIDS – EXPLANATION AND VERIFICATION OF NUMERICAL ANALYSIS

#### 4.1. Introduction

Experimental data presented in the theoretical analysis part of Chapter 3 shows that the convective heat transfer enhancement of nanofluids exceeds the enhancement expected due to the increase in the thermal conductivity. There are several mechanisms recently proposed to explain this additional enhancement in convective heat transfer; such as, particle migration [113] and thermal dispersion [17]. At present, there is controversy about the relative significance of these mechanisms. Therefore, further studies are required for the clarification of the situation.

The validity of the proposed mechanisms can be investigated by solving a heat transfer problem by using the associated model and analyzing the results. Due to the complexity of the heat transfer of nanofluids, numerical analysis is an important tool to perform such a study. In this chapter, a numerical approach for the analysis of convective heat transfer of nanofluids based on a thermal dispersion model is described. Issues related to the geometry in consideration, modeling of nanofluid flow, governing equations, and the numerical method are explained and the accuracy of the numerical method is verified. Results of the numerical analysis of nanofluid heat transfer are presented in Chapter 5.

#### 4.2. Geometry in Consideration

In the numerical study, forced convection heat transfer performance of  $\text{Al}_2\text{O}_3$ /water nanofluid in the laminar flow regime in a straight circular tube is analyzed. Velocity profile is fully developed and the flow is considered as

incompressible. Such a flow condition is common in practical applications in which the flow becomes hydrodynamically fully developed in an unheated entrance region.

#### 4.2.1. Constant Wall Temperature Boundary Condition

For constant wall temperature boundary condition, the schematic view of the configuration is shown in Fig. 14. In order to obtain a proper comparison between the numerical results and experimental data, tube dimensions are selected to be the same as the test section utilized by Heris et al. [15] in their study. As a consequence, tube diameter is 5 mm and tube length is 1 m. In the numerical analysis, depending on Peclet number, the domain is sometimes selected to be longer than 1 m for obtaining thermally fully developed condition at the exit, but only the 1-m part is considered in the determination of heat transfer parameters.

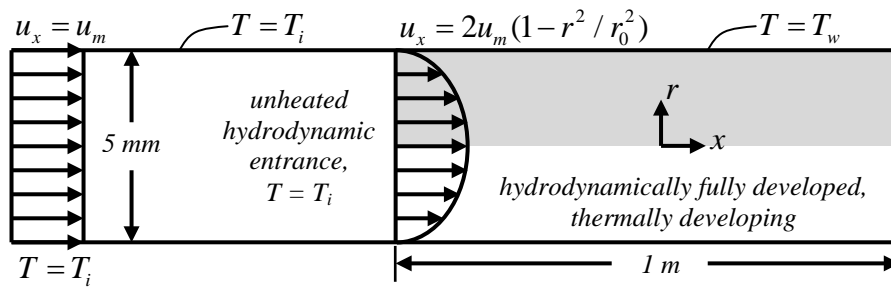


**Figure 14.** Schematic view of the problem considered in the numerical analysis. Boundary condition is constant wall temperature. Gray part is the solution domain.

#### 4.2.2. Constant Wall Heat Flux Boundary Condition

For constant wall heat flux boundary condition, the schematic view of the configuration is shown in Figure 15. In order to obtain a proper comparison between the numerical results and experimental data, tube dimensions are selected to be the same as the test section utilized by Kim et al. [110] in their study. As a consequence, tube diameter is 4.57 mm and tube length is 2 m. In the numerical

analysis, depending on Peclet number, the domain is sometimes selected to be longer than 2 m for obtaining thermally fully developed condition at the exit, but only the 2-m part is considered in the determination of heat transfer parameters.

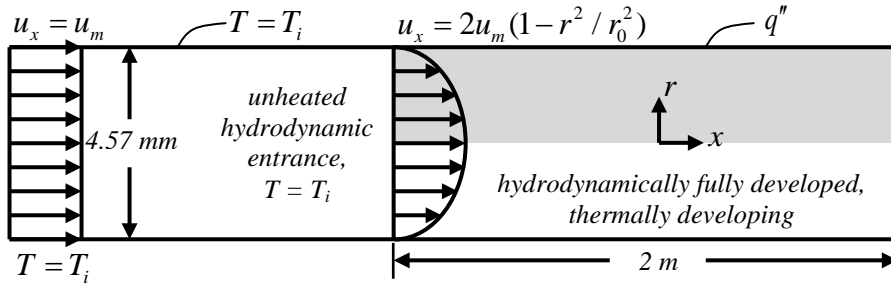


**Figure 15.** Schematic view of the problem considered in the numerical analysis. Boundary condition is constant wall heat flux. Gray part is the solution domain.

### 4.3. Modeling of Nanofluid Flow

#### 4.3.1. Single Phase Approach

In the literature, there are mainly two approaches for the modeling of nanofluid flow. In the first approach, the nanofluid is considered as a single phase fluid due to the fact that the particles are very small and they fluidize easily [116]. In this approach, the effect of nanoparticles can be taken into account by using the thermophysical properties of the nanofluid in the governing equations. In the second approach, the problem is analyzed as a two-phase flow and the interactions between nanoparticles and the liquid matrix are modeled [119].

In the present analysis, the nanofluid is considered as a single phase fluid. Such an approach is a more practical way of analyzing heat transfer of nanofluids. However, the validity of the single phase assumption needs verification. It should be noted that solely substituting the thermophysical properties of the nanofluid to the governing equations is not much different than using the classical correlations of convective heat transfer with thermophysical properties of the nanofluid. In the theoretical analysis part (Section 3.4), it was shown that such an approach

underestimates the experimental results. Therefore, the single phase analysis requires some modifications in order to account for the additional enhancement. For this purpose, the thermal dispersion model proposed by Xuan and Roetzel [17] is used.

#### 4.3.2. Thermal Dispersion Model

Xuan and Roetzel [17] noted that thermal dispersion occurs in nanofluid flow due to the random motion of nanoparticles. By considering the fact that the random motion of the particles creates small perturbations in velocity and temperature, they showed that the effective thermal conductivity in the energy equation takes the following form.

$$k_{eff} = k_{nf} + k_d . \quad (105)$$

In the present analysis,  $k_{nf}$  is calculated according to Eq. (82).  $k_d$  is dispersed thermal conductivity and it was proposed that it can be calculated by using the following expression [17].

$$k_d = C(\rho c_p)_{nf} u_x \phi d_p r_0 . \quad (106)$$

$\rho$  is density,  $c_p$  is specific heat,  $u_x$  is axial velocity,  $\phi$  is particle volume fraction,  $d_p$  is nanoparticle diameter, and  $r_0$  is tube radius.  $C$  is an empirical constant that should be determined by matching experimental data. Eqs. (105, 106) are used in the present analysis for both axial and radial thermal conduction terms and the variation of dispersed thermal conductivity in radial direction due to the variation of axial velocity in radial direction is taken into account.

#### 4.3.3. Thermophysical Properties

In the numerical analysis, for the determination of nanofluid density, specific heat, viscosity and thermal conductivity, Eqs. (75, 77, 81, 82) are used, respectively.

#### 4.3.4. Variation of Thermal Conductivity with Temperature

Variation of thermophysical properties with temperature is an important issue for the modeling of nanofluid flow. Experimental studies show that especially thermal conductivity of nanofluids significantly changes with temperature. As a consequence, constant thermal conductivity assumption in the numerical analysis may lead to erroneous results. Therefore, in the present analysis, variation of thermal conductivity with temperature is taken into account.

#### 4.4. Governing Equations

For the analysis of heat transfer in the present problem, the governing equations are the continuity, momentum and energy equations. For cylindrical coordinates, incompressible and steady continuity equation is as follows [133].

$$\frac{\partial u_r}{\partial r} + \frac{u_r}{r} + \frac{1}{r} \frac{\partial u_\theta}{\partial \theta} + \frac{\partial u_x}{\partial x} = 0. \quad (107)$$

$u_x$ ,  $u_r$ , and  $u_\theta$  are axial, radial and tangential components of flow velocity, respectively.

In the problem considered, the flow is hydrodynamically fully developed. Therefore, the velocity of the flow does not change in  $x$  direction and derivatives of the velocity components in  $x$ -direction are zero. Furthermore, since the flow is axisymmetric, all terms with  $\partial/\partial\theta$  are also zero. Then the continuity equation becomes the following.

$$\frac{\partial u_r}{\partial r} + \frac{u_r}{r} = 0. \quad (108)$$

Noting that  $u_r(r_0) = 0$  where  $r_0$  is the tube radius, it can be obtained

$$u_r = 0. \quad (109)$$

$r$ -momentum,  $\theta$ -momentum and  $x$ -momentum equations in the absence of body forces for cylindrical coordinates are as follows, respectively [133].

$$u_r \frac{\partial u_r}{\partial r} + \frac{u_\theta}{r} \frac{\partial u_r}{\partial \theta} - \frac{u_\theta^2}{r} + u_x \frac{\partial u_r}{\partial x} = -\frac{1}{\rho_{nf}} \frac{\partial p}{\partial r} + \nu_{nf} \left\{ \frac{\partial}{\partial r} \left[ \frac{1}{r} \frac{\partial}{\partial r} (ru_r) \right] + \frac{1}{r^2} \frac{\partial^2 u_r}{\partial \theta^2} - \frac{2}{r^2} \frac{\partial u_\theta}{\partial \theta} + \frac{\partial^2 u_r}{\partial x^2} \right\}, \quad (110)$$

$$u_r \frac{\partial u_\theta}{\partial r} + \frac{u_\theta}{r} \frac{\partial u_\theta}{\partial \theta} + \frac{u_r u_\theta}{r} + u_x \frac{\partial u_\theta}{\partial x} = -\frac{1}{\rho_{nf} r} \frac{\partial p}{\partial \theta} + \nu_{nf} \left\{ \frac{\partial}{\partial r} \left[ \frac{1}{r} \frac{\partial}{\partial r} (ru_\theta) \right] + \frac{1}{r^2} \frac{\partial^2 u_\theta}{\partial \theta^2} + \frac{2}{r^2} \frac{\partial u_r}{\partial \theta} + \frac{\partial^2 u_\theta}{\partial x^2} \right\}, \quad (111)$$

$$u_r \frac{\partial u_x}{\partial r} + \frac{u_\theta}{r} \frac{\partial u_x}{\partial \theta} + u_x \frac{\partial u_x}{\partial x} = -\frac{1}{\rho_{nf} r} \frac{\partial p}{\partial x} + \nu_{nf} \left\{ \frac{1}{r} \frac{\partial}{\partial r} \left( r \frac{\partial u_x}{\partial r} \right) + \frac{1}{r^2} \frac{\partial^2 u_x}{\partial \theta^2} + \frac{\partial^2 u_x}{\partial x^2} \right\}. \quad (112)$$

$\nu_{nf}$  is kinematic viscosity of the nanofluid and  $p$  is pressure. It should be noted that pressure does not change with  $\theta$  due to axisymmetry. Applying the simplifications regarding the  $x$ - and  $\theta$ -derivatives to Eq. (111):

$$0 = \frac{\partial}{\partial r} \left[ \frac{1}{r} \frac{\partial}{\partial r} (ru_\theta) \right]. \quad (113)$$

Noting that  $u_\theta(r_0) = 0$ , it can be obtained

$$u_\theta = 0. \quad (114)$$

Eqs. (110, 112) can also be rewritten by applying the simplifications regarding the  $x$ - and  $\theta$ -derivatives and substituting Eqs. (109, 114):

$$0 = -\frac{1}{\rho_{nf}} \frac{\partial p}{\partial r}, \quad (115)$$

$$0 = -\frac{1}{\rho_{nf} r} \frac{\partial p}{\partial x} + \nu_{nf} \left\{ \frac{1}{r} \frac{\partial}{\partial r} \left( r \frac{\partial u_x}{\partial r} \right) \right\}. \quad (116)$$

Associated boundary conditions are,

$$u_x = 0 \text{ at } r = r_0, \quad (117)$$

$$\frac{\partial u_x}{\partial r} = 0 \text{ at } r = 0. \quad (118)$$

By using Eqs. (115-118), axial component of flow velocity can be determined as:



$$u_x = 2u_m \left( 1 - \frac{r^2}{r_0^2} \right), \quad (119)$$

where  $u_m$  is mean flow velocity.

After the determination of the velocity distribution in the domain, heat transfer in the system can be analyzed by considering the energy equation which is as follows [133].

$$(\rho c_p)_{nf} \frac{DT}{Dt} = \nabla \cdot (k_{eff} \nabla T) + \dot{q} + \Phi, \quad (120)$$

where

$$\frac{D}{Dt} = \frac{\partial}{\partial t} + u_r \frac{\partial}{\partial r} + \frac{u_\theta}{r} \frac{\partial}{\partial \theta} + u_x \frac{\partial}{\partial x}, \quad (121)$$

$$\nabla \cdot (k_{eff} \nabla T) = \frac{1}{r} \frac{\partial}{\partial r} \left( r k_{eff} \frac{\partial T}{\partial r} \right) + \frac{1}{r^2} \frac{\partial}{\partial \theta} \left( k_{eff} \frac{\partial T}{\partial \theta} \right) + \frac{\partial}{\partial x} \left( k_{eff} \frac{\partial T}{\partial x} \right), \quad (122)$$

and

$$\Phi = 2\mu_{nf} \left\{ \begin{aligned} & \left[ \left( \frac{\partial u_r}{\partial r} \right)^2 + \left[ \frac{1}{r} \left( \frac{\partial u_\theta}{\partial \theta} + u_r \right) \right]^2 + \left( \frac{\partial u_x}{\partial x} \right)^2 + \frac{1}{2} \left( \frac{\partial u_\theta}{\partial x} + \frac{1}{r} \frac{\partial u_x}{\partial \theta} \right)^2 \right] \\ & + \frac{1}{2} \left( \frac{\partial u_x}{\partial r} + \frac{\partial u_r}{\partial x} \right)^2 + \frac{1}{2} \left[ \frac{1}{r} \frac{\partial u_r}{\partial \theta} + r \frac{\partial}{\partial r} \left( \frac{u_\theta}{r} \right) \right]^2 \end{aligned} \right\}. \quad (123)$$

$\dot{q}$  is the volumetric heat generation rate and  $\Phi$  is the dissipation function. It should be noted that the thermal conductivity term in the energy equation is replaced by the effective thermal conductivity ( $k_{eff}$ ) according to the thermal dispersion model (Eqs. 105, 106). Applying the simplifications regarding the  $x$ - and  $\theta$ -derivatives to Eq. (120) and substituting Eqs. (109, 114, 119, 121-123):

$$(\rho c_p)_{nf} \left[ \frac{\partial T}{\partial t} + 2u_m \left( 1 - \frac{r^2}{r_0^2} \right) \frac{\partial T}{\partial x} \right] = \frac{1}{r} \frac{\partial}{\partial r} \left( k_{eff} r \frac{\partial T}{\partial r} \right) + \frac{\partial}{\partial x} \left( k_{eff} \frac{\partial T}{\partial x} \right) + \mu_{nf} \left( \frac{\partial u_x}{\partial r} \right)^2. \quad (124)$$

The term with the time derivative is conserved in the energy equation because the numerical solution method utilized reaches the steady-state solution by marching in time. Therefore, the problem is considered as if it is transient.

For the proper analysis of the problem, nondimensionalization should be applied to Eq. (124). Nondimensionalizations for constant wall temperature boundary condition and constant wall heat flux boundary condition are slightly

different. Because of this, the associated discussion is presented in two different sections.

#### 4.4.1. Constant Wall Temperature Boundary Condition

For constant wall temperature boundary condition, following nondimensional parameters are defined:

$$\theta = \frac{T - T_w}{T_i - T_w}, \quad (125)$$

$$x^* = \frac{x}{r_0}, \quad (126)$$

$$r^* = \frac{r}{r_0}, \quad (127)$$

$$t^* = \frac{\alpha_{nf,b} t}{r_0^2}, \quad (128)$$

$$k^* = \frac{k_{eff,T}}{k_{nf,b}}, \quad (129)$$

$$Pe_{nf} = \frac{u_m d}{\alpha_{nf,b}}, \quad (130)$$

$$Br_{nf} = \frac{\mu_{nf,b} u_m^2}{k_{nf,b} (T_i - T_w)}. \quad (131)$$

$T_i$  and  $T_w$  are inlet and wall temperatures, respectively, and  $d$  is tube diameter. By using these nondimensional parameters, Eq. (124) becomes:

$$\frac{\partial \theta}{\partial t^*} + Pe_{nf} (1 - r^{*2}) \frac{\partial \theta}{\partial x^*} = \frac{1}{r^*} \frac{\partial}{\partial r^*} \left( k^* r^* \frac{\partial \theta}{\partial r^*} \right) + \frac{\partial}{\partial x^*} \left( k^* \frac{\partial \theta}{\partial x^*} \right) + 16 r^{*2} Br_{nf}. \quad (132)$$

$Br_{nf}$  is the nanofluid Brinkman number, which is a measure of viscous effects in the flow. For the present flow conditions,  $Br_{nf}$  is on the order of  $10^{-7}$ , therefore viscous dissipation is negligible. As a result, the final form of the energy equation is:

$$\frac{\partial \theta}{\partial t^*} + Pe_{nf} (1 - r^{*2}) \frac{\partial \theta}{\partial x^*} = \frac{1}{r^*} \frac{\partial}{\partial r^*} \left( k^* r^* \frac{\partial \theta}{\partial r^*} \right) + \frac{\partial}{\partial x^*} \left( k^* \frac{\partial \theta}{\partial x^*} \right). \quad (133)$$

The boundary conditions for the above equation are as follows:

$$\frac{\partial \theta}{\partial r^*} = 0 \text{ at } r^* = 0, \quad (134)$$

$$\theta = 0 \text{ at } r^* = 1, \quad (135)$$

$$\theta = 1 \text{ at } x^* = 0. \quad (136)$$

#### 4.4.2. Constant Wall Heat Flux Boundary Condition

For constant wall heat flux boundary condition, the definitions of the nondimensional parameters,  $x^*$ ,  $r^*$ ,  $t^*$ ,  $k^*$ , and  $Pe_{nf}$  are the same as the constant wall temperature case, which are defined by Eqs. (126-130), respectively. The differences are in the definitions of  $\theta$  and  $Br$ :

$$\theta = \frac{k_{nf}(T - T_i)}{q_w'' r_0}, \quad (137)$$

$$Br = \frac{\mu_{nf} u_m^2}{q_w'' r_0}, \quad (138)$$

where  $q_w''$  is the wall heat flux. It is positive when heat is transferred to the working fluid. Application of nondimensionalization to the energy equation results in exactly the same differential equation as in the case of constant wall temperature (Eqs. 132, 133). The boundary conditions are as follows:

$$\frac{\partial \theta}{\partial r^*} = 0 \text{ at } r^* = 0, \quad (139)$$

$$\frac{\partial \theta}{\partial r^*} = \frac{1}{k^*} \text{ at } r^* = 1, \quad (140)$$

$$\theta = 0 \text{ at } x^* = 0. \quad (141)$$

For both constant wall temperature and constant wall heat flux boundary conditions, all of the thermophysical properties are calculated at the bulk mean temperature of the flow, which is indicated by the subscript  $b$  in the associated expressions, except the thermal conductivity. Nondimensional thermal conductivity,  $k^*$ , is defined as the effective thermal conductivity at the local

temperature divided by the nanofluid thermal conductivity at the bulk mean temperature. Bulk mean temperature is:

$$T_b = \frac{T_i + T_o}{2}. \quad (142)$$

It should be noted that  $k^*$  is a function of temperature and local axial velocity due to Eqs. (105, 106, 129).

#### 4.5. Numerical Method

In the numerical solution, finite difference method is utilized by using C programming language. Finite difference method is a practical and efficient method for simple geometries such as the geometry in consideration. Since the flow is axisymmetric, only half of the  $x$ - $r$  plane is considered in the solution, as illustrated in Figs. 14 and 15.

A general flowchart of the numerical solution is provided in Appendix B.

##### 4.5.1. Finite Difference Method

In Eq. (133), all of the terms are discretized by second order differencing. In order to ensure stability, backward differencing is used for the convection term (second term on the left-hand side of Eq. 133). For other terms, central differencing is used. Node distribution is not uniform across the domain, and for such a configuration, central and backward differencing expressions for the first derivative are as follows, respectively.

$$\frac{\partial \theta_i}{\partial x} = \frac{1}{\Delta x_{i-1} + \Delta x_{i+1}} \left[ \frac{\Delta x_{i-1}}{\Delta x_{i+1}} (\theta_{i+1} - \theta_i) + \frac{\Delta x_{i+1}}{\Delta x_{i-1}} (\theta_i - \theta_{i-1}) \right], \quad (143)$$

$$\frac{\partial \theta_i}{\partial x} = \frac{1}{\Delta x_{i-1} - \Delta x_{i-2}} \left[ \frac{\Delta x_{i-2}}{\Delta x_{i-1}} (\theta_{i-1} - \theta_i) + \frac{\Delta x_{i-1}}{\Delta x_{i-2}} (\theta_i - \theta_{i-2}) \right]. \quad (144)$$

For second derivative, associated formulations are as follows, for central and backward differencing, respectively.

$$\frac{\partial^2 \theta_i}{\partial x^2} = \frac{2}{\Delta x_{i-1} + \Delta x_{i+1}} \left[ \frac{\theta_{i+1} - \theta_i}{\Delta x_{i+1}} + \frac{\theta_{i-1} - \theta_i}{\Delta x_{i-1}} \right], \quad (145)$$

$$\frac{\partial^2 \theta_i}{\partial x^2} = \frac{2}{\Delta x_{i-1} - \Delta x_{i-2}} \left[ \frac{\theta_{i-1} - \theta_i}{\Delta x_{i-1}} + \frac{\theta_i - \theta_{i-2}}{\Delta x_{i-2}} \right]. \quad (146)$$

In the above expressions, the subscripts defining the  $r$ -coordinate are not included for simplicity.  $\Delta x$  terms are defined as follows.

$$\Delta x_{i-2} = x_i - x_{i-2}, \quad (147)$$

$$\Delta x_{i-1} = x_i - x_{i-1}, \quad (148)$$

$$\Delta x_{i+1} = x_{i+1} - x_i, \quad (149)$$

$$\Delta x_{i+2} = x_{i+2} - x_i. \quad (150)$$

#### 4.5.2. Discretization of the Boundary Nodes

Discretization of the nodes at the boundaries needs special attention. At the inlet, the temperature is known; therefore, there is no need of discretization at those nodes. For the second column of nodes from the inlet, it is not possible to utilize second order backward differencing for the convection term. Therefore, first order differencing is used for the associated terms. At the exit, both convection and conduction terms are discretized by using second order backward differencing and the need for the introduction of a specific boundary condition is eliminated.

The problem is symmetric with respect to the tube center due to Eqs. (134, 139). For the nodes at  $r^* = 0$ , this symmetry is used to introduce a ghost node below the tube center which enables the discretization of the center nodes as if they are interior nodes. Since the dimensionless temperature values at the ghost nodes are equal to their symmetric counterparts, this approach does not result in additional unknown nodes.

When it comes to the wall boundaries, the formulation for constant wall temperature and constant wall heat flux boundary conditions are different. For constant wall temperature case, since the temperature values are known, there is no need of discretization of the associated nodes. For constant wall heat flux case,

the boundary condition at the wall is given by Eq. (140). This equation is discretized by second order backward differencing and the resulting equation is directly used as the finite difference equation for the associated nodes.

### 4.5.3. Alternating Direction Implicit Scheme

As the solution scheme, Alternating Direction Implicit (ADI) scheme is used [134]. When the scheme is applied to the present problem, the resulting finite difference equations are lengthy and they are not practical for the explanation of the ADI scheme. For the illustration of the scheme, a simpler equation, the two dimensional transient heat conduction equation in Cartesian coordinates is considered:

$$\frac{\partial T}{\partial t} = \alpha \left( \frac{\partial^2 T}{\partial x^2} + \frac{\partial^2 T}{\partial y^2} \right). \quad (151)$$

ADI scheme consists of two time steps that are repeated iteratively. In the first time step, discretization is made such that the discretizations in  $x$ -coordinate are implicit and the discretizations in  $y$ -coordinate are explicit. For simplicity of the illustration, central differencing with uniform node distribution is considered for spatial coordinates. Then Eq. (151) becomes the following.

$$\frac{T_{i,j}^{n+1} - T_{i,j}^n}{\Delta t} = \alpha \left( \frac{T_{i-1,j}^{n+1} - 2T_{i,j}^{n+1} + T_{i+1,j}^{n+1}}{\Delta x^2} + \frac{T_{i,j-1}^n - 2T_{i,j}^n + T_{i,j+1}^n}{\Delta y^2} \right) \quad (152)$$

where  $i$ ,  $j$  and  $n$  correspond to  $x$ ,  $y$ , and  $t$ . In the second time step, the discretizations in  $x$ -coordinate are explicit and the discretizations in  $y$ -coordinate are implicit:

$$\frac{T_{i,j}^{n+2} - T_{i,j}^{n+1}}{\Delta t} = \alpha \left( \frac{T_{i-1,j}^{n+1} - 2T_{i,j}^{n+1} + T_{i+1,j}^{n+1}}{\Delta x^2} + \frac{T_{i,j-1}^{n+2} - 2T_{i,j}^{n+2} + T_{i,j+1}^{n+2}}{\Delta y^2} \right). \quad (153)$$

These two steps are repeated iteratively to obtain the transient solution of the problem. In the present analysis, the objective is to obtain the steady-state solution of the problem. Therefore, in the solution, time steps are selected to be large and solution is progressed in time until the variation of temperature distribution with time becomes negligible.

ADI scheme combines some advantages of simple explicit and implicit schemes. In simple explicit scheme, the solution procedure is straightforward since there is no system of equations to be simultaneously solved. However, in that approach, time steps should be selected to be smaller than a specific value for stability. This limiting value can be very small depending on the node distribution which increases the computation time greatly, and this usually offsets the advantage of the scheme.

When it comes to implicit schemes, such as the Crank-Nicolson scheme, the advantage is that there is no restriction regarding the time steps, that is, the schemes are unconditionally stable. The problem related to these schemes is that the number of linear equations that should be simultaneously solved is very large which requires great amount of memory and computational effort. In two and three dimensional geometries, although the resulting coefficient matrix is sparse, it is not diagonal which prevents the application of efficient algorithms for the solution of the system of equations such as Thomas algorithm.

ADI scheme is implicit only in one direction at a time; and as a result, the size of the coefficient matrix is much smaller than the size of the coefficient matrix obtained in implicit methods. Furthermore, the coefficient matrix is pentadiagonal which allows the application of an efficient solution algorithm. In addition to these advantages, ADI scheme is unconditionally stable similar to the case of implicit schemes. The only disadvantage of the scheme is that the solution algorithm is more complex when compared with the other methods.

It should be noted that one can also directly solve the steady-state form of the energy equation without progressing in time. However, that approach also has some stability problems. The advantage of the method might be the fact that the solution is reached by solving the system of equations only once. But for the case of variable thermal conductivity, this method also requires an iterative approach. Therefore, for the present problem, direct solution of the steady-state form of the energy equation does not provide a significant advantage.

## 4.6. Code Verification

In numerical methods, choosing correct solution parameters is very important for obtaining high accuracy with minimum computational effort. By utilizing large number of nodes and by performing sufficient number of iterations, one can obtain an accurate solution. However, the associated computation time is also an important consideration and therefore, the objective is to obtain quick and sufficiently accurate solutions. There are several parameters that affect the accuracy and speed of the numerical solution, and in the present analysis, their optimum values are determined by trying different values for all of the parameters. The associated discussion is presented in Section 4.6.1.

Numerical solution should also be verified by analyzing its theoretical validity. For that purpose, numerical results are compared with the Graetz solution in Section 4.6.2.

### 4.6.1. Determination of Optimum Solution Parameters

In the analysis, optimum values of solution parameters are determined by considering the flow of pure water, for simplicity. The values obtained by that analysis also apply to the nanofluid flow since the main form of the temperature distribution is similar.

One of the most important solution parameters is the number of nodes used in the solution. For determining proper values, numerical results obtained by utilizing 400x100, 200x50, 100x25, and 50x12 grids are compared in terms of the variation of local Nusselt number in axial direction (first numbers are the number of nodes in  $x$ -direction whereas second numbers indicate the number of nodes in  $r$ -direction).

For constant wall temperature boundary condition, the associated results are provided in Fig. 16 for  $Pe = 2500$ . When the figure is examined, it is seen that 50x12 grid solution is completely erroneous. It is also seen that 100x25 solution deviates from the 200x50 and 400x100 solutions at high axial positions. On the other hand, the difference between the 200x50 and 400x100 solutions is not



significant. Therefore, 200x50 grid is sufficient for the accurate analysis of the problem.

For constant wall heat flux boundary condition, the associated results are provided in Figure 17 for  $Pe = 2500$ . In the analysis it is observed that 100x25, 200x50, and 400x100 grids provide nearly the same results. Therefore, in order to emphasize grid dependence, a 25x6 grid is also considered and 400x100 grid is not shown in the figure. When the figure is examined, it is seen that 25x6 grid solution is completely erroneous. It is also seen that 50x12 solution deviates from the 100x25 and 200x50 solutions at high axial positions. On the other hand, the difference between the 100x25 and 200x50 solutions is not significant. Therefore, 100x25 grid is sufficient for the accurate analysis of the constant wall heat flux case.

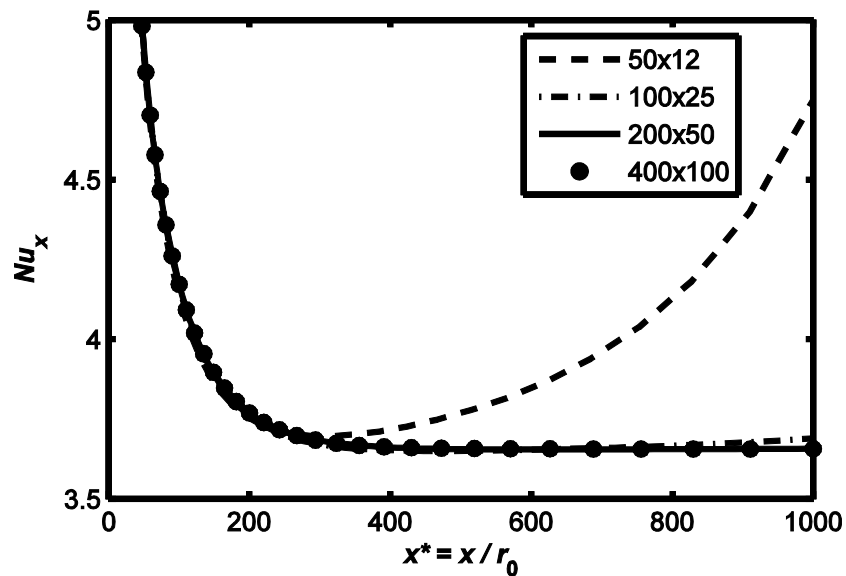


**Figure 16.** Variation of local Nusselt number in axial direction for the solutions with different number of nodes.  $Pe = 2500$ . Boundary condition is constant wall temperature.

It should be noted that the efficiency of the ratio of 4 between the number of nodes in axial and radial directions is also examined by trying different combinations of grid sizes such as 200x10, 200x25, 200x50 and 200x100 for

constant wall temperature boundary condition. The results of these grids are compared, and 200x50 grid is found to be appropriate. The same analysis is repeated for constant wall heat flux case and 100x25 grid is selected.

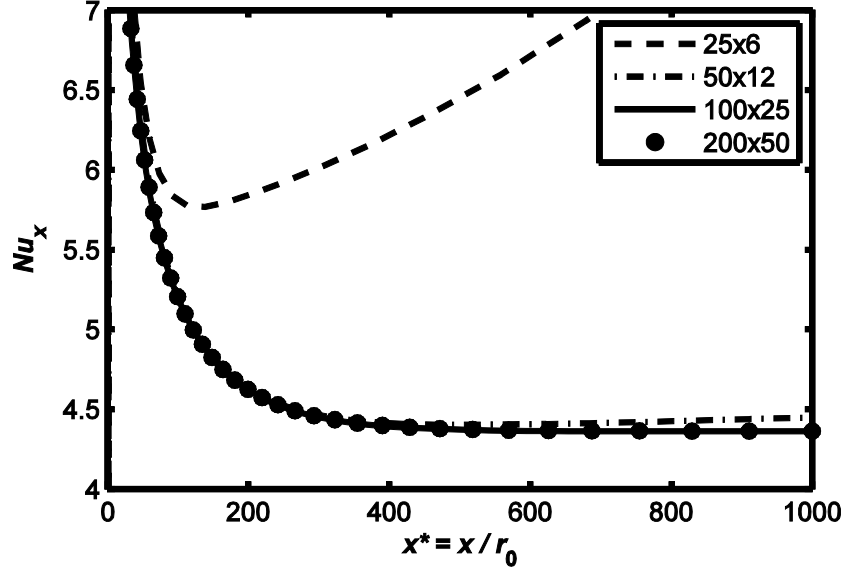


**Figure 17.** Variation of local Nusselt number in axial direction for the solutions with different number of nodes.  $Pe = 2500$ . Boundary condition is constant wall heat flux.

For the minimization of the number of nodes used in the solution, a nonuniform distribution of nodes is preferred in numerical studies. In this study, nodes are concentrated at the entrance region and near the tube wall, since the temperature gradients are more significant at those regions. There are various ways for the application of variable node distribution. In the present analysis, the distances between the nodes are gradually increased in  $x$ -direction and  $-r$ -direction and the variation is defined in terms of the ratio of maximum distance between two nodes to the minimum distance between two nodes. Similar to the previous parameters, different values for this ratio are considered and 1000 is found to be appropriate in both  $x$ - and  $r$ -directions:

$$\frac{\max(\Delta x)}{\min(\Delta x)} = \frac{\max(\Delta r)}{\min(\Delta r)} = 1000. \quad (154)$$

It should also be noted that the ratio of successive distances between nodes is taken as a constant:

$$\frac{\Delta x_{i+1}}{\Delta x_i} = C_x, \quad \frac{\Delta r_{j+1}}{\Delta r_j} = C_r. \quad (155)$$

The values of the constants  $C_x$  and  $C_r$  are calculated according to Eq. (154).

#### 4.6.2. Comparison of the Results with Graetz Solution

The consistency of the numerical solution is shown by the analysis presented in the previous section. However, the numerical results should also be theoretically examined for ensuring the validity of the analysis. For that purpose, numerical results are compared with the results of Graetz solution for parabolic velocity profile in the following two sections, for constant wall temperature and constant wall heat flux boundary conditions, respectively.

##### 4.6.2.1. Constant Wall Temperature Boundary Condition

Numerical results for constant wall temperature boundary condition are compared with the predictions of Graetz solution [135] for parabolic velocity profile, which is discussed in detail in Kakaç and Yener [133]. According to Graetz solution, local Nusselt number is as follows:

$$Nu_x = \frac{h_x d}{k} = \frac{\sum_{n=0}^{\infty} A_n e^{-\lambda_n^2 \xi}}{2 \sum_{n=0}^{\infty} \frac{A_n}{\lambda_n^2} e^{-\lambda_n^2 \xi}}, \quad (156)$$

where

$$\xi = \frac{x / r_0}{Pe}. \quad (157)$$

$A_n$  and  $\lambda_n$  values are provided by Lipkis [136]. Fig. 18 provides the associated comparison in terms of the variation of local Nusselt number in axial direction for the flow of pure water for  $Pe = 2500, 4500,$  and  $6500$ . When the figure is

examined, it is seen that there is perfect agreement between the numerical results and the predictions of the Graetz solution.

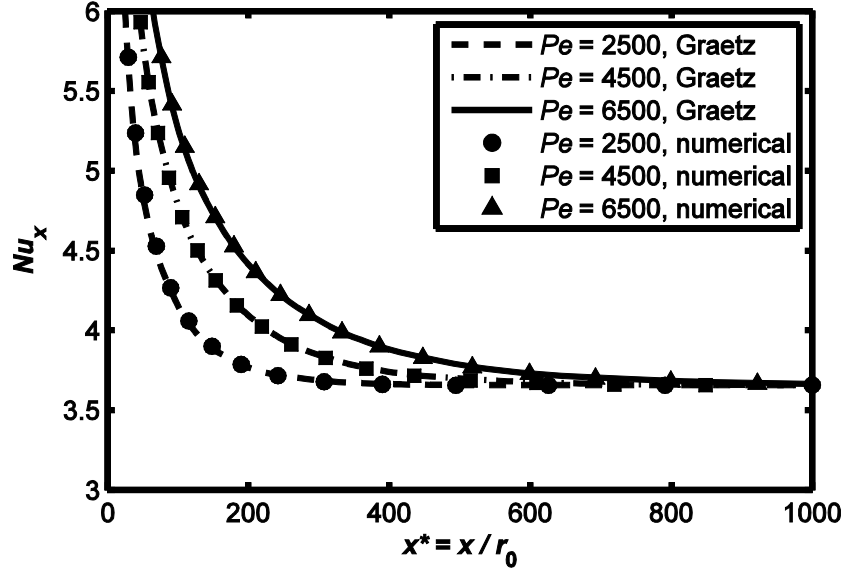


**Figure 18.** Variation of local Nusselt number in axial direction according to the numerical results and Graetz solution. Boundary condition is constant wall temperature.

#### 4.6.2.2. Constant Wall Heat Flux Boundary Condition

Similar to the previous case, the results of constant wall heat flux boundary condition are compared with the predictions of the associated Graetz solution [135] for parabolic velocity profile, which is discussed in detail in Kakaç and Yener [133]. According to Graetz solution, local Nusselt number is as follows [137]:

$$Nu_x = \frac{h_x d}{k} = \left[ \frac{11}{48} - \frac{1}{2} \sum_{n=1}^{\infty} \frac{e^{-\beta_n^2 \xi}}{A_n \beta_n^4} \right]^{-1} \quad (158)$$

$\xi$  is given by Eq. (157) and  $A_n$  and  $\beta_n$  values are provided by Siegel et al. [137]. Fig. 19 provides the associated comparison in terms of the variation of local Nusselt number in axial direction for the flow of pure water for  $Pe = 2500, 4500,$

and 6500. When the figure is examined, it is seen that there is perfect agreement between the numerical results and the predictions of the Graetz solution.

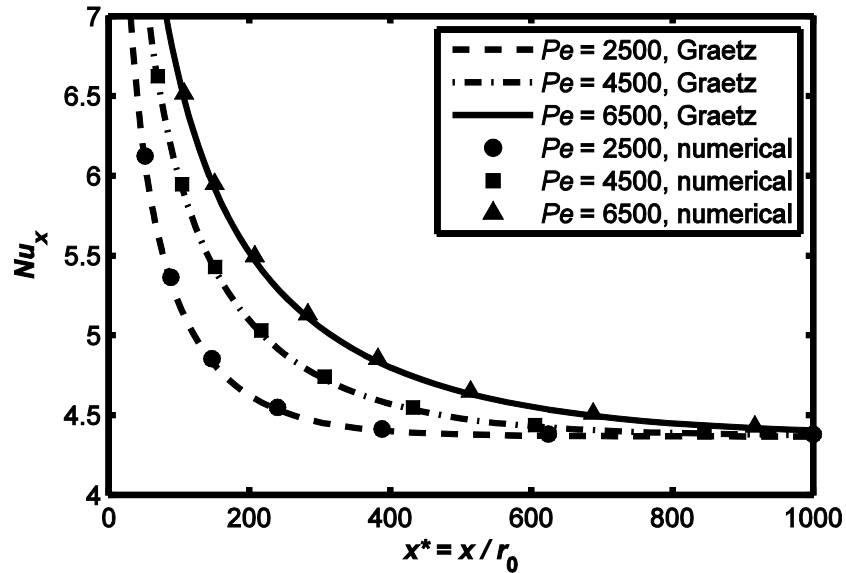


**Figure 19.** Variation of local Nusselt number in axial direction according to the numerical results and Graetz solution. Boundary condition is constant wall heat flux.

#### 4.7. Concluding Remarks

In this chapter, the numerical approach utilized for the analysis of convective heat transfer of nanofluids is explained in terms of geometry in consideration, modeling of nanofluid flow, governing equations, and numerical method. The accuracy of the numerical method is verified by comparing the results with the predictions of the Graetz solution for the flow of pure water. In the following chapter, the results of the numerical analysis of convective heat transfer of nanofluids are presented.

## CHAPTER 5

### CONVECTIVE HEAT TRANSFER WITH NANOFLUIDS – RESULTS OF NUMERICAL ANALYSIS

#### 5.1. Introduction

In this chapter, results of the numerical analysis of convective heat transfer of nanofluids are presented in detail. The analysis is performed by using the numerical code whose accuracy is verified in Chapter 4. Some important issues about the analysis, such as the geometry in consideration, calculation of thermophysical properties, governing equations, and numerical method are discussed in Chapter 4.

The discussion is presented under two main headings, constant wall temperature boundary condition and constant wall heat flux boundary condition, respectively.

#### 5.2. Constant Wall Temperature Boundary Condition

For the constant wall temperature boundary condition, the results are first analyzed in terms of the average heat transfer coefficient enhancement ratio (heat transfer coefficient of nanofluid divided by the heat transfer coefficient of corresponding base fluid). The associated results are compared with the experimental and numerical studies of Heris et al. [15,117]. Then the variation of local Nusselt number in axial direction is examined for different particle volume fractions. Finally, effects of particle size, heating and cooling are discussed in terms of heat transfer coefficient enhancement ratio.

## 5.2.1. Heat Transfer Coefficient Enhancement

### 5.2.1.1. Comparison of Results with Experimental Data

There is limited experimental data for nanofluid flow under the constant wall temperature boundary condition in the literature. In this part, numerical results of the present study are compared with the experimental data of Heris et al. [15]. Heris et al. considered the laminar flow of  $\text{Al}_2\text{O}_3(20 \text{ nm})/\text{water}$  nanofluid. The flow is hydrodynamically developed and thermally developing. Nanofluid flows inside a circular tube with a diameter of 5 mm and length of 1 m. The numerical analysis is performed by using exactly the same nanofluid parameters and flow configuration for obtaining a meaningful analysis.

In Fig. 20, numerical results of the present analysis and experimental data of Heris et al. are presented in terms of the variation of average heat transfer coefficient enhancement ratio with Peclet number for different particle volume fractions. Enhancement ratios are calculated by comparing the nanofluid with the pure fluid at the same Peclet number in order to focus on the sole effect of the increased thermal conductivity and thermal dispersion.

In order to stress the importance of the application of thermal dispersion model, the numerical results without thermal dispersion are also included in the figure. When the figure is examined, it is seen that there is good agreement between the experimental data and the numerical results with thermal dispersion. On the other hand, the analysis without thermal dispersion underpredicts the experimental data. In addition, the analysis without thermal dispersion also fails to predict the increasing enhancement with Peclet number.

The small discrepancies between experimental data and the solution with thermal dispersion might be explained by the fact that the particle volume fraction of a nanofluid may unexpectedly affect the thermal conductivity due to the complicated variation of clustering characteristics with particle volume fraction. Another important point is that, although an empirical constant,  $C$  is present for the determination of the effective thermal conductivity in the analysis (Eq. 106),

since that constant simultaneously defines the magnitude of dispersed thermal conductivity and the variation of it with Peclet number, it does not assure the complete agreement with experimental data. Therefore, the present agreement between numerical analysis and experimental data can be considered as an indication of the convenience of the single phase approach combined with thermal dispersion model for the analysis of convective heat transfer of nanofluids.

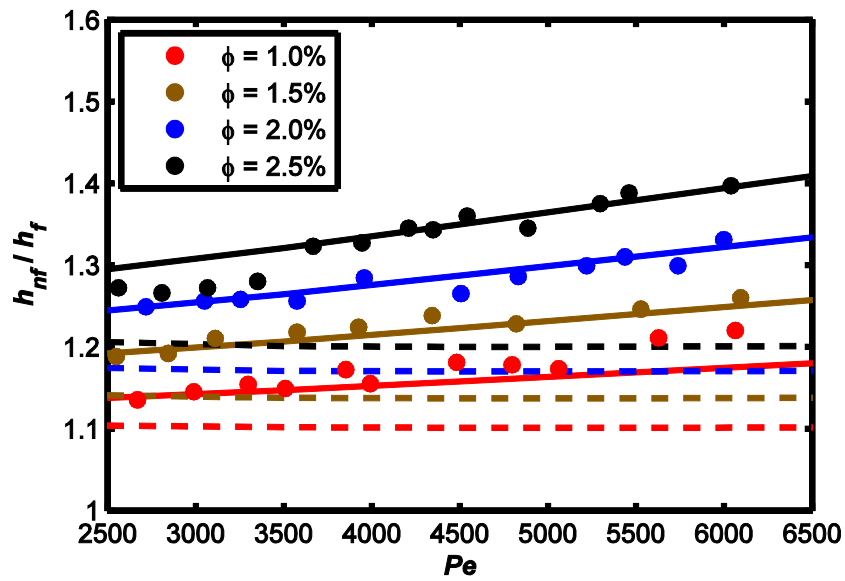


**Figure 20.** Variation of average heat transfer coefficient enhancement ratio with Peclet number for different particle volume fractions of the  $\text{Al}_2\text{O}_3/\text{water}$  nanofluid. Markers: Experimental data of Heris et al. [15]. Dashed lines: Numerical results without thermal dispersion. Solid lines: Numerical results with thermal dispersion.  $Pe$ :  $Pe_{nf}$  for nanofluid,  $Pe_f$  for pure fluid.

### 5.2.1.2. Comparison of Results with Numerical Data

In the present numerical study, variation of nanofluid thermal conductivity with temperature and variation of dispersed thermal conductivity with local axial velocity are taken into account. In order to stress the importance of these in nanofluid heat transfer analysis, the numerical results of the present study are compared with the numerical study of Heris et al. [117]. They [117] considered the same problem that is analyzed in the previous section. However, in their study,



thermal conductivity of nanofluid and dispersed thermal conductivity of the flow were taken to be constants.

Fig. 21 presents the associated comparison in terms of the variation of average heat transfer coefficient enhancement ratio with Peclet number for different particle volume fractions.

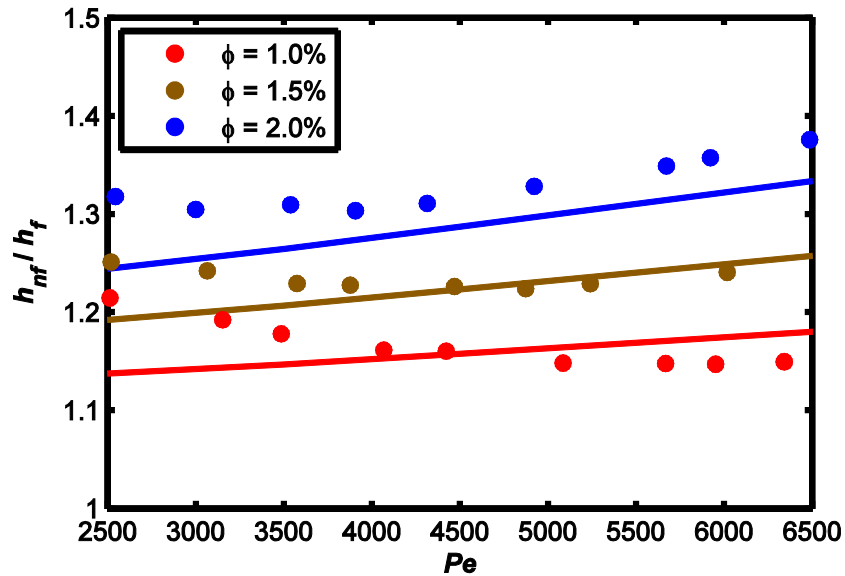


**Figure 21.** Variation of average heat transfer coefficient enhancement ratio with Peclet number for different particle volume fractions of the  $\text{Al}_2\text{O}_3/\text{water}$  nanofluid. Solid lines: Numerical results of the present study with thermal dispersion. Markers: Numerical results of Heris et al. [117].  $Pe_{nf}$  for nanofluid,  $Pe_f$  for pure fluid.

It is seen that the results of Heris et al. [117] predict decreasing heat transfer coefficient enhancement ratio with increasing Peclet number, especially for particle volume fractions of 1.0% and 1.5%, which is not in agreement with the experimental data presented in Fig. 20. For the 2.0 vol.% nanofluid, there is significant difference between the results of the two numerical studies and Fig. 20 shows that the present numerical study is in very good agreement with the experimental data for 2.0 vol.% nanofluid. Therefore, it can be concluded that taking variable thermal conductivity and variable thermal dispersion into account in nanofluid analysis significantly improves the accuracy.

## 5.2.2. Further Analysis

### 5.2.2.1. Local Nusselt Number

In this section, the same flow configuration analyzed numerically in the previous sections is investigated in terms of the axial variation of local Nusselt number. However, in order to determine the fully developed Nusselt number as well, the flow inside a longer tube is considered (5 m). Figure 22 shows the associated results for the flow of pure water and  $\text{Al}_2\text{O}_3/\text{water}$  nanofluid at a Peclet number of 6500. In the figure, it is seen that the local Nusselt number is larger for nanofluids throughout the tube. This is mainly due to the thermal dispersion in the flow. Thermal dispersion results in a higher effective thermal conductivity at the center of the tube which flattens the radial temperature profile. Flattening of temperature profile increases the temperature gradient at the tube wall and as a consequence, Nusselt number becomes higher when compared to the flow of pure water. Figure 22 also shows that increasing particle volume fraction increases Nusselt number. This is due to the fact that the effect of thermal dispersion becomes more pronounced with increasing particle volume fraction.

It should be noted that the fully developed nanofluid Nusselt number values are also higher than pure water case. Associated values for different particle volume fractions of the  $\text{Al}_2\text{O}_3/\text{water}$  nanofluid are presented in Table 6. It is seen that increasing particle volume fraction increases the fully developed Nusselt number. The results presented in the table are for  $Pe = 6500$  and since thermal dispersion is dependent on flow velocity (Eq. 106), fully developed Nusselt number increases also with Peclet number for the case of nanofluids. In Table 6, fully developed heat transfer coefficient values are also provided. It should be noted that heat transfer coefficient enhancement ratios are larger than Nusselt number enhancement ratios since the former shows the combined effect of Nusselt number enhancement and thermal conductivity enhancement with nanofluids.

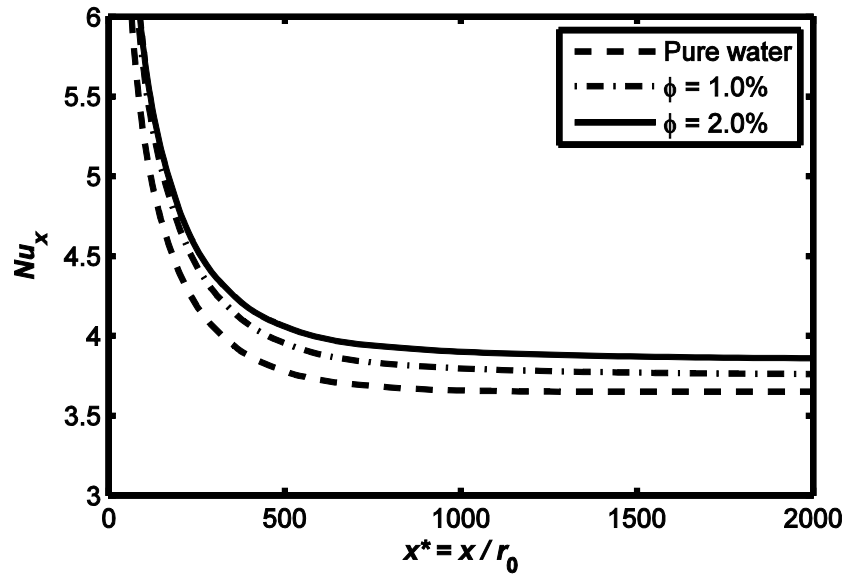


**Figure 22.** Variation of local Nusselt number with dimensionless axial position for pure water and  $\text{Al}_2\text{O}_3/\text{water}$  nanofluid.  $Pe_{nf} = Pe_f = 6500$ .

**Table 6.** Fully developed Nusselt number and heat transfer coefficient values obtained from the numerical solution for pure water and  $\text{Al}_2\text{O}_3/\text{water}$  nanofluid with different particle volume fractions.  $Pe_f = Pe_{nf} = 6500$ .

Fluid	$Nu_{fd}$	$Nu$ Enhancement Ratio ( $Nu_{fd,nf} / Nu_{fd,f}$ )	$h_{fd}$ [W/m <sup>2</sup> K]	$h$ Enhancement Ratio ( $h_{fd,nf} / h_{fd,f}$ )
Water	3.66	–	480	–
<b>Nanofluid</b>				
1.0 vol.%	3.77	1.030	562	1.172
1.5 vol.%	3.82	1.044	594	1.238
2.0 vol.%	3.86	1.057	624	1.300
2.5 vol.%	3.91	1.069	653	1.361

#### 5.2.2.2. Effect of Particle Size

In Chapter 2, it was shown that most of the experimental data in the literature indicates increasing thermal conductivity with decreasing particle size. On the

other hand, decreasing particle size decreases the effect of thermal dispersion through Eq. (106). In order to understand the relative significance of these effects, average heat transfer coefficient enhancement ratio is plotted in Fig. 23 with respect to Peclet number for 1 vol.%  $\text{Al}_2\text{O}_3$ /water nanofluids with different particle sizes. The flow configuration in consideration is the same as the one utilized in the previous sections.

When Fig. 23 is examined, it is seen that heat transfer coefficient enhancement ratio generally increases with increasing particle size, which shows that particle size dependence of thermal dispersion is more pronounced than the associated dependence of thermal conductivity. There is an exception for particle sizes below 25 nm at low Peclet numbers, therefore variation of thermal conductivity with particle size is more effective for those cases.

Although there is very limited experimental data about the effect of particle size on convective heat transfer, Anoop et al. [109] showed that increasing particle size decreases heat transfer for the laminar flow of  $\text{Al}_2\text{O}_3$ /water nanofluids under constant wall heat flux boundary condition, which indicates a disagreement with the results of the present analysis.

The results presented in Fig. 23 are obtained by utilizing the same value for the empirical constant  $C$  in Eq. (106) for all particle sizes, which results in a linear increase in dispersed thermal conductivity with particle size. However, it should be noted that the effect of Brownian motion of nanoparticles increase with decreasing particle size, and decreasing particle size also increases the specific surface area of nanoparticles in the nanofluid, which improves heat transport. Therefore, the present analysis might be modified by considering the empirical expression  $C$  as a function of particle size so that its value decreases with increasing particle size. For proper application of such an approach, a theoretical model should be developed that defines the relation between  $C$  and particle size. Moreover, a systematic set of experimental data is required for the verification of the results of the approach, which is missing in the literature for the time being.

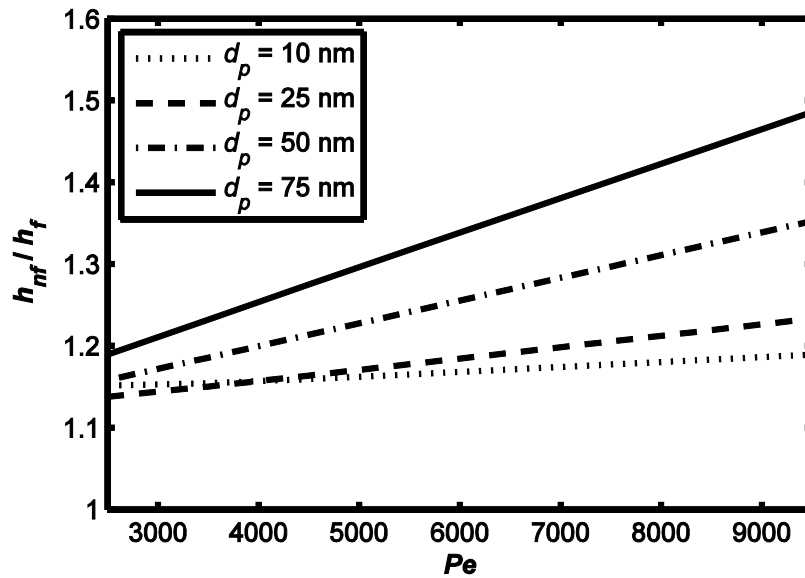


**Figure 23.** Variation of average heat transfer coefficient enhancement ratio with Peclet number for different particle sizes of the 1 vol.%  $\text{Al}_2\text{O}_3$ /water nanofluid

### 5.2.2.3. Effects of Heating and Cooling

Thermal conductivity distribution of the working fluid inside the tube is an important parameter in heat transfer. Especially, thermal conductivity at the wall significantly affects heat transfer. Since thermal conductivity of nanofluids is a strong function of temperature, heat transfer performance of nanofluids depends on whether the working fluid is heated or cooled. Thermal conductivity of nanofluids increases with temperature, and as a consequence, convective heat transfer coefficient and associated enhancement ratio are larger for the heating of the nanofluid in which  $T_w$  has a higher value.

In Fig. 24, this difference is illustrated in terms of the variation of average heat transfer coefficient enhancement ratio with Peclet number for heating and cooling of 2.0 vol.%  $\text{Al}_2\text{O}_3$ /water nanofluid.

The flow configuration in consideration is the same as the one utilized in the previous sections. For heating case,  $T_i = 20^\circ\text{C}$ , and  $T_w = 65^\circ\text{C}$  whereas for cooling  $T_i = 65^\circ\text{C}$ , and  $T_w = 20^\circ\text{C}$ . It is seen that the enhancement difference between the two cases exceeds 5% at low Peclet numbers. Increasing the

difference between inlet and wall temperatures, and increasing the particle volume fraction of the nanofluid might result in larger differences in enhancement values.

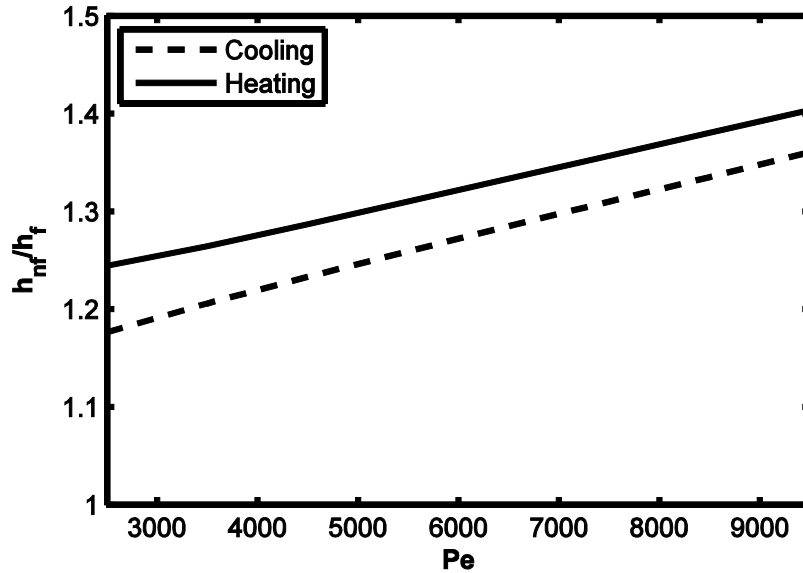


**Figure 24.** Variation of average heat transfer coefficient enhancement ratio with Peclet number for heating and cooling of the 2 vol.%  $\text{Al}_2\text{O}_3$ /water nanofluid

The results presented in this section show that nanofluids provide higher heat transfer enhancement in heating applications when compared to cooling cases. This fact should be taken into account for the proper design of heat transfer processes with nanofluids.

### 5.3. Constant Wall Heat Flux Boundary Condition

For constant wall heat flux boundary condition, results are usually presented in terms of the variation of local heat transfer coefficient in axial direction in the literature. Same approach is followed in the present discussion.

Similar to the constant wall temperature boundary condition case, the results are compared with experimental and numerical data, and effects of particle size, heating and cooling are also discussed.

### 5.3.1. Local Heat Transfer Coefficient

#### 5.3.1.1. Comparison of Results with Experimental Data

The results of the present numerical analysis are compared with the experimental data of Kim et al. [110]. In the study, Kim et al. investigated the laminar and turbulent flow of  $\text{Al}_2\text{O}_3$ /water nanofluid. Constant wall heat flux boundary condition is analyzed in the study by utilizing a test section with 4.57 mm inner diameter and 2 m length. In the experiments, nanofluid entered the tube at  $22^\circ\text{C}$  and total heating power was 60 W throughout the analysis. It was indicated that nanoparticle size distribution is 20 – 50 nm.

By using the same flow parameters, the experiment performed by Kim et al. [110] was simulated numerically. For the particle size, the average value of 35 nm is used in the calculations. In Fig. 25, the associated numerical results are compared with the experimental data, in terms of the local heat transfer coefficient. The presented results are for 3 vol.%  $\text{Al}_2\text{O}_3$ /water nanofluid, which is the only particle volume fraction considered in the experiments. Experimental data for the flow of pure water and associated numerical results are also presented in the figure. It is seen that good agreement exists between numerical and experimental data for both pure water and nanofluid cases.

In the paper of Kim et al. [110], the variation of local heat transfer coefficient in axial direction was only presented for  $Re = 1460$ . Therefore, it is not possible to provide a similar comparison for other Reynolds numbers. Nevertheless, further comparison is made by using the experimental data regarding the variation of local heat transfer coefficient at a specific point with Reynolds number. The available data is the local heat transfer coefficient at  $x^* = x / r_0 = 44$ , for the flow of pure water and 3 vol.%  $\text{Al}_2\text{O}_3$ /water nanofluid. Associated experimental results are compared with the numerical data in Fig. 26. It is seen that there is good agreement between numerical results and experimental data.

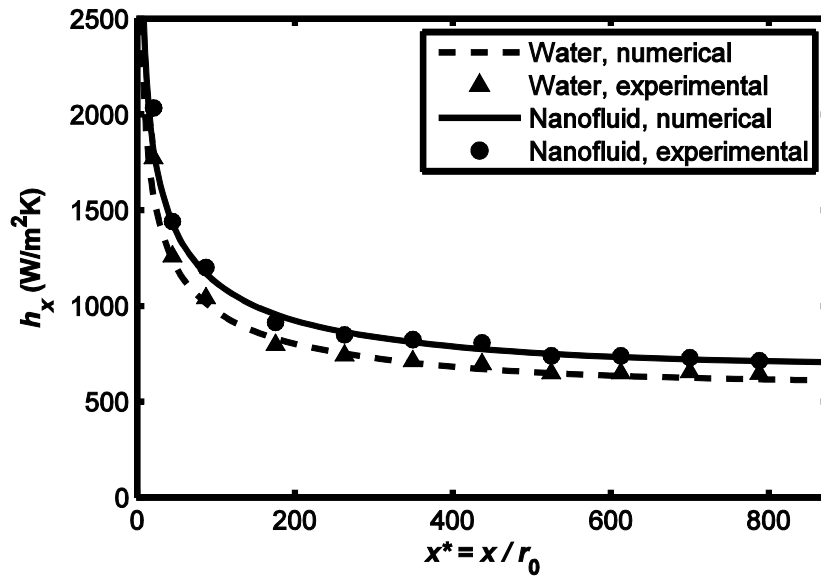


**Figure 25.** Variation of local heat transfer coefficient with dimensionless axial position for pure water and 3 vol.%  $\text{Al}_2\text{O}_3$ /water nanofluid.  $\text{Re}_{nf} = \text{Re}_f = 1460$ . Markers indicate experimental results of Kim et al. [110].

### 5.3.1.2. Comparison of Results with Numerical Data

In this section, numerical results of the present analysis are compared with the numerical analysis of Bianco et al. [119]. In their numerical study, Bianco et al. investigated the laminar flow of  $\text{Al}_2\text{O}_3$ (100 nm)/water nanofluid inside a straight circular tube with a diameter of 1 cm and length of 1 m. Nanofluid enters the tube at a uniform temperature of 20°C. Bianco et al. [119] applied two different approaches in the analysis; namely, single phase and two-phase approaches. For both of these approaches, constant thermal conductivity and variable thermal conductivity solutions were performed.

In order to obtain a meaningful comparison, same flow parameters used in the study of Bianco et al. [119] are utilized in the present numerical study. Associated results are presented in Table 7 in terms of average heat transfer coefficient values at  $\text{Re} = 250$ . First of all, it is seen that constant thermal conductivity solutions of Bianco et al. [119] are significantly different from their variable thermal conductivity solutions. Therefore, constant thermal conductivity



solutions are inaccurate and as a consequence, considering the associated results in the comparison does not provide any information.

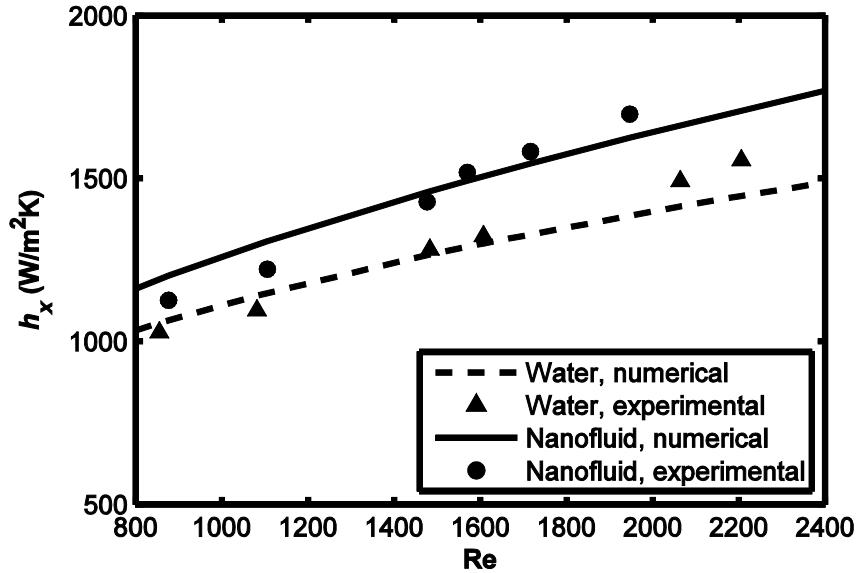


**Figure 26.** Variation of local heat transfer coefficient with Reynolds number for pure water and 3 vol.%  $\text{Al}_2\text{O}_3$ /water nanofluid.  $x^* = x / r_0 = 44$ . Re:  $\text{Re}_{nf}$  for nanofluid,  $\text{Re}_f$  for pure fluid. Markers indicate experimental results of Kim et al. [110].

For 4 vol.% nanofluid, it is seen that present study is in agreement with single phase variable thermal conductivity and two-phase variable thermal conductivity solutions of Bianco et al. [119]. This can be considered as an indication of the validity of the single phase approach since single phase and two-phase analyses provide very close results. However, when it comes to 1 vol.% nanofluid, results are significantly different from each other. For this particle volume fraction, the difference between the present study and single phase variable thermal conductivity solution of Bianco et al. [119] can be explained by the fact that different thermal conductivity models are used for the determination of the thermal conductivity of nanofluids which may alter the associated results. On the other hand, associated result of two-phase variable thermal conductivity

solution is much higher than all of the other cases which requires further investigation.

In summary, more systematical numerical studies are needed for the clarification of the difference between the single phase and two-phase approaches. Studies focusing on the effects of particle volume fraction and particle size will provide a better understanding about the validity of different approaches of nanofluid heat transfer analysis.

**Table 7.** Average heat transfer coefficient of Al<sub>2</sub>O<sub>3</sub>/water nanofluid according to the present numerical study and the numerical study of Bianco et al. [119].  $Re = 250$ .

Al <sub>2</sub> O <sub>3</sub> /water nanofluid	$h$ [W/m <sup>2</sup> K]				
	Present study	Study of Bianco et al. [119]			
		Single phase, constant $k$	Single phase, variable $k$	Two-phase, constant $k$	Two-phase, variable $k$
1.0 vol. %	385	364	398	396	421
4.0 vol. %	450	414	444	422	446

### 5.3.2. Further Analysis

#### 5.3.2.1. Local Nusselt Number

In this section, the same flow configuration analyzed numerically in the previous sections (test section of Kim et al. [110]) is investigated in terms of the axial variation of local Nusselt number. Figure 27 shows the associated results for the flow of pure water and Al<sub>2</sub>O<sub>3</sub>/water nanofluid at a Peclet number of 12000 ( $Re \approx 2000$ ). In the figure, it is seen that the local Nusselt number is larger for nanofluids throughout the tube, similar to the case of constant wall temperature boundary condition. The underlying reasons of the observed trends are the same as those discussed in the case of constant wall temperature (Section 5.2.2.1) and they are not repeated here.

The difference between the nanofluid Nusselt number and pure water Nusselt number is smaller for the present case when compared to constant wall temperature boundary condition. This is mainly due to the fact that the utilized empirical constant  $C$  (Eq. 106) is smaller for the present case when compared to constant wall temperature case, which is selected to be so in order to match the experimental data of Kim et al. [110].

It should be noted that the fully developed nanofluid Nusselt number values are also higher than pure water case. Associated values for different particle volume fractions of the  $\text{Al}_2\text{O}_3/\text{water}$  nanofluid are presented in Table 8. It is seen that increasing particle volume fraction increases the fully developed Nusselt number. The results presented in the table are for  $Pe = 12000$ . In Table 8, fully developed heat transfer coefficient values are also provided. It should be noted that heat transfer coefficient enhancement ratios are larger than Nusselt number enhancement ratios since the former shows the combined effect of Nusselt number enhancement and thermal conductivity enhancement with nanofluids.

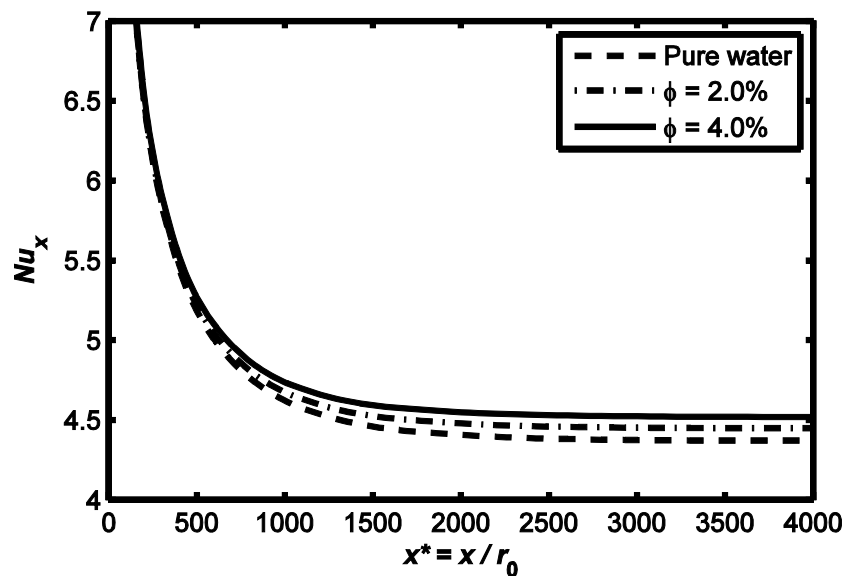


**Figure 27.** Variation of local Nusselt number with dimensionless axial position for pure water and  $\text{Al}_2\text{O}_3/\text{water}$  nanofluid.  $Pe_{nf} = Pe_f = 12000$ .

**Table 8.** Fully developed Nusselt number and heat transfer coefficient values obtained from the numerical solution for pure water and Al<sub>2</sub>O<sub>3</sub>/water nanofluid with different particle volume fractions.  $Pe_f = Pe_{nf} = 12000$ .

Fluid	$Nu_{fd}$	$Nu$ Enhancement Ratio ( $Nu_{fd,nf} / Nu_{fd,f}$ )	$h_{fd}$ [W/m <sup>2</sup> K]	$h$ Enhancement Ratio ( $h_{fd,nf} / h_{fd,f}$ )
Water	4.36	–	588	–
<b>Nanofluid</b>				
1.0 vol.%	4.41	1.011	655	1.115
2.0 vol.%	4.45	1.019	697	1.187
3.0 vol.%	4.48	1.027	737	1.255
4.0 vol.%	4.51	1.035	776	1.320

### 5.3.2.2. Effect of Particle Size

Effect of particle size on heat transfer is previously investigated in Section 5.2.2.2 for constant wall temperature boundary condition. A similar analysis is performed in this section for constant wall heat flux boundary condition. In the analysis, the flow configuration and associated parameters are the same as the ones utilized in the experiments of Kim et al. [110]. Numerical results are presented in Fig. 28 in terms of the variation of local heat transfer coefficient with axial direction. In the figure,  $Pe = 2500$  and 4 vol.% Al<sub>2</sub>O<sub>3</sub>/water nanofluid is considered.

When the figure is examined, it is seen that heat transfer coefficient increases with decreasing particle size. This is mainly due to the fact that the particle size dependence of thermal conductivity is more pronounced than the particle size dependence of thermal dispersion due to the relatively low empirical constant  $C$  used in Eq. (106). In constant wall temperature case,  $C$  was chosen to be higher to match experimental data and thermal dispersion dominated the particle size dependence of heat transfer as a consequence. This resulted in increasing enhancement with increasing particle size in constant wall temperature

case. For higher values of Peclet number, a similar trend can also be observed for the constant wall heat flux boundary condition.

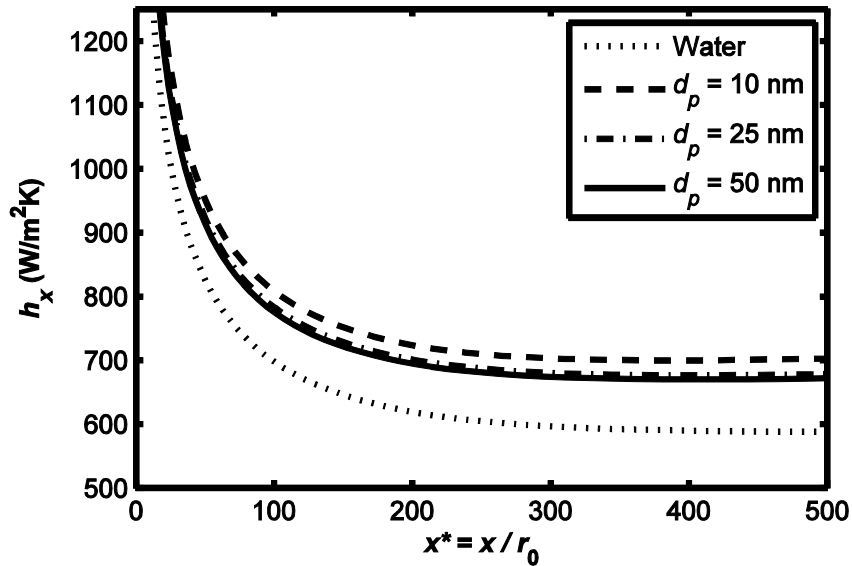


**Figure 28.** Variation of local heat transfer coefficient with dimensionless axial position for different particle sizes of 4 vol.%  $\text{Al}_2\text{O}_3$ /water nanofluid

Particle size dependence of heat transfer enhancement with nanofluids depends on empirical constant  $C$  and Peclet number due to the thermal dispersion model. As these two parameters increase, the dependence tends to become increasing enhancement with increasing particle size.

### 5.3.2.3. Effects of Heating and Cooling

Effects of heating and cooling on heat transfer enhancement are previously discussed for the case of constant wall temperature boundary condition. In that case, heating of the working fluid provided higher enhancement since thermal conductivity of the working fluid at the wall significantly affects the heat transfer. When it comes to the constant wall heat flux, the analysis is performed by firstly considering the heating case according to the parameters in the study of Kim et al.

[110] (with a longer tube to emphasize temperature variation) and exit temperature is determined ( $62^{\circ}\text{C}$ ). For cooling case, that exit temperature is substituted as inlet temperature and the direction of heat flux at the wall is reversed. As a consequence, exit temperature of the cooling case ( $22^{\circ}\text{C}$ ) is equal to the inlet temperature of the heating case.

The results for these two cases are presented in terms of the variation of local heat transfer coefficient with axial direction in Fig. 29. 4 vol.%  $\text{Al}_2\text{O}_3$ /water nanofluid is considered and the results for the flow of pure water are also presented for comparison purposes.

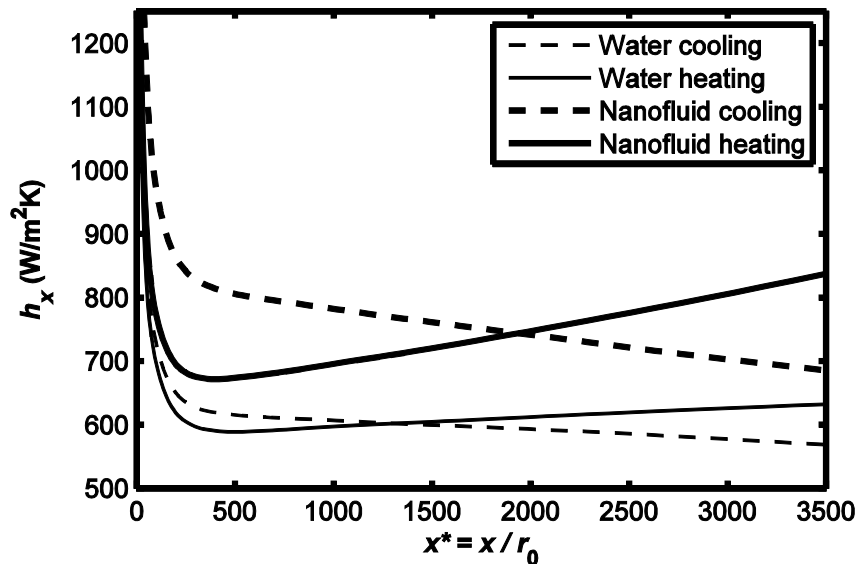


**Figure 29.** Variation of local heat transfer coefficient with dimensionless axial position for heating and cooling of the 4 vol.%  $\text{Al}_2\text{O}_3$ /water nanofluid and pure water.  $Pe = 2500$ .

It is seen that for both the nanofluid and pure water, heat transfer coefficient is higher for cooling case at the beginning since temperature of the fluid is higher in the associated region when compared to heating case. At larger values of axial position, heating case has higher heat transfer coefficient since the temperature of the flow exceeds the corresponding temperature of the cooling case. The important issue here is that the difference between the cooling and

heating cases for the nanofluid is much higher than the associated difference for the pure water. Therefore, for the case of nanofluids, heat transfer performance is significantly more dependent on temperature when compared to pure fluids. This fact should be taken into account for the proper design of heat transfer processes with nanofluids.

#### **5.4. Concluding Remarks**

The theoretical analysis presented in Chapter 3 shows that the classical heat transfer correlations underpredict the heat transfer enhancement of nanofluids. Therefore, convective heat transfer analysis of nanofluids cannot be made accurately by utilizing those correlations. On the other hand, a recently proposed empirical correlation based on a thermal dispersion model provides accurate results.

In order to examine the validity of the thermal dispersion approach, a numerical analysis of forced convection heat transfer of nanofluids is performed. Comparison of numerical results with experimental data indicates good agreement. As a consequence, it is thought that utilizing the thermal dispersion model with single phase assumption is a proper way of analyzing convective heat transfer of nanofluids. It should also be noted that this approach requires less computational effort when compared to two-phase analysis, which is important for practical applications.

In constant wall temperature case, the importance of taking the variation of thermal conductivity and thermal dispersion into account in nanofluid heat transfer analysis is emphasized by comparing the results of the present numerical study with another numerical study which assumes constant values for the associated parameters. When it comes to constant wall heat flux case, present numerical results are compared with the results of a two-phase analysis and good agreement is observed for 4 vol.% nanofluid whereas there is significant discrepancy for 1 vol.% nanofluid.

Examination of local Nusselt number of nanofluids revealed that thermal dispersion enhances Nusselt number, which can be explained by the flattening in the radial temperature profile.

Further verification of the accuracy of the thermal dispersion model requires more systematic experimental studies, such as the investigation of the effect of particle size and tube diameter on convective heat transfer. In addition, thermal conductivity of nanofluids is a key issue for the proper analysis of convective heat transfer of nanofluids. Therefore, further experimental and theoretical research in that area is also needed for more reliable analyses of the problem.



## CHAPTER 6

### CONCLUSION

#### 6.1. Summary

In Chapter 1, some introductory information is presented about nanofluids. Advantages of nanofluids over classical suspensions of solid particles in fluids are explained and main parameters that define a nanofluid are summarized. In addition, common production methods of nanoparticles and nanofluids are briefly discussed.

In Chapter 2, a detailed literature review about the thermal conductivity of nanofluids is presented. After a brief explanation of nanofluid thermal conductivity measurement methods, effects of some parameters, such as particle volume fraction, particle size, and temperature on thermal conductivity of nanofluids are discussed. Discrepancies in experimental data are indicated and some explanations for the contradictory results are provided. Theoretical studies performed in order to explain the thermal conductivity enhancement of nanofluids are summarized and associated thermal conductivity models are explained. In the last part of the chapter, predictions of some thermal conductivity models are compared with the experimental data available in the literature.

In Chapter 3, firstly a literature survey about the forced convection heat transfer of nanofluids is presented and associated experimental, theoretical, and numerical studies are summarized. In addition, determination of nanofluid thermophysical properties, namely, density, specific heat, and viscosity are briefly discussed.

In the following sections, a theoretical analysis of forced convection heat transfer of nanofluids is performed. In the analysis, validity of usage of classical heat transfer correlations for the prediction of nanofluid heat transfer is examined.

Predictions of a recent heat transfer correlation developed especially for nanofluids are also investigated.

In Chapter 4, the numerical approach for the analysis of forced convection heat transfer of nanofluids is described and the accuracy of the numerical method is verified. In the presented approach, nanofluid is considered as a single phase fluid and a thermal dispersion model is applied to the governing energy equation. In addition, variation of thermal conductivity with temperature is taken into account in the analysis.

In Chapter 5, results of the numerical analysis described in Chapter 4 for the hydrodynamically fully developed, thermally developing laminar flow of  $\text{Al}_2\text{O}_3$ /water nanofluid inside a straight circular tube under constant wall temperature and constant wall heat flux boundary conditions are presented. Numerical results are compared with experimental and numerical data available in the literature. Effects of particle size, heating and cooling on heat transfer enhancement are investigated. Variation of local Nusselt number with axial position is determined in order to gain insight to the effects of thermal dispersion and variation of thermal conductivity on heat transfer enhancement.

## **6.2. Conclusion**

As a result of the review of the nanofluid thermal conductivity research in the literature, it is seen that there is significant discrepancy in experimental data. The discrepancy may be due to some specific parameters of nanofluids whose effects on thermal conductivity are not closely observed in most of the studies. These parameters are extent of clustering of nanoparticles, particle size distribution of nanoparticles, duration and severity of ultrasonic vibration applied to the nanofluid, and pH value of the nanofluid.

Although there is significant discrepancy in experimental data, it is still possible to reach some conclusions about the dependence of thermal conductivity on some parameters. It is seen that nanofluid thermal conductivity increases with increasing particle volume fraction and temperature. On the other hand, most of

the experimental results indicate increasing thermal conductivity with decreasing particle size but contradictory results are also present.

There are several mechanisms proposed to explain the thermal conductivity enhancement of nanofluids, such as Brownian motion of nanoparticles, clustering of nanoparticles and liquid layering around nanoparticles. Due to the lack of systematic experimental data in the literature, it is difficult to analyze the relative significance of these mechanisms. Most of the theoretical models based on these mechanisms include some empirical constants. It is possible to correctly predict experimental results to some extent by adjusting the values of these constants accordingly. On the other hand, at present, a complete theoretical model of thermal conductivity that takes all of the parameters into account is not available.

When it comes to the convective heat transfer of nanofluids, in the theoretical analysis part of Chapter 3, it is shown that the classical correlations for pure fluids underpredict the experimental data of nanofluids. On the other hand, a recent heat transfer correlation developed for nanofluids based on a thermal dispersion model provides accurate results.

In Chapter 5, it is seen that application of the thermal dispersion model to the governing energy equation provides meaningful results which are in agreement with the available experimental data in the literature. This can be considered as an indication of the validity of the thermal dispersion model for nanofluid heat transfer analysis. Furthermore, it can be concluded that single phase analysis of nanofluid heat transfer is sufficiently accurate for practical applications as long as variation of thermal conductivity with temperature is taken into account in the associated calculations.

Examination of local Nusselt number for the flow of nanofluids shows that Nusselt number is higher for the case of nanofluids which is mainly due to the flattening in the radial temperature profile as a consequence of thermal dispersion. Fully developed Nusselt numbers and heat transfer coefficients are also determined for nanofluids with different particle volume fractions and it is seen

that the effect of thermal conductivity enhancement on heat transfer coefficient enhancement is more pronounced than the effect of Nusselt number enhancement.

Investigation of the effect of nanofluid particle size on heat transfer results in complicated trends due to the opposing effects of thermal conductivity and thermal dispersion on heat transfer in terms of particle size dependence. It is seen that if empirical constant  $C$  in dispersed thermal conductivity expression is sufficiently small, the effect of thermal conductivity dominates particle size dependence which results in increasing heat transfer with decreasing particle size. On the other hand, if  $C$  is large, heat transfer increases with increasing particle size.

Investigation of the effects of cooling and heating on nanofluid heat transfer revealed that for the constant wall heat flux boundary condition, heat transfer (and associated enhancement) is higher when flow temperature is higher. When it comes to the constant wall temperature boundary condition, the dominant parameter that affects the heat transfer is the wall temperature. As the wall temperature increases, the heat transfer and the associated enhancement increases. These facts should be taken into account for the practical application of nanofluids in heat transfer devices.

### **6.3. Suggestions for Future Work**

At present, there is significant discrepancy in thermal conductivity data of nanofluids. For the practical application of nanofluids in heat transfer devices, these discrepancies should be eliminated by systematically investigating the effects of some parameters on thermal conductivity of nanofluids. In the literature, the research about the effects of clustering, pH value, and ultrasonic vibration on thermal conductivity is very limited and further research is required regarding the effects of these parameters.

When it comes to the theoretical studies about the thermal conductivity of nanofluids, it is seen that the relative significance of the proposed enhancement mechanisms of thermal conductivity are not known. Development of new

theoretical models that combine the effects of numerous enhancement mechanisms and comparison of these models' predictions with systematically obtained experimental data will provide insight to the theoretical explanation of anomalous thermal conductivity enhancement with nanofluids.

In the literature, there are different theoretical approaches for the analysis of convective heat transfer of nanofluids. In order to understand the validity of the proposed approaches, numerical analyses that are based on those approaches are useful. At present, numerical studies in the literature about this issue are not sufficient to reach a conclusion about the accuracy of the approaches. On the other hand, there is very limited experimental data about forced convection heat transfer of nanofluids and this prevents the systematic comparison of numerical results with experimental findings.

Similar to the case of thermal conductivity, convective heat transfer of nanofluids is also dependent on many parameters such as particle volume fraction, particle size, particle material, temperature, and base fluid type. Detailed experimental investigation of the effects of most of these parameters on heat transfer has not been performed yet. Systematic studies about these aspects of nanofluid heat transfer will provide valuable information for the optimization of heat transfer enhancement obtained with nanofluids.

## REFERENCES

- [1] Wang, B., Zhou, L., and Peng, X., 2003, "A Fractal Model for Predicting the Effective Thermal Conductivity of Liquid with Suspension of Nanoparticles," *Int. J. Heat Mass Tran.*, **46**(14), pp. 2665-2672.
- [2] Keblinski, P., Phillpot, S. R., Choi, S. U. S., and Eastman, J. A., 2002, "Mechanisms of Heat Flow in Suspensions of Nano-Sized Particles (Nanofluids)," *Int. J. Heat Mass Tran.*, **45**(4), pp. 855-863.
- [3] Masuda, H., Ebata, A., Teramae, K., and Hishinuma, N., 1993, "Alteration of Thermal Conductivity and Viscosity of Liquid by Dispersing Ultra-Fine Particles (Dispersion of  $\gamma$ -Al<sub>2</sub>O<sub>3</sub>, SiO<sub>2</sub>, and TiO<sub>2</sub> Ultra-Fine Particles)," *Netsu Bussei*, **4**(4), pp. 227-233.
- [4] Choi, S. U. S., 1995, "Enhancing Thermal Conductivity of Fluids with Nanoparticles," *Developments and Applications of Non-Newtonian Flows*, D. A. Siginer, and H. P. Wang, eds., The American Society of Mechanical Engineers, New York, **FED-Vol. 231 / MD-Vol.66**, pp. 99-105.
- [5] Chein, R., and Chuang, J., 2007, "Experimental Microchannel Heat Sink Performance Studies using Nanofluids," *Int. J. Therm. Sci.*, **46**(1), pp. 57-66.
- [6] Lee, J., and Mudawar, I., 2007, "Assessment of the Effectiveness of Nanofluids for Single-Phase and Two-Phase Heat Transfer in Micro-Channels," *Int. J. Heat Mass Tran.*, **50**(3-4), pp. 452-463.
- [7] Eastman, J. A., Choi, S. U. S., Li, S., Yu, W., and Thompson, L. J., 2001, "Anomalously Increased Effective Thermal Conductivities of Ethylene Glycol-Based Nanofluids Containing Copper Nanoparticles," *Appl. Phys. Lett.*, **78**(6), pp. 718-720.
- [8] Yu, W., France, D. M., Routbort, J. L., and Choi, S. U. S., 2008, "Review and Comparison of Nanofluid Thermal Conductivity and Heat Transfer Enhancements," *Heat Transfer Eng.*, **29**(5), pp. 432-460.
- [9] Romano, J. M., Parker, J. C., and Ford, Q. B., 1997, "Application Opportunities for Nanoparticles Made from the Condensation of Physical Vapors," *Adv. Pm. Part.*, pp. 12-13.

- [10] Chon, C. H., Kihm, K. D., Lee, S. P., and Choi, S. U. S., 2005, "Empirical Correlation Finding the Role of Temperature and Particle Size for Nanofluid ( $\text{Al}_2\text{O}_3$ ) Thermal Conductivity Enhancement," *Appl. Phys. Lett.*, **87**(15), 153107.
- [11] Das, S. K., Putra, N., Thiesen, P., and Roetzel, W., 2003, "Temperature Dependence of Thermal Conductivity Enhancement for Nanofluids," *J. Heat Transfer*, **125**(4), pp. 567-574.
- [12] Li, C. H., and Peterson, G. P., 2006, "Experimental Investigation of Temperature and Volume Fraction Variations on the Effective Thermal Conductivity of Nanoparticle Suspensions (Nanofluids)," *J. Appl. Phys.*, **99**(8), 084314.
- [13] Pak, B. C., and Cho, Y. I., 1998, "Hydrodynamic and Heat Transfer Study of Dispersed Fluids with Submicron Metallic Oxide Particles," *Exp. Heat Transfer*, **11**(2), pp. 151-170.
- [14] Hwang, K. S., Jang, S. P., and Choi, S. U. S., 2009, "Flow and Convective Heat Transfer Characteristics of Water-Based  $\text{Al}_2\text{O}_3$  Nanofluids in Fully Developed Laminar Flow Regime," *Int. J. Heat Mass Tran.*, **52**(1-2), pp. 193-199.
- [15] Heris, S. Z., Esfahany, M. N., and Etemad, S., 2007, "Experimental Investigation of Convective Heat Transfer of  $\text{Al}_2\text{O}_3$ /Water Nanofluid in Circular Tube," *Int. J. Heat Fluid Fl.*, **28**(2), pp. 203-210.
- [16] Heris, S. Z., Etemad, S., and Esfahany, M. N., 2006, "Experimental Investigation of Oxide Nanofluids Laminar Flow Convective Heat Transfer," *Int. Commun. Heat Mass*, **33**(4), pp. 529-535.
- [17] Xuan, Y., and Roetzel, W., 2000, "Conceptions for Heat Transfer Correlation of Nanofluids," *Int. J. Heat Mass Tran.*, **43**(19), pp. 3701-3707.
- [18] Özerinç, S., Kakaç, S., and Yazıcıoğlu, A. G., 2010, "Enhanced Thermal Conductivity of Nanofluids: A State-of-the-Art Review," *Microfluid. Nanofluid.*, **8**(2), pp. 145-170.
- [19] Wang, X., and Mujumdar, A. S., 2007, "Heat Transfer Characteristics of Nanofluids: A Review," *Int. J. Therm. Sci.*, **46**(1), pp. 1-19.
- [20] Murshed, S., Leong, K., and Yang, C., 2008, "Thermophysical and Electrokinetic Properties of Nanofluids - A Critical Review," *Appl. Therm. Eng.*, **28**(17-18), pp. 2109-2125.
- [21] Chandrasekar, M., and Suresh, S., 2009, "A Review on the Mechanisms of Heat Transport in Nanofluids," *Heat Transfer Eng.*, **30**(14), pp. 1136-1150.

- [22] Choi, S. U. S., 2009, "Nanofluids: From Vision to Reality through Research," *J. Heat Transfer*, **131**(3), 033106.
- [23] Wen, D., Lin, G., Vafaei, S., and Zhang, K., 2009, "Review of Nanofluids for Heat Transfer Applications," *Particuology*, **7**(2), pp. 141-150.
- [24] Ding, Y., Alias, H., Wen, D., and Williams, R. A., 2006, "Heat Transfer of Aqueous Suspensions of Carbon Nanotubes (CNT Nanofluids)," *Int. J. Heat Mass Tran.*, **49**(1-2), pp. 240-250.
- [25] Zhu, H. T., Zhang, C. Y., Tang, Y. M., and Wang, J. X., 2007, "Novel Synthesis and Thermal Conductivity of CuO Nanofluid," *J. Phys. Chem. C*, **111**(4), pp. 1646-1650.
- [26] Hong, T., Yang, H., and Choi, C. J., 2005, "Study of the Enhanced Thermal Conductivity of Fe Nanofluids," *J. Appl. Phys.*, **97**(6), 064311-4.
- [27] Beck, M., Yuan, Y., Warriar, P., and Teja, A., 2009, "The Effect of Particle Size on the Thermal Conductivity of Alumina Nanofluids," *J. Nanopart. Res.*, **11**(5), pp. 1129-1136.
- [28] Wang, X., Choi, S. U. S., and Xu, X., 1999, "Thermal Conductivity of Nanoparticle - Fluid Mixture," *J. Thermophys. Heat Tran.*, **13**(4), pp. 474-480.
- [29] Czarnetzki, W., and Roetzel, W., 1995, "Temperature Oscillation Techniques for Simultaneous Measurement of Thermal Diffusivity and Conductivity," *Int. J. Thermophys.*, **16**(2), pp. 413-422.
- [30] Ju, Y. S., Kim, J., and Hung, M., 2008, "Experimental Study of Heat Conduction in Aqueous Suspensions of Aluminum Oxide Nanoparticles," *J. Heat Transfer*, **130**(9), 092403-6.
- [31] Putnam, S. A., Cahill, D. G., Braun, P. V., Ge, Z., and Shimmin, R. G., 2006, "Thermal Conductivity of Nanoparticle Suspensions," *J. Appl. Phys.*, **99**(8), 084308-6.
- [32] Lee, S., Choi, S. U. S., Li, S., and Eastman, J. A., 1999, "Measuring Thermal Conductivity of Fluids Containing Oxide Nanoparticles," *J. Heat Transfer*, **121**(2), pp. 280-289.
- [33] Murshed, S., Leong, K., and Yang, C., 2005, "Enhanced Thermal Conductivity of TiO<sub>2</sub>-Water Based Nanofluids," *Int. J. Therm. Sci.*, **44**(4), pp. 367-373.
- [34] Choi, S. U. S., Zhang, Z. G., Yu, W., Lockwood, F. E., and Grulke, E. A., 2001, "Anomalous Thermal Conductivity Enhancement in Nanotube Suspensions," *Appl. Phys. Lett.*, **79**(14), pp. 2252-2254.



- [35] Chopkar, M., Sudarshan, S., Das, P., and Manna, I., 2008, "Effect of Particle Size on Thermal Conductivity of Nanofluid," *Metall. Mater. Trans. A*, **39**(7), pp. 1535-1542.
- [36] Assael, M. J., Metaxa, I. N., Arvanitidis, J., Christofilos, D., and Lioutas, C., 2005, "Thermal Conductivity Enhancement in Aqueous Suspensions of Carbon Multi-Walled and Double-Walled Nanotubes in the Presence of Two Different Dispersants," *Int. J. Thermophys.*, **26**(3), pp. 647-664.
- [37] Maxwell, J. C., 1873, *A Treatise on Electricity and Magnetism*, Clarendon Press, Oxford.
- [38] Xuan, Y., Li, Q., and Hu, W., 2003, "Aggregation Structure and Thermal Conductivity of Nanofluids," *AIChE Journal*, **49**(4), pp. 1038-1043.
- [39] Lee, D., 2007, "Thermophysical Properties of Interfacial Layer in Nanofluids," *Langmuir*, **23**(11), pp. 6011-6018.
- [40] Xie, H., Wang, J., Xi, T., Liu, Y., and Ai, F., 2002, "Dependence of the Thermal Conductivity of Nanoparticle-Fluid Mixture on the Base Fluid," *J. Mater. Sci. Lett.*, **21**(19), pp. 1469-1471.
- [41] Hasselman, D., and Johnson, L. F., 1987, "Effective Thermal Conductivity of Composites with Interfacial Thermal Barrier Resistance," *J. Compos. Mater.*, **21**(6), pp. 508-515.
- [42] Liu, M., Lin, M. C., Huang, I., and Wang, C., 2005, "Enhancement of Thermal Conductivity with Carbon Nanotube for Nanofluids," *Int. Commun. Heat Mass*, **32**(9), pp. 1202-1210.
- [43] Eastman, J. A., Choi, S. U. S., Li, S., Yu, W., and Thompson, L. J., 2001, "Anomalously Increased Effective Thermal Conductivities of Ethylene Glycol-Based Nanofluids Containing Copper Nanoparticles," *Appl. Phys. Lett.*, **78**(6), pp. 718-720.
- [44] Hamilton, R. L., and Crosser, O. K., 1962, "Thermal Conductivity of Heterogeneous Two-Component Systems," *Ind. Eng. Chem. Fund.*, **1**(3), pp. 187-191.
- [45] Chopkar, M., Das, P. K., and Manna, I., 2006, "Synthesis and Characterization of Nanofluid for Advanced Heat Transfer Applications," *Scripta Mater.*, **55**(6), pp. 549-552.
- [46] Mintsas, H. A., Roy, G., Nguyen, C. T., and Doucet, D., 2009, "New Temperature Dependent Thermal Conductivity Data for Water-Based Nanofluids," *Int. J. Therm. Sci.*, **48**(2), pp. 363-371.

- [47] Murshed, S., Leong, K., and Yang, C., 2008, "Investigations of Thermal Conductivity and Viscosity of Nanofluids," *Int. J. Therm. Sci.*, **47**(5), pp. 560-568.
- [48] Chon, C. H., and Kihm, K. D., 2005, "Thermal Conductivity Enhancement of Nanofluids by Brownian Motion," *J. Heat Transfer*, **127**(8), p. 810.
- [49] Prasher, R., Phelan, P. E., and Bhattacharya, P., 2006, "Effect of Aggregation Kinetics on the Thermal Conductivity of Nanoscale Colloidal Solutions (Nanofluid)," *Nano Lett.*, **6**(7), pp. 1529-1534.
- [50] Feng, Y., Yu, B., Xu, P., and Zou, M., 2007, "The Effective Thermal Conductivity of Nanofluids Based on the Nanolayer and the Aggregation of Nanoparticles," *J. Phys. D: Appl. Phys.*, **40**(10), pp. 3164-3171.
- [51] Xie, H., Wang, J., Xi, T., and Liu, Y., 2002, "Thermal Conductivity of Suspensions Containing Nanosized SiC Particles," *Int. J. Thermophys.*, **23**(2), pp. 571-580.
- [52] Timofeeva, E. V., Routbort, J. L., and Singh, D., 2009, "Particle Shape Effects on Thermophysical Properties of Alumina Nanofluids," *J. Appl. Phys.*, **106**(1), 014304-10.
- [53] Li, C. H., Williams, W., Buongiorno, J., Hu, L., and Peterson, G. P., 2008, "Transient and Steady-State Experimental Comparison Study of Effective Thermal Conductivity of Al<sub>2</sub>O<sub>3</sub>/Water Nanofluids," *J. Heat Transfer*, **130**(4), 042407-7.
- [54] Turgut, A., Tavman, I., Chirtoc, M., Schuchmann, H., Sauter, C., and Tavman, S., 2009, "Thermal Conductivity and Viscosity Measurements of Water-Based TiO<sub>2</sub> Nanofluids," *Int. J. Thermophys.*, **30**(4), pp. 1213-1226.
- [55] Zhang, X., Gu, H., and Fujii, M., 2006, "Effective Thermal Conductivity and Thermal Diffusivity of Nanofluids Containing Spherical and Cylindrical Nanoparticles," *J. Appl. Phys.*, **100**(4), 044325-5.
- [56] Zhang, X., Gu, H., and Fujii, M., 2006, "Experimental Study on the Effective Thermal Conductivity and Thermal Diffusivity of Nanofluids," *Int. J. Thermophys.*, **27**(2), pp. 569-580.
- [57] Roy, G., Nguyen, C. T., Doucet, D., Suiro, S., and Maré, T., 2006, "Temperature Dependent Thermal Conductivity Evaluation of Alumina Based Nanofluids," *Proceedings of the 13th International Heat Transfer Conference*, G. D. V. Davis, and E. Leonardi, eds., Begell House Inc.
- [58] Hong, K. S., Hong, T., and Yang, H., 2006, "Thermal Conductivity of Fe Nanofluids Depending on the Cluster Size of Nanoparticles," *Appl. Phys. Lett.*, **88**(3), 031901-3.

- [59] Zhu, H., Zhang, C., Liu, S., Tang, Y., and Yin, Y., 2006, "Effects of Nanoparticle Clustering and Alignment on Thermal Conductivities of  $\text{Fe}_3\text{O}_4$  Aqueous Nanofluids," *Appl. Phys. Lett.*, **89**(2), 023123-3.
- [60] Xie, H., Wang, J., Xi, T., Liu Y., Ai, F., and Wu, Q., 2002, "Thermal Conductivity Enhancement of Suspensions Containing Nanosized Alumina Particles," *J. Appl. Phys.*, **91**(7), pp. 4568-4572.
- [61] Wang, X., Zhu, D., and Yang, S., 2009, "Investigation of pH and SDBS on Enhancement of Thermal Conductivity in Nanofluids," *Chem. Phys. Lett.*, **470**(1-3), pp. 107-111.
- [62] Murshed, S. M. S., Leong, K. C., and Yang, C., 2008, "Characterization of Electrokinetic Properties of Nanofluids," *J. Nanosci. Nanotechnol.*, **8**, pp. 5966-5971.
- [63] Li, Y., Qu, W., and Feng, J., 2008, "Temperature Dependence of Thermal Conductivity of Nanofluids," *Chinese Phys. Lett.*, **25**(9), pp. 3319-3322.
- [64] Bhattacharya, P., Saha, S. K., Yadav, A., Phelan, P. E., and Prasher, R. S., 2004, "Brownian Dynamics Simulation to Determine the Effective Thermal Conductivity of Nanofluids," *J. Appl. Phys.*, **95**(11), pp. 6492-6494.
- [65] Prasher, R., Bhattacharya, P., and Phelan, P. E., 2005, "Thermal Conductivity of Nanoscale Colloidal Solutions (Nanofluids)," *Phys. Rev. Lett.*, **94**(2), 025901.
- [66] Li, C., and Peterson, G., 2007, "Mixing Effect on the Enhancement of the Effective Thermal Conductivity of Nanoparticle Suspensions (Nanofluids)," *Int. J. Heat Mass Tran.*, **50**(23-24), pp. 4668-4677.
- [67] Evans, W., Fish, J., and Keblinski, P., 2006, "Role of Brownian Motion Hydrodynamics on Nanofluid Thermal Conductivity," *Appl. Phys. Lett.*, **88**(9), 093116-3.
- [68] He, Y., Jin, Y., Chen, H., Ding, Y., Cang, D., and Lu, H., 2007, "Heat Transfer and Flow Behaviour of Aqueous Suspensions of  $\text{TiO}_2$  Nanoparticles (Nanofluids) Flowing Upward through a Vertical Pipe," *Int. J. Heat Mass Tran.*, **50**(11-12), pp. 2272-2281.
- [69] Evans, W., Prasher, R., Fish, J., Meakin, P., Phelan, P., and Keblinski, P., 2008, "Effect of Aggregation and Interfacial Thermal Resistance on Thermal Conductivity of Nanocomposites and Colloidal Nanofluids," *Int. J. Heat Mass Tran.*, **51**(5-6), pp. 1431-1438.
- [70] Nan, C., Birringer, R., Clarke, D. R., and Gleiter, H., 1997, "Effective Thermal Conductivity of Particulate Composites with Interfacial Thermal Resistance," *J. Appl. Phys.*, **81**(10), pp. 6692-6699.

- [71] Keblinski, P., Prasher, R., and Eapen, J., 2008, "Thermal Conductance of Nanofluids: Is the Controversy Over?," *J. Nanopart. Res.*, **10**(7), pp. 1089-1097.
- [72] Yu, C., Richter, A. G., Datta, A., Durbin, M. K., and Dutta, P., 1999, "Observation of Molecular Layering in Thin Liquid Films Using X-ray Reflectivity," *Phys. Rev. Lett.*, **82**(11), pp. 2326-2329.
- [73] Yu, W., and Choi, S. U. S., 2003, "The Role of Interfacial Layers in the Enhanced Thermal Conductivity of Nanofluids: A Renovated Maxwell Model," *J. Nanopart. Res.*, **5**(1), pp. 167-171.
- [74] Xie, H., Fujii, M., and Zhang, X., 2005, "Effect of Interfacial Nanolayer on the Effective Thermal Conductivity of Nanoparticle-Fluid Mixture," *Int. J. Heat Mass Tran.*, **48**(14), pp. 2926-2932.
- [75] Sitprasert, C., Dechaumphai, P., and Juntasaro, V., 2009, "A Thermal Conductivity Model for Nanofluids Including Effect of the Temperature-Dependent Interfacial Layer," *J. Nanopart. Res.*, **11**(6), pp. 1465-1476.
- [76] Tillman, P., and Hill, J. M., 2007, "Determination of Nanolayer Thickness for a Nanofluid," *Int. Commun. Heat Mass*, **34**(4), pp. 399-407.
- [77] Xue, L., Keblinski, P., Phillpot, S. R., Choi, S. U. S., and Eastman, J. A., 2004, "Effect of Liquid Layering at the Liquid-Solid Interface on Thermal Transport," *Int. J. Heat Mass Tran.*, **47**(19-20), pp. 4277-4284.
- [78] Geiger, G. H., and Poirier, D. R., 1973, *Transport Phenomena in Metallurgy*, Addison-Wesley, Reading, PA.
- [79] Nie, C., Marlow, W., and Hassan, Y., 2008, "Discussion of Proposed Mechanisms of Thermal Conductivity Enhancement in Nanofluids," *Int. J. Heat Mass Tran.*, **51**(5-6), pp. 1342-1348.
- [80] Domingues, G., Volz, S., Joulain, K., and Greffet, J., 2005, "Heat Transfer between Two Nanoparticles through Near Field Interaction," *Phys. Rev. Lett.*, **94**(8), 085901.
- [81] Ben-Abdallah, P., 2006, "Heat Transfer through Near-Field Interactions in Nanofluids," *Appl. Phys. Lett.*, **89**(11), 113117-3.
- [82] Jang, S. P., and Choi, S. U. S., 2004, "Role of Brownian Motion in the Enhanced Thermal Conductivity of Nanofluids," *Appl. Phys. Lett.*, **84**(21), pp. 4316-4318.
- [83] Einstein, A., 1956, *Investigation on the Theory of Brownian Movement*, Dover, New York.

- [84] Koo, J., and Kleinstreuer, C., 2004, "A New Thermal Conductivity Model for Nanofluids," *J. Nanopart. Res.*, **6**(6), pp. 577-588.
- [85] Xu, J., Yu, B., Zou, M., and Xu, P., 2006, "A New Model for Heat Conduction of Nanofluids Based on Fractal Distributions of Nanoparticles," *J. Phys. D: Appl. Phys.*, **39**(20), pp. 4486-4490.
- [86] Tomotika, S., Aoi, T., and Yosinobu, H., 1953, "On the Forces Acting on a Circular Cylinder Set Obliquely in a Uniform Stream at Low Values of Reynolds Number," *Proceedings of the Royal Society of London, Series A, Mathematical and Physical Sciences*, **219**(1137), pp. 233-244.
- [87] Li, Q., and Xuan, Y., 2000, "Experimental Investigation on Transport Properties of Nanofluids," *Heat Transfer Science and Technology 2000*, B. Wang, ed., Higher Education Press, Beijing, pp. 757-762.
- [88] Chen, H., Witharana, S., Jin, Y., Kim, C., and Ding, Y., 2009, "Predicting Thermal Conductivity of Liquid Suspensions of Nanoparticles (Nanofluids) Based on Rheology," *Particuology*, **7**(2), pp. 151-157.
- [89] Krieger, I. M., and Dougherty, T. J., 1959, "A Mechanism for Non-Newtonian Flow in Suspensions of Rigid Spheres," *J. Rheol.*, **3**(1), pp. 137-152.
- [90] Bruggeman, D. A. G., 1935, "The Calculation of Various Physical Constants of Heterogeneous Substances. I. The Dielectric Constants and Conductivities of Mixtures Composed of Isotropic Substances," *Ann. Phys.*, **416**(7), pp. 636-664.
- [91] Nan, C. W., Shi, Z., and Lin, Y., 2003, "A Simple Model for Thermal Conductivity of Carbon Nanotube-Based Composites," *Chem. Phys. Lett.*, **375**(5-6), pp. 666-669.
- [92] Schwartz, L. M., Garboczi, E. J., and Bentz, D. P., 1995, "Interfacial Transport in Porous Media: Application to DC Electrical Conductivity of Mortars," *J. Appl. Phys.*, **78**(10), pp. 5898-5908.
- [93] Yu, W., and Choi, S., 2004, "The Role of Interfacial Layers in the Enhanced Thermal Conductivity of Nanofluids: A Renovated Hamilton-Crosser Model," *J. Nanopart. Res.*, **6**(4), pp. 355-361.
- [94] Xue, Q., 2003, "Model for Effective Thermal Conductivity of Nanofluids," *Phys. Lett. A*, **307**(5-6), pp. 313-317.
- [95] Zhou, L. P., and Wang, B. X., 2002, "Experimental Research on the Thermophysical Properties of Nanoparticle Suspensions Using the Quasi-Steady State Method," *Proceedings of the 11th Annual Conference of Chinese Society of Engineering Thermophysics*, Shanghai, pp. 889-892.

- [96] Xue, Q., and Xu, W., 2005, "A Model of Thermal Conductivity of Nanofluids with Interfacial Shells," *Mater. Chem. Phys.*, **90**(2-3), pp. 298-301.
- [97] Chen, G., 1996, "Nonlocal and Nonequilibrium Heat Conduction in the Vicinity of Nanoparticles," *J. Heat Transfer*, **118**(3), pp. 539-545.
- [98] Einstein, A., 1906, "A New Determination of the Molecular Dimensions," *Ann. Phys.*, **324**(2), pp. 289-306.
- [99] Leong, K., Yang, C., and Murshed, S., 2006, "A Model for the Thermal Conductivity of Nanofluids – The Effect of Interfacial Layer," *J. Nanopart. Res.*, **8**(2), pp. 245-254.
- [100] Oh, D., Jain, A., Eaton, J. K., Goodson, K. E., and Lee, J. S., 2008, "Thermal Conductivity Measurement and Sedimentation Detection of Aluminum Oxide Nanofluids by Using the  $3\omega$  Method," *Int. J. Heat Fluid Fl.*, **29**(5), pp. 1456-1461.
- [101] Wen, D., and Ding, Y., 2004, "Experimental Investigation into Convective Heat Transfer of Nanofluids at the Entrance Region under Laminar Flow Conditions," *Int. J. Heat Mass Tran.*, **47**(24), pp. 5181-5188.
- [102] Nimtz, G., Marquardt, P., and Gleiter, H., 1990, "Size-Induced Metal-Insulator Transition in Metals and Semiconductors," *J. Cryst. Growth*, **86**(1-4), pp. 66-71.
- [103] Eastman, J., Choi, S. U. S., Li, S., Thompson, L., and Lee, S., 1997, "Enhanced Thermal Conductivity through the Development of Nanofluids," *Proceedings of the Symposium on Nanophase and Nanocomposite Materials II*, Materials Research Society, Boston, **457**, pp. 3-11.
- [104] Patel, H., Sundararajan, T., and Das, S., 2010, "An Experimental Investigation into the Thermal Conductivity Enhancement in Oxide and Metallic Nanofluids," *J. Nanopart. Res.*, **12**(3), pp. 1015-1031.
- [105] Tsai, T., Kuo, L., Chen, P., and Yang, C., 2008, "Effect of Viscosity of Base Fluid on Thermal Conductivity of Nanofluids," *Appl. Phys. Lett.*, **93**(23), 233121-3.
- [106] Li, Q., and Xuan, Y., 2002, "Convective Heat Transfer and Flow Characteristics of Cu-Water Nanofluid," *Sci. China Ser. E*, **45**(4), pp. 408-416.
- [107] Chen, H., Yang, W., He, Y., Ding, Y., Zhang, L., Tan, C., Lapkin, A. A., and Bavykin, D. V., 2008, "Heat Transfer and Flow Behaviour of Aqueous Suspensions of Titanate Nanotubes (Nanofluids)," *Powder Technol.*, **183**(1), pp. 63-72.

- [108] Kulkarni, D. P., Namburu, P. K., Ed Bargar, H., and Das, D. K., 2008, "Convective Heat Transfer and Fluid Dynamic Characteristics of SiO<sub>2</sub> Ethylene Glycol/Water Nanofluid," *Heat Transfer Eng.*, **29**(12), pp. 1027-1035.
- [109] Anoop, K., Sundararajan, T., and Das, S. K., 2009, "Effect of Particle Size on the Convective Heat Transfer in Nanofluid in the Developing Region," *Int. J. Heat Mass Tran.*, **52**(9-10), pp. 2189-2195.
- [110] Kim, D., Kwon, Y., Cho, Y., Li, C., Cheong, S., Hwang, Y., Lee, J., Hong, D., and Moon, S., 2009, "Convective Heat Transfer Characteristics of Nanofluids under Laminar and Turbulent Flow Conditions," *Current Applied Physics*, **9**(2, Supplement 1), pp. 119-123.
- [111] Kakaç, S., and Pramuanjaroenkij, A., 2009, "Review of Convective Heat Transfer Enhancement with Nanofluids," *Int. J. Heat Mass Tran.*, **52**(13-14), pp. 3187-3196.
- [112] Godson, L., Raja, B., Mohan Lal, D., and Wongwises, S., 2010, "Enhancement of Heat Transfer Using Nanofluids-An Overview," *Renew. Sust. Energ. Rev.*, **14**(2), pp. 629-641.
- [113] Ding, Y., and Wen, D., 2005, "Particle Migration in a Flow of Nanoparticle Suspensions," *Powder Technol.*, **149**(2-3), pp. 84-92.
- [114] Buongiorno, J., 2006, "Convective Transport in Nanofluids," *J. Heat Transfer*, **128**(3), pp. 240-250.
- [115] Mansour, R. B., Galanis, N., and Nguyen, C. T., 2007, "Effect of Uncertainties in Physical Properties on Forced Convection Heat Transfer with Nanofluids," *Appl. Therm. Eng.*, **27**(1), pp. 240-249.
- [116] Maïga, S. E. B., Nguyen, C. T., Galanis, N., and Roy, G., 2004, "Heat Transfer Behaviours of Nanofluids in a Uniformly Heated Tube," *Superlattices and Microstructures*, **35**(3-6), pp. 543-557.
- [117] Heris, S. Z., Esfahany, M. N., and Etemad, G., 2007, "Numerical Investigation of Nanofluid Laminar Convective Heat Transfer through a Circular Tube," *Numer. Heat Tr. A-Appl.*, **52**(11), pp. 1043-1058.
- [118] Behzadmehr, A., Saffar-Avval, M., and Galanis, N., 2007, "Prediction of Turbulent Forced Convection of a Nanofluid in a Tube with Uniform Heat Flux Using a Two Phase Approach," *Int. J. Heat Fluid Fl.*, **28**(2), pp. 211-219.
- [119] Bianco, V., Chiacchio, F., Manca, O., and Nardini, S., 2009, "Numerical Investigation of Nanofluids Forced Convection in Circular Tubes," *Appl. Therm. Eng.*, **29**(17-18), pp. 3632-3642.

- [120] Wang, X., and Mujumdar, A., 2008, "A Review on Nanofluids - Part I: Theoretical and Numerical Investigations," *Braz. J. Chem. Eng.*, **25**(4), pp. 613-630.
- [121] Nguyen, C., Desgranges, F., Roy, G., Galanis, N., Maré, T., Boucher, S., and Angue Mintsa, H., 2007, "Temperature and Particle-Size Dependent Viscosity Data for Water-Based Nanofluids - Hysteresis Phenomenon," *Int. J. Heat Fluid Fl.*, **28**(6), pp. 1492-1506.
- [122] Chen, L., Xie, H., Li, Y., and Yu, W., 2008, "Nanofluids Containing Carbon Nanotubes Treated by Mechanochemical Reaction," *Thermochim. Acta*, **477**(1-2), pp. 21-24.
- [123] Kulkarni, D. P., Das, D. K., and Chukwu, G. A., 2006, "Temperature Dependent Rheological Property of Copper Oxide Nanoparticles Suspension (Nanofluid)," *J. Nanosci. Nanotechnol.*, **6**, pp. 1150-1154.
- [124] Chen, H., Ding, Y., and Lapkin, A., 2009, "Rheological Behaviour of Nanofluids Containing Tube / Rod-Like Nanoparticles," *Powder Technol.*, **194**(1-2), pp. 132-141.
- [125] Prasher, R., Song, D., Wang, J., and Phelan, P., 2006, "Measurements of Nanofluid Viscosity and Its Implications for Thermal Applications," *Appl. Phys. Lett.*, **89**(13), 133108-3.
- [126] Pastoriza-Gallego, M. J., Casanova, C., Paramo, R., Barbes, B., Legido, J. L., and Pineiro, M. M., 2009, "A Study on Stability and Thermophysical Properties (Density and Viscosity) of Al<sub>2</sub>O<sub>3</sub> in Water Nanofluid," *J. Appl. Phys.*, **106**(6), 064301-8.
- [127] Brinkman, H. C., 1952, "The Viscosity of Concentrated Suspensions and Solutions," *J. Chem. Phys.*, **20**(4), p. 571.
- [128] Batchelor, G. K., 1977, "The Effect of Brownian Motion on the Bulk Stress in a Suspension of Spherical Particles," *J. Fluid Mech.*, **83**(1), pp. 97-117.
- [129] Yu, W., France, D. M., Choi, S. U. S., Routbort, J. L., and Systems, E., 2007, "Review and Assessment of Nanofluid Technology for Transportation and Other Applications," Argonne National Laboratory, Energy Systems Division, Argonne, Illinois.
- [130] Tseng, W. J., and Lin, K., 2003, "Rheology and Colloidal Structure of Aqueous TiO<sub>2</sub> Nanoparticle Suspensions," *Mater. Sci. Eng. A*, **355**(1-2), pp. 186-192.
- [131] Shah, R. K., and London, A. L., 1978, *Laminar Flow Forced Convection in Ducts, Supplement 1 to Advances in Heat Transfer*, Academic Press, New York.



- [132] Sieder, E. N., and Tate, G. E., 1936, "Heat Transfer and Pressure Drop of Liquids in Tubes," *Ind. Eng. Chem.*, **28**(12), pp. 1429-1435.
- [133] Kakaç, S., and Yener, Y., 1995, *Convective Heat Transfer: Second Edition*, CRC-Press, Boca Raton.
- [134] Özışık, M. N., 1994, *Finite Difference Methods in Heat Transfer*, CRC-Press, Boca Raton.
- [135] Graetz, L., 1883, "Über die Wärmeleitungs fähigkeit von Flüssigkeiten," *Ann. Phys. Chem.*, **18**, pp. 79-94.
- [136] Lipkis, R. P., 1954, "Heat Transfer to an Incompressible Fluid in Laminar Motion," M.Sc. Thesis, University of California, Los Angeles.
- [137] Siegel, R., Sparrow, E. M., and Hallman, T. M., 1958, "Steady Laminar Heat Transfer in a Circular Tube with Prescribed Wall Heat Flux," *Applied Scientific Research*, **7A**, pp. 386-392.

## APPENDIX A

### SAMPLE CALCULATIONS

In the first part of this appendix, a sample calculation for the determination of average heat transfer coefficient enhancement ratio of a laminar nanofluid flow inside a straight circular tube under constant wall temperature boundary condition is provided. Complete results of the associated analysis are provided in Section 3.4.2.2.

In the second part of the appendix, a similar discussion for the determination of fully developed heat transfer coefficient of a laminar nanofluid flow is presented. Complete results of the associated analyses are provided in Section 3.4.3.

Throughout the discussion, the numerical values are provided in SI units, unless otherwise noted.

#### A.1. Average Heat Transfer Coefficient Enhancement Ratio

In this part, average heat transfer coefficient enhancement ratio is determined for the case of 2 vol.% Al<sub>2</sub>O<sub>3</sub>/water nanofluid. The nanofluid is considered to contain spherical particles with a diameter of 20 nm. The flow configuration is the same as the experimental test section of Heris et al. [15]. The nanofluid flows inside a straight circular tube whose diameter is 5 mm and length is 1 m. For constant wall temperature boundary condition, determination of average heat transfer coefficient enhancement ratio is explained in Section 3.4.2.2 in detail. As a result of the derivation, following expression is obtained.

$$\frac{h_{nf}}{h_f} = \left( \frac{\rho_{nf} c_{p,nf}}{\rho_f c_{p,f}} \right)^{1/3} \left( \frac{k_{nf}}{k_f} \right)^{2/3}. \quad (159)$$

In order to perform the associated calculation, density, specific heat and thermal conductivity of the nanofluid should be determined. Density of the nanofluid can be determined as follows.

$$\rho_{nf} = \phi\rho_p + (1-\phi)\rho_f = 0.02(3700) + (1-0.02)(994.0) = 1048 \text{ kg/m}^3. \quad (160)$$

Specific heat of the nanofluid can be determined in a similar way:

$$\begin{aligned} c_{p,nf} &= \frac{\phi(\rho c_p)_p + (1-\phi)(\rho c_p)_f}{\rho_{nf}} \\ &= \frac{0.02(3700)(880) + (1-0.02)(994.0)(4179)}{1048} = 3946 \text{ J/kgK} \end{aligned} \quad (161)$$

For the determination of the thermal conductivity of the nanofluid, the model provided by Chon et al. [10] is used.

$$\frac{k_{nf}}{k_f} = 1 + 64.7\phi^{0.7460} \left(\frac{d_f}{d_p}\right)^{0.3690} \left(\frac{k_p}{k_f}\right)^{0.7476} \text{Pr}^{0.9955} \text{Re}^{1.2321}. \quad (162)$$

Here,  $d_f$  is the diameter of the fluid molecules. Prandtl number and Reynolds number are defined as follows.

$$\text{Pr} = \frac{\mu_f}{\rho_f \alpha_f}, \quad (163)$$

$$\text{Re} = \frac{\rho_f V_{Br} d_p}{\mu_f}. \quad (164)$$

$V_{Br}$  is the Brownian velocity of the nanoparticles and it is calculated by using the following expression.

$$V_{Br} = \frac{\kappa_B T}{3\pi\mu_f d_p \lambda_f}. \quad (165)$$

Substituting this expression into Eq. (164), Reynolds number can be rewritten as

$$\text{Re} = \frac{\rho_f \kappa_B T}{3\pi\mu_f^2 \lambda_f}. \quad (166)$$

$\lambda_f$  is mean-free path of the fluid molecules, and it is 0.17 nm for water. Substituting the associated values for 2 vol.%  $\text{Al}_2\text{O}_3$ /water nanofluid, Prandtl number and Reynolds number are obtained as follows.

$$\text{Pr} = \frac{\mu_f}{\rho_f \alpha_f} = \frac{7.207 \cdot 10^{-4}}{(994.0)(1.494 \cdot 10^{-7})} = 4.853, \quad (167)$$

$$\text{Re} = \frac{\rho_f \kappa_B T}{3\pi \mu_f^2 \lambda_f} = \frac{(994.0)(1.3807 \cdot 10^{-23})(308)}{3\pi(7.207 \cdot 10^{-4})^2(0.17 \cdot 10^{-9})} = 0.005079. \quad (168)$$

After the determination of Prandtl and Reynolds numbers, Eq. (162) can be utilized for the determination of the nanofluid thermal conductivity as follows.

$$\frac{k_{nf}}{0.6210} = 1 + 64.7(0.02)^{0.7460} \left( \frac{0.28 \cdot 10^{-9}}{20 \cdot 10^{-9}} \right)^{0.3690} \left( \frac{36}{0.6210} \right)^{0.7476}, \quad (169)$$

$$4.853^{0.9955} 0.005079^{1.2321}$$

$$k_{nf} = 0.6881 \text{ W/mK}. \quad (170)$$

By using this result, one can calculate the average heat transfer coefficient enhancement ratio by substituting the associated parameters into Eq. (159):

$$\frac{h_{nf}}{h_f} = \left( \frac{\rho_{nf} c_{p,nf}}{\rho_f c_{p,f}} \right)^{1/3} \left( \frac{k_{nf}}{k_f} \right)^{2/3} = \left( \frac{1048 \ 3946}{994.0 \ 4179} \right)^{1/3} \left( \frac{0.6881}{0.6210} \right)^{2/3} = 1.069. \quad (171)$$

Therefore, a 6.9% enhancement is obtained in average heat transfer coefficient by using 2.0 vol.% Al<sub>2</sub>O<sub>3</sub>/water nanofluid, according to the approach of direct application of classical correlations.

## A.2. Fully Developed Heat Transfer Coefficient

In this sample calculation, fully developed heat transfer coefficient value is determined for the case of 4 vol.% Al<sub>2</sub>O<sub>3</sub>/water nanofluid at room temperature. The nanofluid is considered to contain spherical particles with a diameter of 47 nm. For constant wall temperature boundary condition, fully developed Nusselt number is as follows.

$$Nu_{fd} = 3.657. \quad (172)$$

By utilizing the definition of Nusselt number,

$$Nu = \frac{hd}{k}, \quad (173)$$

fully developed heat transfer coefficient can be obtained as

$$h_{fd} = \frac{Nu_{fd}k}{d}. \quad (174)$$

where  $k$  is working fluid thermal conductivity and  $d$  is tube diameter. Therefore, thermal conductivity of the nanofluid should be calculated for the determination of the heat transfer coefficient of the nanofluid flow. For the room temperature case, Hamilton and Crosser model [44] can be utilized for thermal conductivity calculation. The associated expression is as follows:

$$k_{nf} = \frac{k_p + (n-1)k_f - (n-1)\phi(k_f - k_p)}{k_p + (n-1)k_f + \phi(k_f - k_p)} k_f \quad (175)$$

where

$$n = \frac{3}{\psi}. \quad (176)$$

For spherical particles,  $\psi = 1$ , and as a result,  $n = 3$ . At room temperature, thermal conductivities of  $Al_2O_3$  and water are as follows.

$$k_{Al_2O_3} = 46 \text{ W/mK}, \quad (177)$$

$$k_{water} = 0.606 \text{ W/mK}. \quad (178)$$

The value provided above is the bulk thermal conductivity of  $Al_2O_3$ . For nanometer sized particles, thermal conductivity should be calculated according to the following expression [97].

$$k_p = \frac{3r^*/4}{3r^*/4+1} k_b. \quad (179)$$

$k_b$  is thermal conductivity of the bulk material, and  $r^* = r_p / \lambda$ , where  $r_p$  is particle radius and  $\lambda$  is the mean-free path of phonons (35 nm for  $Al_2O_3$  [2]). Then,  $r^*$  for the present case becomes:

$$r^* = \frac{23.5 \text{ nm}}{35 \text{ nm}} = 0.671. \quad (180)$$

Substituting the associated values into Eq. (179), nanoparticle thermal conductivity can be obtained as follows.

$$k_p = \frac{3(0.671)/4}{3(0.671)/4+1} 46 = 15.4 \text{ W/mK}. \quad (181)$$

After the determination of the nanoparticle thermal conductivity, Eq. (175) can be used to obtain the nanofluid thermal conductivity:

$$k_{nf} = \frac{15.4 + (3-1)(0.606) - (3-1)0.04(0.606-15.4)}{15.4 + (3-1)0.606 + 0.04(0.606-15.4)} 0.606 = 0.673 \text{ W/mK} . \quad (182)$$

Associated thermal conductivity ratio is:

$$\frac{k_{nf}}{k_f} = \frac{0.673}{0.606} = 1.111 . \quad (183)$$

Assuming a tube diameter of 1 cm, fully developed heat transfer coefficient for the nanofluid flow becomes:

$$h_{fd,nf} = \frac{Nu_{fd} k_{nf}}{d} = \frac{(3.657)(0.673)}{0.01} = 246.2 \text{ W/m}^2\text{K} . \quad (184)$$

Since the tube diameter and the Nusselt number are the same for the case of pure water flow and nanofluid flow, heat transfer coefficient enhancement ratio is equal to the thermal conductivity ratio:

$$\frac{h_{fd,nf}}{h_{fd,f}} = \frac{k_{nf}}{k_f} = 1.111 . \quad (185)$$

Therefore, the enhancement obtained in fully developed heat transfer coefficient by using 4.0 vol.% Al<sub>2</sub>O<sub>3</sub>/water nanofluid is 11.1%, assuming that fully developed Nusselt number is the same for the flow of pure fluids and nanofluids.

## **APPENDIX B**

### **FLOWCHART OF THE NUMERICAL SOLUTION**

In Figure 30, a general flowchart of the numerical analysis of the forced convection heat transfer of nanofluids is provided. The associated numerical approach is explained and verified in Chapter 4 in detail. The results of the numerical analyses are discussed in Chapter 5.

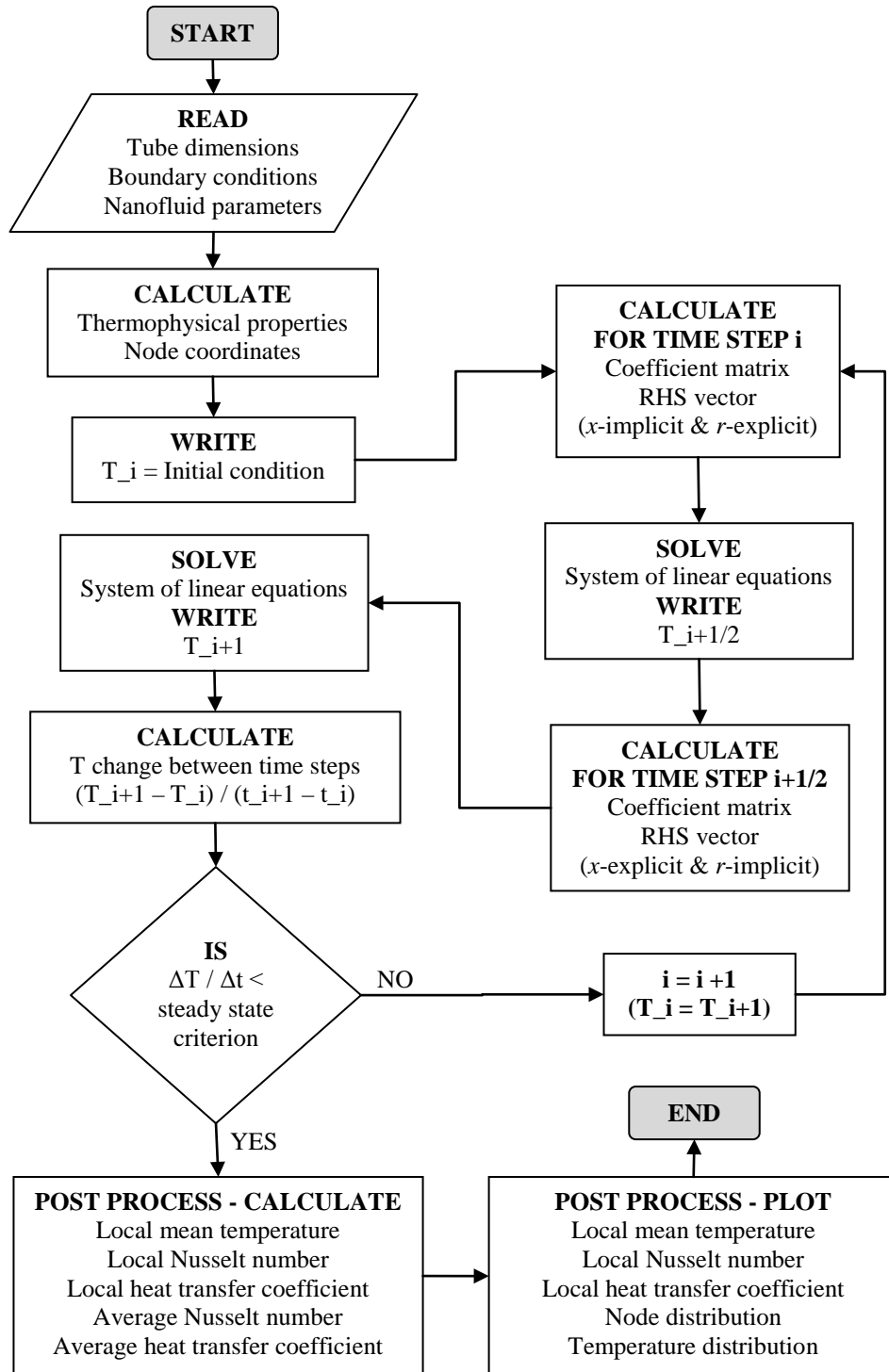


**Figure 30.** Flowchart of the numerical solution discussed in Chapters 4 and 5. T is temperature, and t is time. Subscript i indicates the time step.